Understanding the Mechanism and Chemical Properties of High Valent Iron(IV) Oxo Intermediates in Enzymes Using Quantum Mechanical Methods

Extended Abstract

A thesis submitted to The Babasaheb Bhimrao Ambedkar University for the Award of the degree

of

Doctor in Science

in

Physics

By

Prof. (Dr.) Devesh Kumar, MNASc

Enrollment No.: 1086/18

Advisor

Prof. (Dr.) R. C. Sobti

Department of Physics

2020

IN MEMORIES OF

LATE PARENTS

#

Acknowledgements

First of all I would like to thank the than Vice-Chancellor Prof (Dr.) R. C. Sobti (2018) without whose encouragement and support it was not possible for me to pursue for this degree.

I would also like to thank all the Faculty Members (Prof. (Dr.) B. C. Yadav, Dr. Ramesh Chandra, Dr. Anil K Yadav, Dr. Devendra Singh and Dr. K. B. Thapa) and office staff (Mr. Amit, Mr. Mukesh, Mr. Shtrudhan and Mr. Rahul) of the Deparment of Physics for their continous support.

All the former and present PhD students in my group (Dr Jitendra Kumar, Dr Suresh Kumar, Dr Pranav Upadhyaya, Dr. Deep Kumar, Dr. Devendra Singh, Dr. Dharmveer Singh, Dr. Ashish Kumar, Mr. Narinder Kumar, Miss Rolly Yadav, Miss Anamika Shukla, Miss Nidhi Awasti, Miss Shivani Choudhary), without their active participation in the projects discussed here this dissertation would not have been accomplished is acknowledged.

I also thank the National Service of Computational Chemistry Software (NSCCS), UK for very generous CPU support for our work. Funding from DST, New Delhi for Ramanujan Fellowship and DBT, New Delhi [BT/PR14510/BID/07/334/2010] is acknowledged for resources and person support is thanked.

Due to the interdisciplinary nature of the research, many of the projects described here are in collaboration with either experimentally based or computational research groups. I would like to thank all my collaborators over the years for their valuable contributions and stimulating discussions. In particular, I would like to thank the long-standing collaboration with Prof. (Dr.) C. V. Sastri, IIT, Guwahati.

I also need to give my special thanks to my close computational collaborator, Prof (Dr.) Sam P de Visser, Univrsity of Manchestor, UK who always is interested in working on joint projects with me. Our collaboration started during our joint postdoc in Jerusalem under supervision of Prof Sason Shaik

and continued after my move to initially the Max Planck Institute (with Late Prof Walter Thiel) and the Indian Institute of Chemical Technology in Hyderabad (with Prof G. Narahari Sastry).

Of course, I also thank for continous encouragement and support given by my family.

(Devesh Kumar)

Abstract:

In more than one third of enzymes metal ions play critical roles.These ions use to control an enzyme-catalyzed reaction by modify electron flow in enzyme or substrate. There are no general rules exist through which one may describe the behavior of given metal ion in an enzyme. These ions are usually positively charged and behave as electrophiles, always looking for the possibility of sharing electron pairs with other subgroups or atoms in order to form a bond or charge-charge interaction, hence, these ions behave like hydrogen ions. The ligands are usually negatively charged or neutral atom(s) or group(s) of atoms which can form bond with the metal ion in an electrostatic manner, generally by donating electron density to the metal ion. The number of ligand atoms bound to metal ion is the coordination number of a metal ion. It is viewed in terms of concentric spheres; the inner sphere containing those atoms is in contact with the metal ion while the second sphere containing those atoms is in contact with the inner sphere ligands. The sizes of metal ion as well as the sizes of the ligands decide the number of atoms in these spheres.

The theoretical model calculations, two decades before, had a minor role for explaining mechanisms of redox-active metalloenzymes. The available methods to describe transition metals were too slow for any meaningful applications and they were not accurate enough also. The computational models for the treatment of these enzymes were underdeveloped. But this situation changed now-a-days because of developments of methods as well as insights from applications. The developed density functional theory (DFT) methods with accuracy were not far from accuracy. The major improvements was the incorporation of density gradient terms for the exchange part and of fractions of exact exchange. The application of these methods showed that the accuracy was quite reasonable for transition-metal complexes. The experience of decades on small models with transition-metal complexes was the second important reason for the development in this area, it was surprisingly helpful for understanding many aspects of the mechanisms of large organometallic complexes, at least qualitatively, using small models. It is also observed that

the individual reaction steps as well as transition-state structures are quite insensitive to the size of the model in terms of explaining the mechanisms.

Originally two different approaches were developed to study mechanisms of redox-active metalloenzymes. The cluster model which is used to capture the important features of a mechanism in small quantum mechanical models is used. This model was used firstly in 1997, with DFT methods for understanding the mechanism of methane monooxygenase (MMO). The other approach in which the entire enzyme was treated with quantum mechanically described small core and the rest of enzyme was described with molecular mechanics, known as the quantum mechanics/molecular mechanics (QM/MM) model. The first application of QM/MM on the mechanism of galactose oxidase was made in 2000. Both approaches have been developed over the years from their original form. Now a day, with improvement in computer technology, QM cluster models can handle quite big model i.e. with more than 200 atoms, and even larger QM core can be used in the QM/MM approach.

Today, theoretical model calculations must be considered at least of equal importance for explaining/ determining mechanisms for metalloenzymes as compared with traditional spectroscopic techniques. Although the spectroscopic techniques have the advantage due to its application on the actual system, but their interpretations are often extremely difficult is the disadvantage. In theoretical modeling not only choices of the method but also the modeling of the real system has to be accurate. More than two decades of experience has made the understanding of the applicability and limitations of different models fully grown and it has reached at a mature stage.

Table of Contents:

1. Introduction.

Oxygen activating metalloenzymes are highly versatile in nature and are involved in processes that include biodegradation, metabolism and biosynthesis. Many of the metalloenzymes in nature utilize iron in their active centre, which structurally contains either a heme or a nonheme ligand system. A large – and well studied – class of heme enzymes are the cytochromes P450, which are monoxygenases found, for instance, in the liver, where they catalyze the metabolism of drugs, detoxification processes as well as the biosynthesis of hormones.[1–8] These enzymes use a molecule of O_2 on a heme centre and with assistance of two electrons and two protons create a high-valent iron(IV)-oxo heme cation radical intermediate, $[Fe^{IV}(O)(heme^{+\bullet})]$ also known as Compound I (Cpd I), Eq 1. The monoxygenation reactions catalyzed by P450 enzymes cover a wide range of possible chemical reactions, but generally start from the active species, Cpd I.[8–13] A selection of the most often encountered mechanisms of oxygen atom transfer processes by Cpd I of P450 are given in Figure 1. The most common one of those is aliphatic hydroxylation leading to alcohol products. Other reactions include double bond activation that produces epoxides and challenging processes such as aromatic hydroxylation and heteroatom oxidation, such as sulphoxidation. In addition, the P450s occasionally give products originating from dehydrogenation and ring-closure processes, Figure 1.

$$[Fe^{III}(heme)] + O_2 + 2\ e^- + 2\ H^+ \rightarrow [Fe^{IV}(O)(heme^{+\bullet})] + H_2O \qquad (1)$$

Although the activity of Cpd I in oxygen atom transfer processes was predicted by biomimetic reaction mechanisms many years ago,[14] it was only characterized with spectroscopic methods very recently.[15] Due to the fact that P450 Cpd I was elusive for a long time, studies into its intrinsic electronic properties and reactivity patterns were performed using computational modelling, which characterized it as an extremely versatile oxidant.[4,8,16] Moreover, computational studies established the electronic properties, predicted spectroscopic parameters and reactivity patterns, and, as such guided and supported experiment. These studies gave insight into the nature of the

active species, the effect of ligands to the reaction centre and environmental influences on the oxidants and its activity towards substrates. In this dissertation, an overview will be given on the computational studies into heme and nonheme based iron(IV)-oxo species and synthetic analogues.

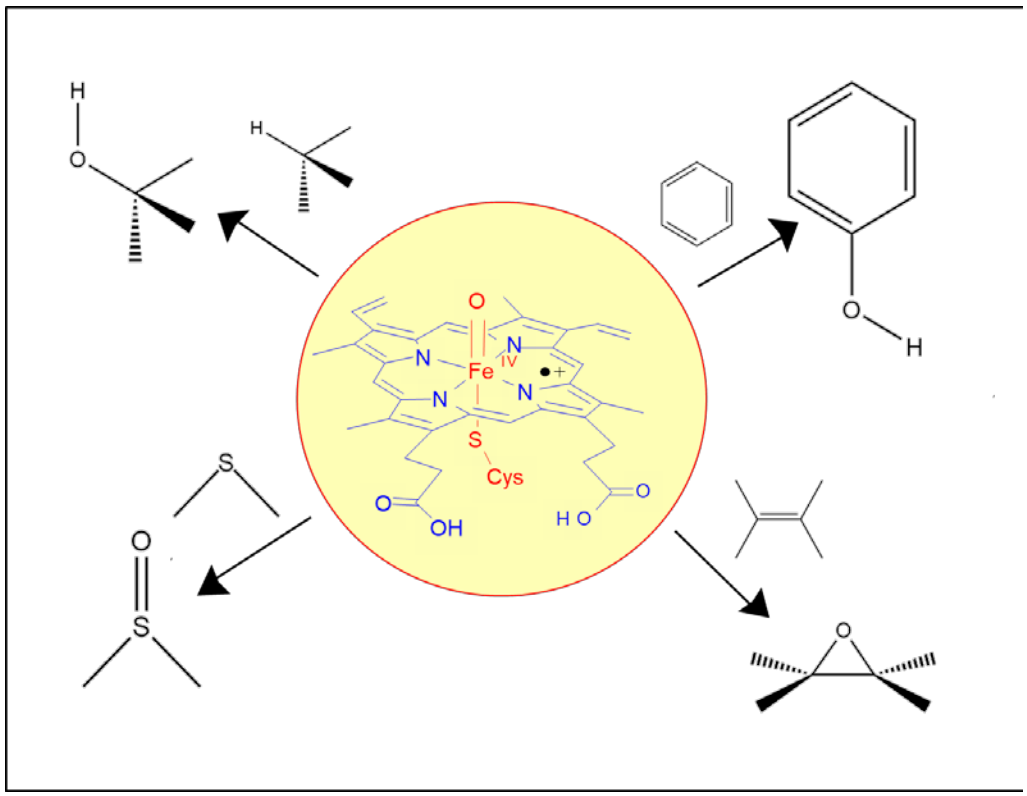

Figure 1: Reactivity patterns of Compound I of P450 enzymes with selected substrates.

Due to experimental difficulties in trapping and characterizing the active species of P450 enzymes, studies in the field moved to biomimetic model complexes and mononuclear nonheme iron enzymes instead. Over the past ten years the field of nonheme iron chemistry has blossomed, especially after the successful spectroscopic characterization of several iron(IV)-oxo complexes well before the first spectroscopic characterization of P450 Cpd I. Computational studies also investigated nonheme iron enzymes and synthetic analogues in detail and explained their reactivity patterns and predicted its chemical properties. Later we will give an overview of key advances in the field obtained from computational modelling. Before discussing the results of

our calculations, let me give a brief overview of heme and nonheme enzymes, their function and properties.

2. Biological nonheme and heme based iron(IV)-oxo intermediates.

Oxygen binding enzymes, generally, come in two varieties, namely with either a heme or a non-heme ligand system. Although in some enzymatic systems, such as methane monoxygenases,[17] a dimetal core is involved in the catalytic reaction mechanism, we will focus here on mononuclear iron systems only. Also oxygenases with other transition metals than iron in the catalytic site will not be covered. In the next sections we will give a brief overview on the mechanism and function of heme and non-heme iron containing mono- and dioxygenases. Subsequently, we will highlight how computational chemistry can assist in gaining understanding in catalytic transformations and the characterization of short-lived intermediates in reaction processes.

2.1 Cytochrome P450s (P450s).

Many heme enzymes utilize molecular oxygen on an iron centre, including monoxygenases, like the P450s,[1–10] but also the catalases and peroxidases.[18–20] The latter detoxify hydrogen peroxide to water, while the catalases convert it to molecular oxygen and water. The first heme enzyme where the complete catalytic cycle was resolved for using crystallographic methods was the one of cytochrome *c* peroxidase (C*c*P) and as a result it has become a template for heme studies in general.[21] However, spectroscopic studies on its Cpd I species as compared to that of other peroxidases and P450s showed that the active species of C*c*P is electronically quite different from the one obtained in other peroxidases, and, therefore, its active species cannot be considered as a model Cpd I species anymore.

The cytochromes P450 are probably, by far, the most extensively studied group of heme enzymes due to their relevance for human health and their potential in biotechnological applications. The name cytochrome P450 comes from the fact that the CO bound ferrous-heme gives a red-shifted strong Soret band through a high-energy π-π^* transition of the porphyrin ring at 450 nm,

due to the strong electron-donating character of the cysteinate axial ligand.[22–24] The P450s catalyze the transfer of one oxygen atom of molecular oxygen to substrates (SubH) concomitant with reduction of the other oxygen atom of O_2 to a water molecule.[1–8] The P450s are widespread in nature and have been found in virtually all forms of life, including bacteria, eukaryotes and fungi.[5,25,26] This is probably due to their versatility and their effectiveness of catalyzing oxidation reactions. They have been linked with the biosynthesis of antibiotics in prokaryotes as well as hormones in eukaryotes. In the human liver the P450s are involved with the metabolism and biodegradation of drugs and xenobiotics.[27] Since the P450s are highly versatile and able to hydroxylate substrates regio- as well as stereospecifically they are of big interest to the biotechnology industry. To gain insight into the fundamental building blocks of the P450s bioinorganic chemists have created biomimetic models of the P450 active site.[12,28–30] Subsequent computational studies have given further insight into the fundamental nature of the heme active site.[8,16,31–33]

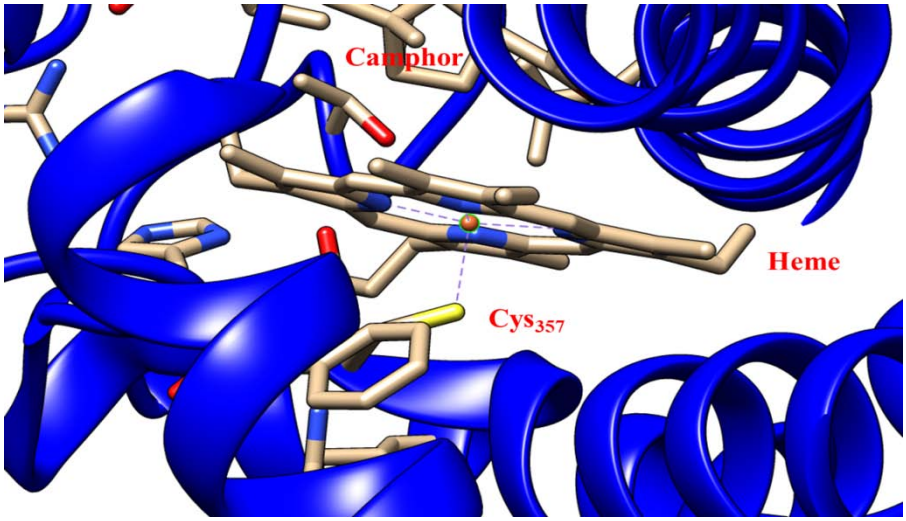

Figure 2: Extract of the crystal structure of substrate bound P450cam as taken from the 1DZ9 pdb file.

Poulos and co-workers were the first to determine an X-ray crystal structure of a P450 isozyme, namely the soluble bacterial $P450_{cam}$ isolated from the bacterium *Pseudomonas putida*,[34] which triggered a range of studies in the field and currently hundreds of P450 crystal structure coordinates are available

from the protein databank.[35] The P450 isozymes show considerable homology and all contain a central heme group, where the catalysis takes place. P450 enzymes contain a single polypeptide chain containing a heme *b* group (iron protoporphyrin IX) linked to a cysteine (Cys) amino acid via the axial ligand of the metal.[9] Figure 2 shows a snapshot of the active site of a typical P450 isozyme, namely $P450_{cam}$, as taken from the 1DZ9 protein databank (pdb) structure.[36] $P450_{cam}$ is a bacterial P450 that catalyses the regioselective hydroxylation of camphor at the C^5 position. It is one of the most extensively studied P450s and generally serves as a template for P450 chemistry.[37,38] The heme *b* group of $P450_{cam}$ is bound to the protein via a thiolate bond of Cys_{357} with the metal and is located deep inside the hydrophobic interior of the enzyme. This is important to accommodate hydrophobic substrates. Note that the axial cysteinate amino acid accepts hydrogen bonds from several neighbouring amino acids, including amide protons of three amino acids including Leu_{358} and Gly_{359}.[39] These hydrogen bonding interactions are believed to fine-tune the catalytic activity of the enzyme and affect the ionization potentials of several intermediates in the catalytic cycle.[40–45] Often the substrates of P450 isozymes bind in a very tight binding pocket where they are locked in position through electrostatic and hydrogen bonding interactions.[35]

The catalytic cycle of the P450s has been extensively studied but only recently the final evidence has been delivered for its mechanism. Thanks to efforts in the fields of enzymology, biomimetic chemistry and computational chemistry over the past four decades, a clear picture on the catalytic activity of P450 enzymes has emerged (Figure 3).[1–10,13,16] Computational modelling provided important insights into the molecular structures, spin states, and chemical and physical properties intermediates and reaction mechanisms.[4,8,16,31–33] Currently many excellent and detailed reviews are available on the catalytic cycle of P450 enzymes and the nature of the individual intermediates during the reaction process.[1–13,16]

The substrate-free resting state (**A**) is the starting (and end) point of the catalytic cycle and contains a six-coordinate low-spin iron(III) state with bound water molecule in the distal ligand position. This is the displaceable

ligand and upon substrate binding into the binding pocket the water molecule is removed as a result of a low-spin to high-spin state transition.[46]

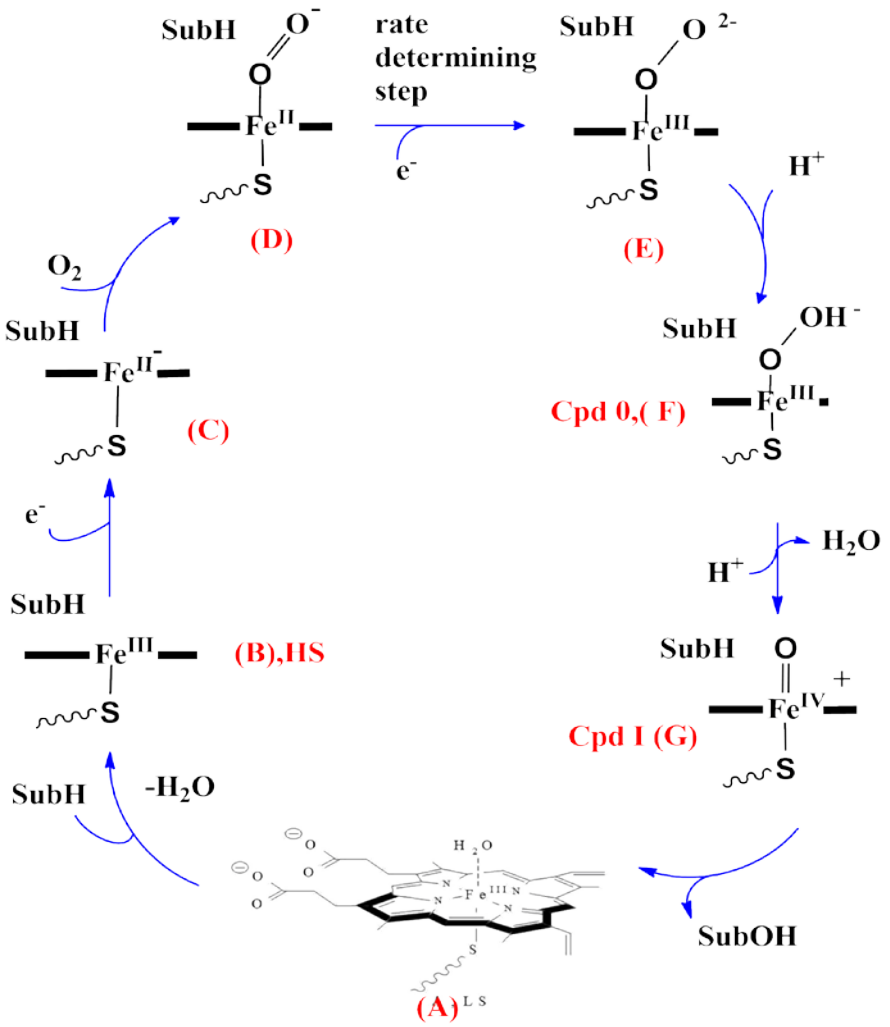

Figure 3: Catalytic cycle of P450 enzymes. SubH is the substrate.

Computational studies indeed confirmed a difference in spin-state ordering for **A** and **B** resulting in a favourable pentacoordinated complex in the high-spin state.[47–51] The spin-state change triggers an electron transfer process from the reductase domain to the heme and reduces the ferric complex **B** to a ferrous complex, **C**.[46] Subsequently, molecular oxygen binds to the ferrous heme to form a ferric-superoxo heme complex (Fe^{III}-O_2^{-}), **D**. The next step in the catalytic cycle is considered the rate-determining step and leads to a second electron transfer from the reductase domain to the heme,[52] to give the ferric-peroxo species (Fe^{III}-O_2^{2-}), **E**. This intermediate picks up a proton from a nearby carboxylic acid group and forms the ferric-hydroperoxo complex, **F**,

that is also known as Compound 0 (Cpd 0). Radiolytic cryoreduction of the ferric-superoxo of cytochrome $P450_{cam}$, **D**, with gradual temperature annealing produced the ferric-peroxo and ferric-hydroperoxo intermediates that were characterized by Electron Paramagnetic Resonance (EPR), Electron-Nuclear Double Resonance (ENDOR), and Ultraviolet-visible (UV-vis) spectroscopies.[36,53–55] A final proton transfer to the ferric-hydroperoxo species, **F**, results in heterolytic O–O bond cleavage to give the iron(IV)-oxo porphyrin π-cation radical intermediate or Cpd I (**G**) and a water molecule. Cpd I has recently been detected and characterized by UV-Visible, resonance Raman and Mössbauer spectroscopy and shown to react with substrates via hydrogen atom abstraction with a large kinetic isotope effect.[15] The spectroscopic properties of Compound I show similarities to the ones observed for the iron(IV)-oxo heme cation radical intermediates of chloroperoxidase (CPO) and horseradish peroxidase (HRP).[41,56] The final step in the catalytic cycle of P450 involves the transfer of the oxygen atom of **G** to the substrate (SubH) to give the alcohol products. This process returns the enzyme back to the resting state.

Due to the short lifetime of several intermediates in the catalytic cycle of P450, however, for a long time, alternative mechanisms have been proposed. One of these suggestions implicated activity of Cpd 0 in substrate epoxidation and sulphoxidation reactions.[57–59] Thus, site-directed mutagenesis studies on $P450_{cam}$ that supposedly blocked the second protonation step in the catalytic cycle and hence terminated the catalytic cycle at Cpd 0 still gave significant activity of the enzyme,[60] which was interpreted as the participation of Cpd 0 as a second electrophilic oxidant in substrate monoxygenation reactions, including olefin epoxidation and sulphoxidation. These mutants gave significant amounts of products originating from olefin epoxidation and sulphoxidation reactions but not from aliphatic hydroxylation reactions.[57–60] Further studies were done using so-called radical-clock substrates that distinguish between a radical and cationic reaction pathways,[61] and implicated ultrashort lifetimes indicative of two active oxidants in the reaction mechanism and hence assigned Cpd I and Cpd 0 as competitive oxidants.[60,62] Site-directed mutants were made where the proton-transfer processes in the catalytic cycle were affected through replacements of key amino acids in $P450_{cam}$ such as the

alcohol side-chain of Thr_{252} and the carboxylic acid group of Asp_{251}. The Thr252Ala mutation gave decreased activity of the enzyme with respect to wild-type and gave significant amounts of decoupling products whereby the ferric-hydroperoxo was converted into ferric-hydrogen peroxide instead and no substrate hydroxylation occured.[57] Interestingly, despite decreased activity of the Thr252Ala mutant with respect to aliphatic hydroxylation, by contrast, double bond epoxidation reactions apparently still proceeded. Based on these studies, a two-oxidant scenario was hypothesized[57] whereby Cpd I was assigned as the oxidant for aliphatic hydroxylation reactions, whereas Cpd 0 is responsible for double bond epoxidation.

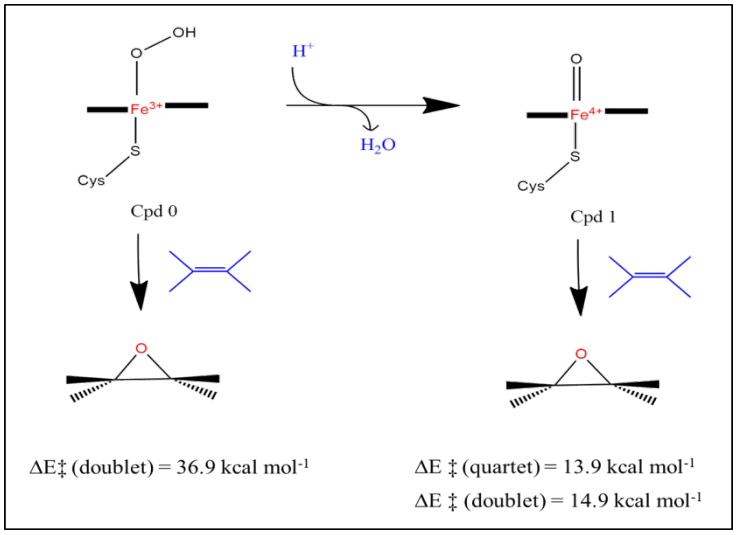

Figure 4: Computational studies of ethene epoxidation by Cpd 0 and Cpd I models of P450 with rate determining barriers in kcal mol–1.

Many computational and biomimetic studies have investigated the two-oxidant hypothesis, but all research showed the iron(III)-hydroperoxo species to be a sluggish oxidant.[63–66] The first evidence against Cpd 0 as an active oxidant came from computational modelling and addressed the relative performance of Cpd I and Cpd 0 in ethene epoxidation.[63] Figure 4 highlights the main results from these studies. Thus, Cpd I reacts with ethene in a stepwise mechanism via a radical intermediate, whereby the initial electrophilic addition is rate determining with a barrier of 13.9 kcal mol^{-1} on the quartet spin state surface and 14.9 kcal mol^{-1} on the doublet spin state surface. By contrast, the epoxidation reaction by Cpd 0 has a much higher reaction barrier of 36.9 kcal

mol^{-1}, and consequently, Cpd 0 is a sluggish oxidant and will not be able to compete with Cpd I.

Further detailed quantum mechanics/molecular mechanics (QM/MM) studies on dimethylsulphide sulphoxidation by Cpd I and Cpd 0 intermediates of P450 confirmed the conclusions of small model complexes and assigned Cpd I as the only viable oxidant in the catalytic cycle.[66] High barriers were found for the reaction mechanism starting from the iron(III)-hydroperoxo species, while much lower barriers for the same reaction by Cpd I were found. The computational studies were supported by biomimetic work on the substrate epoxidation and sulphoxidation reactions by three different nonheme iron(III)-hydroperoxo oxidants, namely $[(N4Py)Fe^{III}(OOH)]^{2+}$, $[(Bn\text{-}tpen)Fe^{III}(OOH)]^{2+}$ and $[(TPA)Fe^{III}(OOH)]^{2+}$ with N4Py = *N*,*N*-bis(2-pyridylmethyl)-*N*-bis(2-pyridyl)-methylamine, Bn-tpen = *N*-benzyl-*N*,*N*′,*N*′-tris(2-pyridylmethyl)ethane-1,2-diamine and TPA = tris(2-pyridylmethyl)amine. The work provided insight into electrophilic and nucleophilic reactivities of nonheme iron(III)-hydroperoxo intermediates.[67] The oxidants were found to be inactive towards thioanisole and cyclohexene, which implies that these intermediates cannot react via sulphoxidation and epoxidation mechanisms in support of the computational studies. The analogous iron(IV)-oxo complexes, by contrast, showed efficient catalysis of olefins and sulphides to their respective oxides and sulphoxides.[67] Similar conclusions were derived from the reaction of a mononuclear nonheme iron(III)-alkylperoxo complex, $[(TPA)Fe^{III}(t\text{-}BuOO)]^{2+}$ (*t*-BuOOH = *t*-butyl hydroperoxide), with substrates, where little reactivity was observed. This is further confirmation that iron(III)-alkylperoxo porphyrin intermediates are sluggish oxidants and that the iron(IV)-oxo intermediate is formed through O–O bond homolysis.[68,69]

Woggon, van Eldik, and their co-workers recently came with spectroscopic evidence for the formation of an iron(IV)-oxo porphyrin cation radical intermediate and its involvement in oxygen atom transfer processes to substrates.[70] Subsequently, they measured rate constants for the formation and decay of intermediates formed in the catalytic reaction of the iron porphyrin complex and *m*-CPBA (*m*-chloroperbenzoic acid) as well as oxygen atom transfer rate constants using low-temperature rapid-scan stopped-flow techniques. Nam and co-workers compared the reactivity of a high-valent

iron(IV)-oxo porphyrin cation radical with an iron(III)-alkylperoxo complex and found evidence that the former is an active oxidant in the catalytic oxygenation of organic substrates, while the latter is a sluggish oxidant.[71]

2.2 Taurine/α-ketoglutarate dioxygenase (TauD).

A large class of mononuclear nonheme iron containing enzymes that utilize molecular oxygen and react as dioxygenases are the α-ketoacid dependent dioxygenases of which α-ketoglutarate dependent dioxygenases (αKDD) are the most extensively studied of those.[8,28–30,72–78] By contrast to the catalytic cycle of the P450s that uses two external electrons and protons, the nonheme iron dioxygenases do neither utilize a cofactor nor a proton source, but instead use a co-substrate (α-ketoglutarate, αKG) to generate an iron(IV)-oxo active species. This intermediate is relatively long-lived and has been characterized by a range of spectroscopic methods, *vide supra*.[77,78] The αKDD are very versatile and catalyze many different reactions in biosystems, ranging from substrate hydroxylation, substrate halogenation and desaturation to ring-closure processes.[28,77–80] As such they catalyze a series of vital processes for human health with examples that include: DNA and RNA base repair in mammals,[81–83] cross-linking processes in collagen,[84] responses to hypoxia,[85] and the biosynthesis of the vancomycin, fosfomycin and carbapenem group of antibiotics in bacteria.[86–88] As both the nonheme iron dioxygenases and the P450 monoxygenases catalyze oxygen atom transfer reactions to substrates and specifically aliphatic hydroxylation reactions, the question remains why nature generated two sets of enzymes with essentially the same function. The detailed computational studies reported here will highlight the differences and comparisons between the heme and nonheme iron complexes in nature.

The nonheme iron dioxygenases, therefore, are highly versatile but show distinct structural differences between isoforms; however, most of them contain a characteristic iron-coordination site, where the metal is bound to the side chains of two histidine and one carboxylic acid (Asp/Glu) residue into a facial 2-His/1-Asp ligand system.[89,90] This motif has been identified in large numbers of nonheme iron dioxygenases, including clavaminic acid synthase,[91] AlkB repair enzymes,[92,93] and prolyl-4-hydroxylase.[94–106] The first nonheme iron enzyme of which the iron(IV)-oxo species was spectroscopically

characterized, and consequently the most extensively studied one, was taurine/α-ketoglutarate dioxygenase (TauD), and, hence, we will describe details of its spectroscopic characterization and reactivity in hydrogen atom abstraction reactions. To highlight the versatility of nonheme iron enzymes, we describe spectroscopic and reactivity studies on an alternative nonheme iron enzyme (cysteine dioxygenase, CDO) with a 3-His ligand system (Figure 5) that catalyzes the sulphoxidation reaction of a substrate. These two case studies highlight the effect of axial and equatorial ligands on the ground state properties of mononuclear nonheme iron(IV)-oxo intermediates and their reactivity patterns.

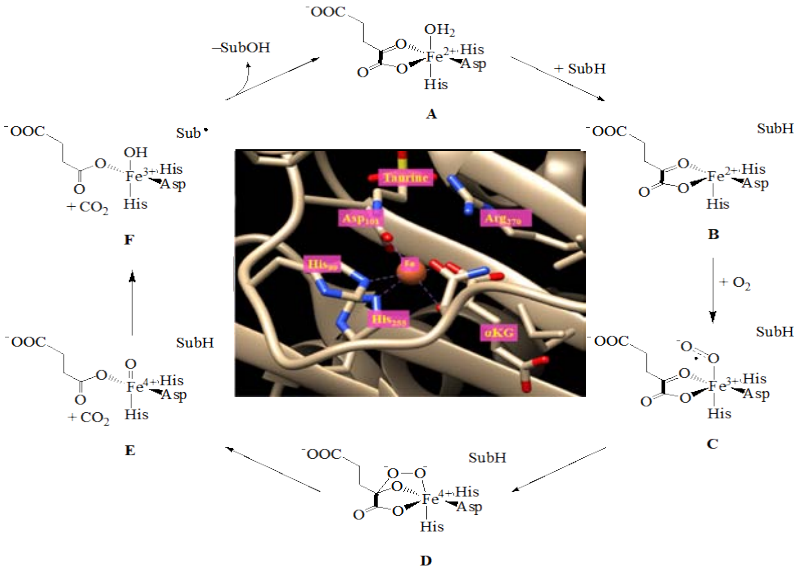

Figure 5: Catalytic cycle of TauD. The central structure is an extract of the 1OS7 pdb structure with key residues highlighted. SubH is substrate

2.3 Cysteine Dioxygenase (CDO).

Another nonheme iron enzyme that utilizes an iron(IV)-oxo species in its catalytic cycle is cysteine dioxygenase (CDO), which catalyzes the conversion of L-cysteine into L-cysteine sulphinic acid products. CDO is a vital enzyme for human health involved in the biodegradation and metabolism of toxic cysteine.[107,108] High concentrations of cysteine in the body are toxic and it precipitates into cystine stones.[109] Moreover, elevated levels of cysteine in the body have been correlated with neurological diseases such as Alzheimer's and

Parkinson's diseases.[110] The metabolism of cysteine is accomplished by a series of enzymes and the first one of these is CDO. Because of its importance in human physiology, the reaction has attracted a lot of scientific attention and is well studied.

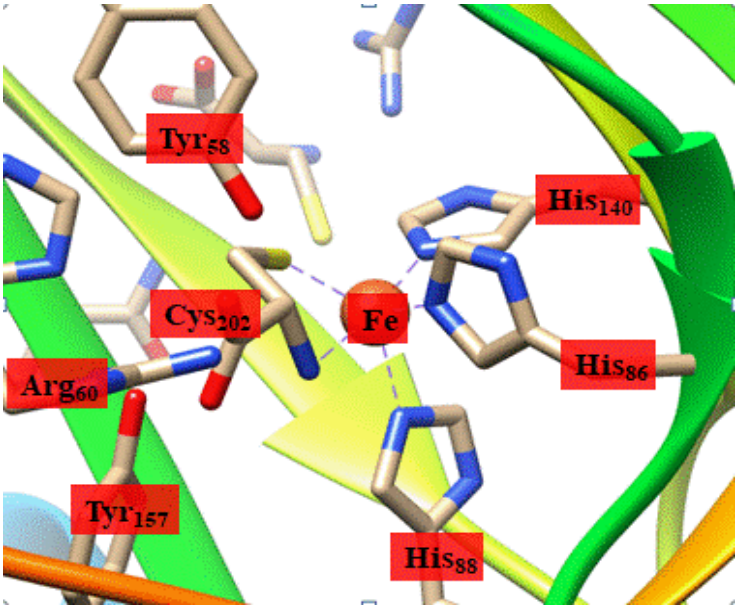

Figure 6: Active site structure of substrate bound CDO as taken from the 2IC1 pdb file with amino acids labelled as in the pdb file

By contrast to the chemical structure of TauD, the catalytic metal ion in CDO is bound into a 3-His ligand structure rather than the typical 2-His/1-Asp facial triad. Figure 6 gives an extract of the crystal structure of CDO enzymes as taken from the 2IC1 pdb file.[111] The metal is bound to the protein backbone via three histidine linkages of the side chains of His_{86}, His_{88} and His_{140}, whereas cysteine binds as a bidentate ligand to the metal with the thiolate group *trans* to His_{88} and the amino group *trans* to His_{140}. The carboxylic acid group of cysteine forms hydrogen bonding interactions with several residues in the binding pocket, including a salt bridge with Arg_{60}, as well as hydrogen bonding interactions with the imidazole side chain of His_{155} and the phenol groups of Tyr_{157} and Tyr_{58}. Because of this, the substrate binding pocket is tight and consequently CDO enzymes are highly substrate specific and will not even catalyze the reaction for structurally similar inhibitors.[112] The last ligand

position of iron is empty in the pdb file but it is the place where molecular oxygen will bind. EPR studies on NO bound CDO provided compelling evidence that substrate binds prior to molecular oxygen to the metal centre.[113] Moreover, experiments with $^{18}O_2$ showed that both oxygen atoms of O_2 are incorporated into cysteine sulphinic acid products.[114]

Another interesting and unusual feature of the enzyme active site is the Tyr_{157}–Cys_{93} crosslink. Currently, it is not clear what its function is, but it was shown to be correlated to substrate binding and catalytic turn-over.[115,116] It may, therefore, affect the active site geometry through structural changes, although recent Mössbauer spectroscopic studies revealed little effect on iron binding.[117] So far few experimental studies managed to stabilize and characterize catalytic cycle intermediates obtained after dioxygen binding, therefore, to gain insight into the dioxygenation reaction of CDO a string of high-level computational studies were performed.[118–120] The only two experimental reports on dioxygen bound intermediates refer to a crystal structure of an iron(III)-persulphenate and the spectroscopic characterization of an iron(III)-superoxo complex.[121,122] QM/MM calculations on the iron(III)-persulphenate structure,[120] however, found no evidence of its involvement of the catalytic mechanism of CDO, and its energy was found to be well higher than the iron(III)-superoxo structure. Therefore, it is more likely to be a by-product from a side reaction. The iron(III)-superoxo intermediate was synthesized from substrate bound CDO and mixed with superoxide generated from xanthine oxidase.[122] This created a transient species with UV-Vis features at 485 and 565 nm, which decayed very slowly. EPR spectroscopic studies on this transient species gave evidence of the septet spin iron(III)-superoxo intermediate with $S = {}^5/_2$ spin on the metal that is ferromagnetically coupled to an S = ½ superoxo radical.

3. Methods and techniques.

3.1 Density functional theory.

Our group uses well benchmarked and calibrated methods that are based on density functional theory (DFT) calculations as implemented in commercially available computational chemistry software packages, such as *Gaussian*, *Jaguar*, *Turbomole* or *Orca*.[123–126] Thus, these software packages describe the

electronic features of molecules with the Schrödinger equation,[127] Eq 2, that relates the wave function of electrical particles (Ψ) to the total energy of the system (E) by taking all perturbations that influence the wave function into account via the Hamilton operator (H). The Hamilton operator within the Born-Oppenheimer approximation includes the kinetic and potential energy of all the electrons and nuclei within a molecule and contains electron-electron, electron-nucleus and nucleus-nucleus interactions as described in Eq 3.[128–130] The distances between protons and electrons are given as r_{Ii}, while the distances between two electrons and two protons is described by either r_{ij} and R_{IJ}, respectively. The first term in Eq 3 represents the kinetic energy of the electrons, the second term is the electron-nuclei attractions and the third term gives the electron-electron repulsions. The final term in Eq 3 gives the nucleus-nucleus repulsions, which within the Born-Oppenheimer approximation is a constant value, because the electronic energy E is calculated for a rigid molecular geometry. In Eq 3, $\hbar$ is Planck's constant divided by 2π, m_{e} is the electron mass, e is the elementary charge and ε_0 represents the permittivity in vacuum. The Laplacian (∇) is defined in Eq 4 and represents the motion of an electron in three-dimensional space. The complexity of the Hamiltonian obviously is dependent on the number of electrons (N_{e}) and the number of protons (N_{p}) of the chemical system. Consequently, an increase of the chemical system with more atoms, i.e. with increased number of electrons and nuclei, gives enhanced complexity of the solution of the Schrödinger equation. As a result of this, the Schrödinger equation can only be solved exactly for the hydrogen atom and the $H_2^{+\bullet}$ molecule and for larger chemical systems approximations have to be used.

$$H\,\Psi = E\,\Psi \tag{2}$$

$$H = -\frac{\hbar^2}{2m_e}\sum_{i}^{N_e}\nabla_i^2 - \sum_{i}^{N_e}\sum_{I}^{N_p}\frac{Z_I e^2}{4\pi\varepsilon_0 r_{Ii}} + \frac{1}{2}\sum_{i,j}^{N_e}\frac{e^2}{4\pi\varepsilon_0 r_{ij}} + \frac{1}{2}\sum_{I,J}^{N_p}\frac{e^2}{4\pi\varepsilon_0 R_{IJ}} \tag{3}$$

$$\nabla_i^2 = \frac{\partial^2}{\partial x^2} + \frac{\partial^2}{\partial y^2} + \frac{\partial^2}{\partial z^2} \tag{4}$$

In Hartree-Fock theory (HF) the Schrödinger equation is solved numerically by multiplication of Eq 2 with the complex conjugate wave function followed by integration of the equation with respect to each individual spin orbital, Eq 5.

Solving Eq 5 gives the HF energy for a particular structure. In a subsequent step, the wave function coefficients are modified and the HF equations recalculated, which is an iterative process that is repeated until self-consistency is obtained, whereby the energy change from one step to the next stays below a certain cut-off value (the convergence energy). During a geometry optimization, this converged wave function is used as the starting point for a modified geometry based on the first derivatives of the energy to all individual distances and angles. The HF equations are again solved for the new structure until self-consistence and the process is repeated until a stationary structure, or minimum energy conformation, is found. This optimized geometry should be on a local minimum on the potential energy surface with first and second derivatives of the energy to the individual coordinates that are zero.

$$\int \Psi^* H \Psi d\tau = E \int \Psi^* \Psi d\tau \qquad (5)$$

Generally, HF gives reasonable geometries but its energies are not good enough for calculations on reaction mechanisms and barrier heights. For these processes, further improvements to the theory are necessary. One such method in wave function chemistry is the second order perturbation theory, such as Møller-Plesset theory or MP2, which gives much more accurate energies and chemical structures.[131] However, these methods are computationally demanding and even with current resources only accessible to chemical systems with less than 30 atoms.[132] To enable studies of larger chemical systems, including biosystems, the search for computationally cheap methods was started. Firstly, the advances in density functional theory (DFT) supplied an alternative to computationally expensive wave function methods such as MP2. Secondly, the development of quantum mechanics/molecular mechanics (QM/MM) opened up opportunities to study enzymatic systems with high accuracy.

In the 1960s Kohn and co-workers[133,134] showed that replacement of the wave function by a functional of the electron density, $\rho(\mathbf{r})$ with $\mathbf{r}$ the distance between two electrons, is more practical. Thus, in DFT the solution to the electronic energy (E_{el}) follows from the sum of the integrals given in Eq 6. Again, the first term represents the kinetic energy of the electrons, the second term the electron-nucleus attractions and the third integral gives the Coulombic

electron-electron repulsions. In addition, in DFT there is an exchange-correlation term E_{xc} for electron pair interactions with an exchange and a correlation component, E_{x} and E_{c}, respectively. The exchange energy, E_{x}, is dependent on ferromagnetic interactions of two electrons with the same spin (α or β) but in different orbitals. By contrast, the correlation energy, E_{c}, reflects the electron pairing energy of two electrons in the same molecular orbital. Unfortunately, no exact equations are known for the exchange and correlation energies so that they need to be approximated using empirical equations.

$$E_{el} = -\frac{1}{2}\sum_{i}\int \phi_i(\mathbf{r}_1)\nabla^2\phi_i(\mathbf{r}_1)d\mathbf{r}_1 + \sum_{A}\int \frac{Z_A}{|\mathbf{R}_A - \mathbf{r}_1|}\rho(\mathbf{r}_1)d\mathbf{r}_1 + \frac{1}{2}\int \frac{\rho(\mathbf{r}_1)\rho(\mathbf{r}_2)}{|\mathbf{r}_1 - \mathbf{r}_2|}d\mathbf{r}_1 d\mathbf{r}_2 + E_{xc} \tag{6}$$

Commonly used exchange and correlation energy equations are the Slater exchange, Eq 7,[135] and the correlation energy due to Vosco, Wilk and Nusair, Eq 8.[136] The Slater exchange uses the exchange scale factor (α_{ex}) that has a value of $^2/_3$ for an electron gas. The correlation energy is calculated per electron in a gas from the correlation functional $\varepsilon_c\left[\rho_1^\alpha, \rho_1^\beta\right]$ using spin densities ρ_1^α and ρ_1^β. The sole use of E_x^{Slater} and E_c^{VWN} gives the Local Density Approximation (LDA), which although it gives an improvement over Hartree-Fock (HF) wave function methods, it is not good enough to compete with, e.g., MP2 methods. As such, further corrections due to non-local interactions are needed. These are, for instance, implemented into the Lee, Yang and Parr (LYP) or Perdew and Wang (PW95) correlation methods.[137,138]

$$E_x^{Slater} = -\frac{9}{4\alpha_{ex}}\left(\frac{3}{4\pi}\right)^{\frac{1}{3}}\sum_{\gamma}\int\left[\rho_1^\gamma(\mathbf{r}_1)\right]^{\frac{4}{3}}d\mathbf{r}_1 \tag{7}$$

$$E_c^{VWN} = \int \rho_1(\mathbf{r}_1)\varepsilon_c\left[\rho_1^\alpha(\mathbf{r}_1), \rho_1^\beta(\mathbf{r}_1)\right]d\mathbf{r}_1 \tag{8}$$

It took until the 1990s until highly accurate density functional methods were developed that were able to accurately predict molecular properties. Thus, Becke developed a three parameter (*A*, *B*, *C*) hybrid density functional method that includes the exchange and correlation functionals of respectively Slater

and VWN in combination with the HF exchange and two correction factors: one for the correlation due to, e.g., LYP (ΔE_c^{LYP}) and the other for the exchange components (ΔE_x^{Becke}), Eq 9.[139] Becke then optimized the three parameters *A*, *B*, and *C* against experimentally determined electron affinities, ionization potentials and proton affinities for a test-set of molecules. As an example, we give the exchange correlation energy for the commonly used B3LYP hybrid density functional method in Eq 9. Obviously, since the hybrid density functional method contains fit-parameters that were calibrated against experiment, this method cannot be considered as an *ab initio* method. Hybrid density functional methods, however, combine high speed with reasonable accuracy, so that these methods are commonly used in computational chemistry problems for calculations on relatively large chemical systems with excess of 50 atoms. Becke's test-set predicted energies within 2 kcal mol^{-1} from experiment,[139] which is a reasonable accuracy to calculate chemical reactions. The Becke test-set, however, did not include transition metal containing complexes and recent calibration methods showed that for those types of chemical systems it is often better to use a modified hybrid density functional method like B3LYP* that uses less HF exchange, i.e. typically 10 or 15% rather than the standard 20%.[140] In addition, the energetics of these complexes often are overestimated due to lack of dispersion in the calculations. Grimme and co-workers developed a dispersion correction expression that gives improved energies, which we label as B3LYP-D.[141] Nevertheless, regardless on the DFT method chosen, the calculated result should be similar. Although often calculations show little sensitivity to the methodology, in transition metal complexes with close-lying spin states the ordering and spin-state energy splitting are occasionally dependent on the chosen method. It is of paramount importance, therefore, to calibrate DFT calculations on transition metal complexes to either experimental data or to do test calculations with alternative methods. In most projects described in this work that was done and examples of these benchmark results will be given later.

$$E_{xc}^{B3LYP} = AE_x^{Slater} + (1-A)E_x^{HF} + B\Delta E_x^{Becke} + E_c^{VWN} + C\Delta E_c^{LYP} \qquad (9)$$

3.2 Basis sets.

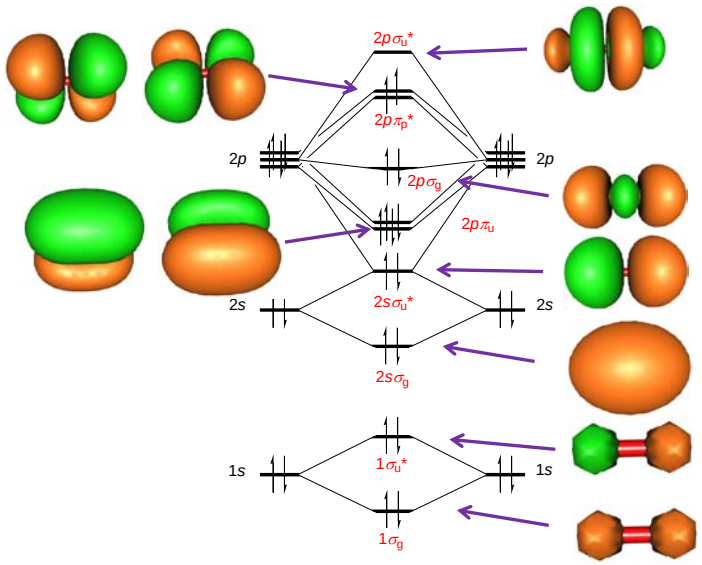

Figure 7: Molecular orbitals of O_2 in the triplet spin state as calculated with MP2/6-31G*.

In order to solve the Schrödinger equation one optimizes the wave function and using the perturbations from the Hamilton operator find the eigenvalues or energies associated with the equation. The wave function of molecules is not as straightforward as that of atoms, where distinct orbital levels can be identified, i.e. 1*s*, 2s, 2*p* etc. To overcome this problem, the molecular wave function, and consequently molecular orbitals, are usually described as a mathematical sum of atomic orbital components through the Linear Combination of Atomic Orbitals (LCAO) approach.[142] This approach takes all occupied and a selection of virtual atomic orbitals (χ) of all atoms in the molecule and creates a set of molecular orbitals (φ_i) through fractions (c_{ri}) of all atomic orbital components, Eq 10. The quality of these molecular orbitals obviously is dependent on the number of active orbitals taken into consideration and in particular the number of virtual orbitals included. Especially for wave function calculations large numbers of virtual orbitals are needed in the calculations as the energy tends to converge to the basis set limit. Since, the coefficients of hybrid density functional theory were benchmarked against experimental data using calculations using a double-ζ quality basis set,

this type of basis set is generally sufficient in DFT calculations for geometry optimizations.

$$\varphi_i = \sum_r c_{ri} \chi_r \qquad (10)$$

As an example of the mixing of atomic orbital components into molecular orbitals, we give in Figure 7 the orbital splitting for molecular oxygen. Thus, the left and right-hand-side levels represent the two individual oxygen atoms with $1s^2\ 2s^2\ 2p^4$ orbital occupation. The atomic orbitals on the two centres mix and form the set of molecular (O_2) orbitals depicted in the middle of Figure 7. The two 1*s* orbitals of the two oxygen atoms mix to form a bonding ($1\sigma_g$) and an anti-bonding ($1\sigma_u$*) pair of molecular orbitals, and the same happens between the atomic 2*s* pair of orbitals to generate the $2s\sigma_g$ and $2s\sigma_u$* set of molecular orbitals. In contrast to the 1σ orbitals the $2s\sigma$ molecular orbitals contain a certain degree of 2*p* character as well, and, therefore, have shapes that differ from the atomic orbitals. This is even more so for the valence orbitals ($2p\sigma$ and $2p\pi$), where several high lying (virtual) atomic orbitals are mixed in. Consequently, the calculated energy from the Schrödinger equation is dependent on the choice of basis set and the number of basis functions used. This is particularly important in wave function methods, such as MP2, where relatively large basis sets are required.

Due to the large number of electrons in transition metal elements there are special basis sets available that include an effective core potential (ECP).[143] Essentially, the core electrons, i.e. 1*s*, 2*s* and 2*p* electrons in Fe, are hardly affected by chemical bonding and, therefore, do not change much with respect to atomic orbitals. These orbitals in the ECP treatment are replaced by an electrical potential in the Hamiltonian. Often the ECP component contains relativistic corrections to the energy and improves the calculated energies. For iron, typical ECP containing basis sets are from the Los Alamos type, e.g. LACVP or LANL2DZ.[144] Generally, in our work we calculated energies using a triple ζ-type basis set (LACV3P+) that includes diffuse and polarization functions on the metal. Test calculations for a substrate hydroxylation potential energy profile by a Cpd I model using two different basis sets, namely BS1 (LACVP on iron and 6-31G on the rest of the atoms) and BS2 (LACV3P+ on

iron and 6-311+G* on the rest of the atoms), showed very little changes in optimized geometries and virtually identical relative energies along a reaction profile.[145] As such, usually geometries are optimized using a double-ζ basis set and the calculation is followed by a single point energy calculations with a triple-ζ basis set.

3.3 Zero point energy (ZPE).

Calculations of potential energy profiles and reaction mechanisms, as we have seen, start off from the Schrödinger equation with a choice of method and basis set. The eigenvalues obtained through this, however, are electronic energies, which are devoid of vibrational and entropical contributions.

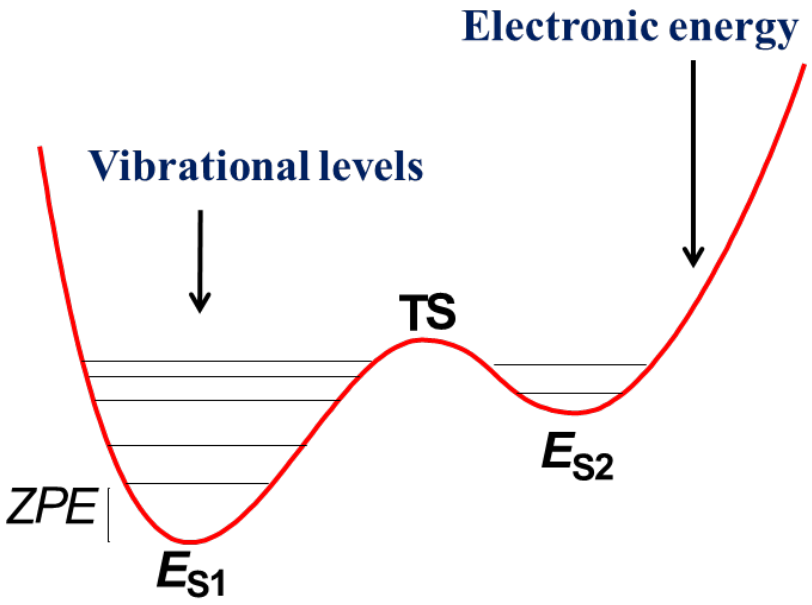

Figure 8: Potential energy profile from reactant state S1 to a product state S2 via a transition state TS. Highlighted are the electronic and ZPE contributions to the total energy.

In order to obtain these corrections to the electronic energy, a frequency calculation is performed that calculates the first and second derivatives of the energy with respect to the distances and angles between the atoms. From these derivatives the vibrational energy levels of a molecule are calculated. Thus, at 0 K temperature, the molecule resides in the lowest vibrational level above the

electronic energy of the local minimum as explained in Figure 8. This Figure gives the hypothetical potential energy profile of a molecule that can exist in two stable conformations, S1 and S2, for which local minima are calculated with energy E_{S1} and E_{S2}, respectively. The zero point energy (*ZPE*) is the lowest vibrational energy level above these electronic energies and hence E_{S1} + *ZPE* is the ground state energy for conformation S1. Calculations on a potential energy profile are given as ΔE + *ZPE* relative to a starting structure.

3.4 Solvent effects.

Calculated energies using computational chemistry methods refer to gas-phase data, whether they use ZPE corrections or not. In order to compare computational results to experiment, the solvent needs to be mimicked in into the calculations. This can be done by simply adding solvent molecules to the chemical model and reoptimizing the structures. However, calculations with large number of atoms require more resources and are not always practical, especially since solvent molecules can exist in several conformations.[146] Instead of addition of solvent molecules to the chemical structure, a more common approach is to add solvent corrections to the energetics using an implicit solvent model. This can either be done at single point level, whereby the energy is recalculated with a solvent model on the gas-phase optimized geometry, or by reoptimizing the structure using a solvent model.

Software packages, such as *Gaussian* and *Jaguar*, include solvent models like the Polarizable Continuum Model (PCM).[147] In PCM calculations the solvent is described as a perturbation of the molecule with a dielectric constant and the molecule is placed in a cavity that is surrounded by the dielectric continuum. The cavity is described as the area around the molecule that contains less than pre-defined amount of electron density of the molecule and is often based on van der Waals radii of atoms. The classical Poisson equations are then used to calculate the electronic potential arising from the molecule-solvent interactions using a defined dielectric constant.

3.5 Quantum mechanics/molecular mechanics (QM/MM).

Another approach to mimic perturbations of a surrounding into the energies of molecules is to use the quantum mechanics/molecular mechanics (QM/MM) approach. In QM/MM the chemical system, such as an enzyme, is divided into two or more regions (shells): the inner core that is calculated with accurate methods and the outer region, which contains the protein and solvent is calculated with computationally cheap methods, like molecular mechanics (MM).[148] The inner core is our region of interest and contains the basic features of the enzyme active site and the substrate, but is held in position by interactions with the rest of the protein. These chemical constraints fix the active site and substrate into a specific conformation that affect their interactions and reactivities. However, those chemical groups that do not contribute to the reaction mechanism and, therefore, are not essential for the quantum mechanical description of the system are not necessary in the QM region and are calculated with an MM force field.

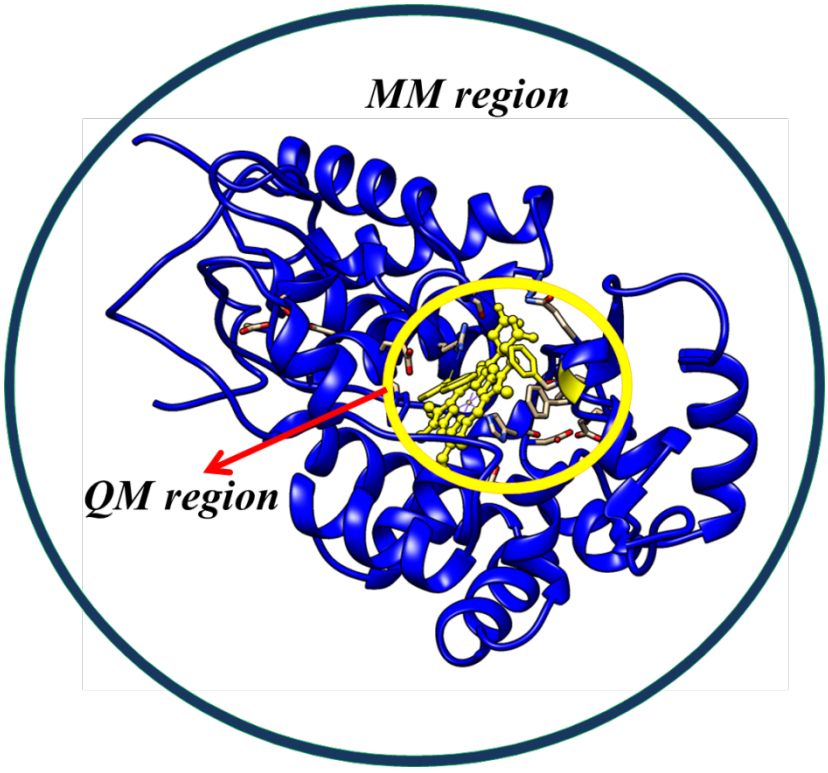

Figure 9: Description of an enzyme via QM/MM and the division of the system into a QM and an MM region.

The division of the system between QM and MM regions is not necessarily straightforward, since it may cut through bonds, and as such there are several methods to describe the interface between the QM and MM region. We use the link-atom approach whereby the region between the QM and MM areas is described with hydrogen link atoms using the charge shift model.[149]

The QM/MM methodology starts off from experimentally determined crystal structure coordinates, i.e. a protein data bank (pdb) file. Many pdb files of proteins are available from the protein databank on the internet.[35] Often these pdb files refer to a resting state structure of the enzyme rather than its catalytically active species. This, therefore, requires some modifications to the starting structure pdb and conversion of it into a later structure in the catalytic cycle. In addition, the pdb files tend not to contain hydrogen atoms, so that they need to be added as well as a solvent layer/box. Generally, this is done in the preliminary set up where the user carefully checks protonation states of residues, salt and disulphide bridges and ions. The pdbtopqr program was used to assign protonation states at pH = 7, whereas all individual histidine residues are manually checked for protonation state. Histidine groups in proteins can exist in one of three protonation states: deprotonated, singly protonated or doubly protonated. All His residues in the structure are manually and visually investigated for likely hydrogen bonding donor and acceptor groups and their protonation states assigned. Counterions are added to the surface to balance the overall charge of the system to neutral. After this initial set up the system is equilibrated and heated to room temperature in a stepwise protocol. First only hydrogen atoms are allowed to change position, but in a later stage also the backbone atoms are free to relax in the geometry optimization. The final molecular dynamics simulation creates a series of low energy snapshots that are used as starting points for the actual QM/MM calculations. There are several force fields available for these MD simulations, such as a universal force field (UFF),[150] Amber,[151] Charmm,[152] etc.

In our calculations we describe the QM region with a DFT method, such as B3LYP, in combination with one of the common basis sets mentioned above, e.g. LANL2DZ+ECP and 6-31G*. Since, the speed of the calculations is dependent on the number of atoms in the QM region, we test several sizes of QM region for consistency. Geometries refer to optimizations of all degrees of

freedom in the QM and MM regions unless otherwise noted. Frequencies are done on the geometry for the QM region only.

4. Results and Discussion.

Our studies use a combination of chemical techniques and are focused on gaining fundamental chemical insight into short-lived intermediates in enzymatic systems. In particular, the work describes the activity of enzymes vital for human health including the heme-based P450s and the nonheme iron dioxygenases. Both systems utilize molecular oxygen on an iron centre, but catalyze different reactions. Their reactivity patterns are still poorly understood, and hence these enzymes are under-used in commercial biotechnological applications. Moreover, due to the transient nature of several key intermediates in the reaction processes and the complications due to multiple possible spin state electromers it is difficult to study these chemical systems with experimental methods. Theoretical modelling assist here and guides experimental work in the field.

4.1 Cytochrome P450s (P450s).

Over the years our group has extensively studied the catalytic mechanism and chemical properties of P450 enzymes. Early studies focussed on establishing the catalytic mechanisms and rate determining steps of aliphatic hydroxylation,[153–155] olefin epoxidation,[154,156,157] sulphoxidation of dialkylsulphides,[65] and the aromatic hydroxylation of arenes by P450 Cpd I.[158] We will not discuss these studies in detail here, as they have been extensively reviewed,[8,13,16,32,33] but will describe more recent work where we have generalized the rate constants of the reaction processes using thermodynamic and valence bond (VB) models and the effect of ligands on the reaction mechanism. Those studies have predictive value and enable one to determine regioselectivities and activities of metal-oxo species. Before discussing the predictive studies, however, let me briefly summarize the key properties of the active species of P450, namely Cpd I.

4.1.1 Compound I of P450.

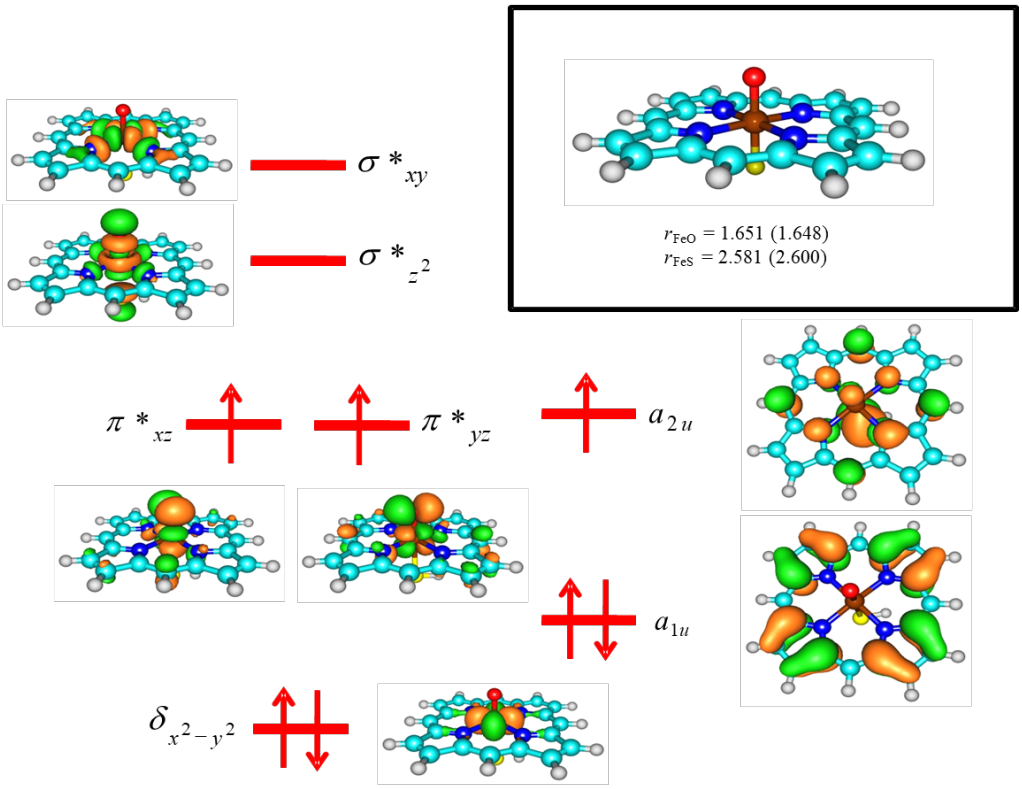

Figure 10: High-lying occupied and low-lying virtual orbitals of 4Cpd I. The inset gives the optimized geometry of 4,2Cpd I with bond lengths in angstroms.

As described above, the active species of the P450s is an iron(IV)-oxo heme cation radical species that is also known as Compound I (Cpd I). Cpd I has a characteristic electronic configuration with three unpaired electrons: two are in orthogonal π^*_{FeO} orbitals (labelled as π^*_{xz} and π^*_{yz}) while the third is in a heme-type π^* orbital with a_{2u} symmetry.[159,160] The latter orbital is known to mix with the axial ligand π-orbitals, and hence, its energy level is influenced by electron donating ligands.[161] In particular, a thiolate ligand of a cysteinate group gives strong mixing of the $3p_S$ orbital with the a_{2u} orbital that raises it in energy. This mixing was also shown to be dependent on environmental effects including donating hydrogen bonds toward thiolate.[161,162] The calculated geometry of Cpd I is shown in Figure 10 together with the key orbitals involved in the oxygen atom transfer reaction to substrates. Five of these orbitals originate from the metal 3*d* orbitals and the other two are π^*-type

porphyrin orbitals with a_{1u} and a_{2u} symmetry. Four electrons occupy the metal 3*d* set of orbitals: two reside into the nonbonding $\delta_x 2_{-y} 2$ orbital in the plane of the heme and two others are in a pair of almost degenerate π^*_{xz} and π^*_{yz} orbitals for the interactions of the $3d_{xz}/3d_{yz}$ iron orbitals with $2p_x/2p_y$ orbitals on oxygen. In a bare porphyrin ring ($PorH_2$) without the central metal ion, the a_{1u} and a_{2u} orbitals are degenerate,[163] but interactions of the a_{2u} with the axial thiolate ligand, raise it in energy. The overall electron configuration of Cpd I is $\delta_x 2_{-y} 2^2\ \pi^*_{xz}{}^1\ \pi^*_{yz}{}^1\ a_{1u}{}^2\ a_{2u}{}^1$ with a total of three unpaired electrons. Since, the interactions between the π^*_{xz}/π^*_{yz} and a_{2u} orbitals is small, the three unpaired electrons either couple to an overall doublet spin state ($\pi^*_{xz}{}^{\uparrow}\ \pi^*_{yz}{}^{\uparrow}\ a_{2u}{}^{\downarrow}$) or a quartet spin state ($\pi^*_{xz}{}^{\uparrow}\ \pi^*_{yz}{}^{\uparrow}\ a_{2u}{}^{\uparrow}$) that are very close in energy.[163] As a result Cpd I reacts with substrates via two-state-reactivity patterns on competing doublet and quartet spin state surfaces.[16,164] In the past we found examples, such as for substrate hydroxylation by *trans*-methylphenylcyclopropane, where the doublet spin mechanism is different from the one on the quartet spin state and consequently the two spin state surfaces give different reaction products.[165] Furthermore, two-state-reactivity was shown to affect and disturb kinetic isotope effects.

4.1.2 Chemical properties of Cpd I of peroxidases and catalases.

Most peroxidases in contrast to the P450s are heme enzymes that contain a histidine group in the axial position rather than a cysteinate residue, yet a tyrosinate group occupies that position in catalases. This, for a long time, was considered as the key chemical reason for the differences in biological function of these three classes of heme enzymes.[18,166,167] The biological function of peroxidases is to detoxify hydrogen peroxide to two water molecules, while catalases convert it to molecular oxygen and water. It has been proposed that a cysteinate axial ligand induces a “push”-effect of electron density toward the heme, whereas a histidine ligand withdraws electron density.[168,169] To understand the electron withdrawing/electron donating properties of the axial ligand and the effect this has on the catalysis of a substrate, we performed a series of DFT calculations on models of Cpd I of P450, horseradish peroxidase (HRP), cytochrome *c* peroxidase (C*c*P) and catalase (Cat).[163,170–172] Figure 11

displays optimized geometries of ^{4,2}Cpd I models of P450, HRP, C*c*P and Cat with relevant group spin densities (ρ) highlighted.

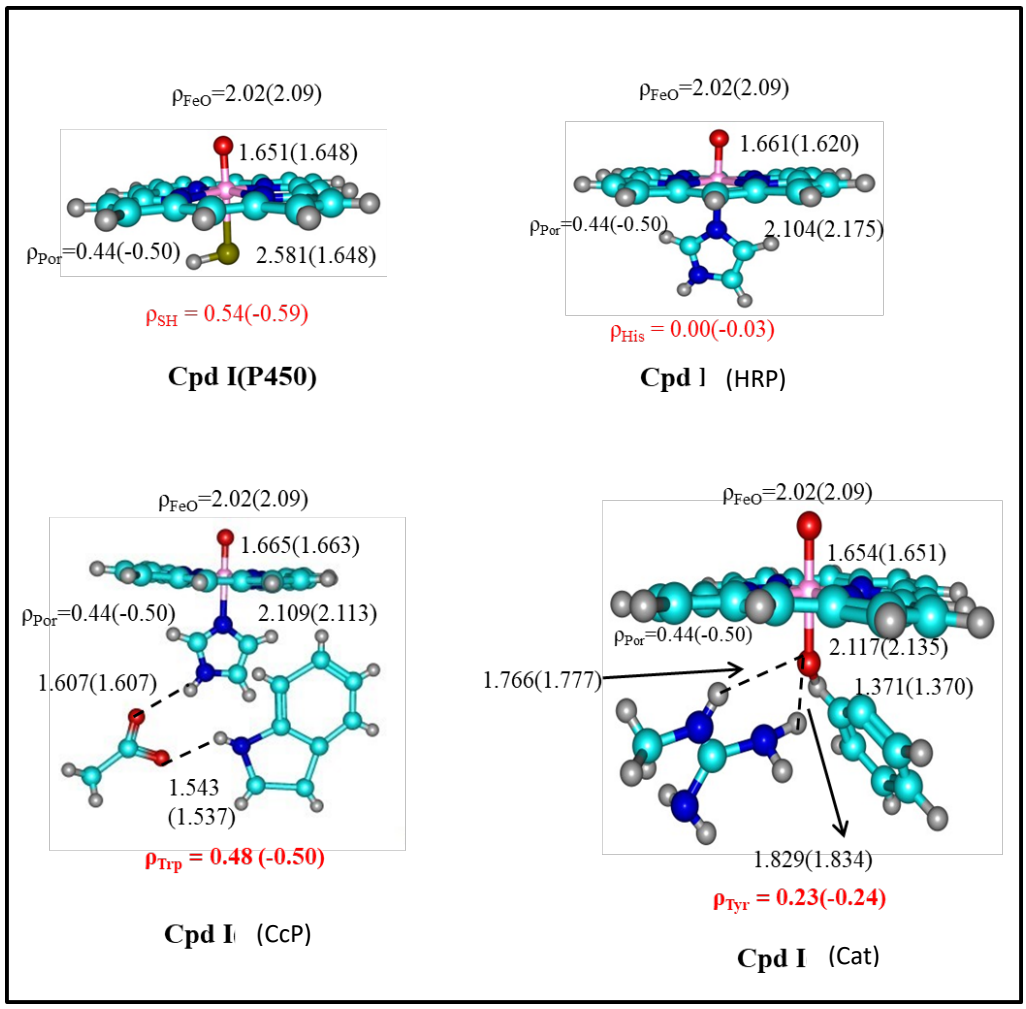

Figure 11: Optimized geometries of ^{4,2}Cpd I models of P450, HRP, CcP and Cat with bond lengths in angstroms and group spin densities (□) in atomic units. Data for the low-spin states are in parenthesis.

Geometrically, little variation is found in the iron(IV)-oxo distance in all Cpd I structures and generally the distance is about 1.66 Å in histidine ligated Cpd I, whereas it is slightly shorter in Cpd I systems with an anionic axial ligand. The group spin densities give a value of about 2 on the FeO group, which reflects single occupation of the π^*_{xz} and π^*_{yz} orbitals. In P450 Cpd I, the third electron is based in a mixed heme and axial ligand orbital as highlighted in Figure 12(*a*). Thus, the a_{2u} orbital mixes with a lone pair orbital (π_L, L = S) on the axial ligand along the O–Fe–S axis and splits into bonding and anti-bonding combination of orbitals ($a_{2u} + \pi_L$) and ($a_{2u} - \pi_L$). The former orbital is doubly occupied, whereas the anti-bonding orbital is destabilized in energy

and singly occupied. Since, this is the highest occupied molecular orbital (HOMO), the electron affinity of Cpd I(P450) is significantly reduced with respect to that of Cpd I(HRP), where this mixing does not occur.

The DFT model calculations on C*c*P Cpd I identify the electronic structure as a mixed state with partial unpaired spin density on the heme, in the a_{2u} orbital and partial single occupation of a tryptophan π-orbital, i.e. $\pi^*_{xz}{}^1\ \pi^*_{yz}{}^1\ a_{2u}{}^1\ \pi_{Trp}{}^2 \leftrightarrow \pi^*_{xz}{}^1\ \pi^*_{yz}{}^1\ a_{2u}{}^2\ \pi_{Trp}{}^1$.[170] In the gas-phase as well as in a solvent mimicked calculation, the energy differences between the two states are very small and hence a mixed state is found. To find out, whether environmental effects can change the ordering of these two states we added a point charge at a distance to our chemical system. Thus, a structurally close enzyme to C*c*P is ascorbate peroxidase (APX), which has a very similar heme active site that also contains a His-Asp-Trp triad, and the only difference in the structure appears to be a K^+ binding site at about 8 Å from the heme.[173] Experimental EPR studies on APX Cpd I, in contrast to those on Cpd I of C*c*P, identified the electronic state as a porphyrin radical rather than a Trp radical.

4.1.3 Aliphatic hydroxylation by P450 Cpd I.

Aliphatic hydroxylation is one of the most common chemical reactions catalyzed by the P450s as a means of detoxification of drugs and xenobiotics in the liver. As a result the P450s are well studied enzymes by the pharmacological industry.[174] Other P450 isozymes, such as the $P450_{BM3}$ isozymes, hydroxylate long-chain fatty acids stereospecifically and regioselectively.[175] Aliphatic C–H hydroxylation is a challenging reaction process, due to the fact that a strong C–H bond needs to be broken, Eq 11. Moreover, often the reaction takes place in a regioselective or stereospecific manner. As it is an important reaction in catalysis many studies have been performed to understand the catalytic mechanism, the origins of the regio- and stereoselectivity of the reaction, the nature of the by-products and predictions of chemical reactivity. However, as Cpd I is short-lived, experimental studies encounter difficulties. Computational modelling, therefore, can assist here and give insight into fast reaction processes of short-lived chemical intermediates.

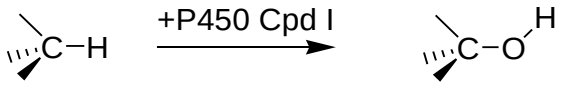

(11)

Technically, the aliphatic hydroxylation by Cpd I can start with a hydrogen atom abstraction, a proton abstraction or a hydride transfer from the substrate. We will start, however, with the most common reaction process that starts with a hydrogen atom abstraction, which essentially is the sum of a proton and electron transfer. In P450 chemistry the electron and proton transfer do not necessarily take place to the same site, so that different electromers can be formed after hydrogen atom abstraction from a substrate (SubH) to Cpd I, [Fe^{IV}=O(heme$^{+\bullet}$)], leading to either an iron(IV)-hydroxo heme or an iron(III)-hydroxo heme cation radical intermediate, Eqs 12 and 13. The reaction enthalpy for Eq 12 and 13 is $\Delta H_{HA,FeIV}$ and $\Delta H_{HA,FeIII}$, respectively.

$$[Fe^{IV}=O(heme^{+\bullet})] + SubH \rightarrow [Fe^{IV}(OH)(heme)] + Sub^{\bullet} + \Delta H_{HA,FeIV} \quad (12)$$

$$[Fe^{IV}=O(heme^{+\bullet})] + SubH \rightarrow [Fe^{III}(OH)(heme^{+\bullet})] + Sub^{\bullet} + \Delta H_{HA,FeIII} \quad (13)$$

Thus, the electron transfer from substrate to doublet or quartet Cpd I can lead to five low-lying radical intermediates (^{2,4}**I**), whereby the electron either fills the porphyrin hole (a_{2u} orbital) or fills the π^*_{xz} orbital with a second electron. Note that there are two isoelectronic doublet spin intermediates with the metal in the iron(III) oxidation state and electronic configuration $\pi^*_{xz}{}^2\ \pi^*_{yz}{}^{\uparrow}\ a_{2u}{}^{\downarrow}\ \phi_{Sub}{}^{\uparrow}$ (^{2}**I**$_{III}$) or $\pi^*_{xz}{}^2\ \pi^*_{yz}{}^{\uparrow}\ a_{2u}{}^{\uparrow}\ \phi_{Sub}{}^{\downarrow}$ (^{2}**I′**$_{III}$) with ϕ_{Sub} the orbital for the radical on Sub$^{\bullet}$. Table 1 gives an example of these five radical intermediates as calculated for hydrogen atom abstraction from propene by a Cpd I model.[176]

Table 1: Electronic configuration and relative energies of optimized geometries of radical intermediates (**I**) obtained after hydrogen atom abstraction from propene by P450 Cpd I.

Label	Electronic configuration	Orbital occupation	ΔE [a]
^{2}**I**$_{IV}$	[Fe^{IV}(OH)(heme)--Sub$^{\bullet}$]	$\pi^*_{xz}{}^{\uparrow}\ \pi^*_{yz}{}^{\uparrow}\ a_{2u}{}^2\ \phi_{Sub}{}^{\downarrow}$	0.0
^{4}**I**$_{IV}$	[Fe^{IV}(OH)(heme)--Sub$^{\bullet}$]	$\pi^*_{xz}{}^{\uparrow}\ \pi^*_{yz}{}^{\uparrow}\ a_{2u}{}^2\ \phi_{Sub}{}^{\uparrow}$	0.4

$^4\mathbf{I}_{III}$	[Fe^{III}(OH)(heme$^{+\bullet}$)--Sub$^{\bullet}$]	$\pi^*_{xz}{}^2\ \pi^*_{yz}{}^{\uparrow}\ a_{2u}{}^{\uparrow}\ \phi_{Sub}{}^{\uparrow}$	6.4
$^2\mathbf{I'}_{III}$	[Fe^{III}(OH)(heme$^{+\bullet}$)--Sub$^{\bullet}$]	$\pi^*_{xz}{}^2\ \pi^*_{yz}{}^{\uparrow}\ a_{2u}{}^{\uparrow}\ \phi_{Sub}{}^{\downarrow}$	6.4
$^2\mathbf{I}_{III}$	[Fe^{III}(OH)(heme$^{+\bullet}$)--Sub$^{\bullet}$]	$\pi^*_{xz}{}^2\ \pi^*_{yz}{}^{\uparrow}\ a_{2u}{}^{\downarrow}\ \phi_{Sub}{}^{\uparrow}$	9.9

[a] Energies in kcal mol^{-1} calculated at UB3LYP/BS2 and taken from Ref 176.

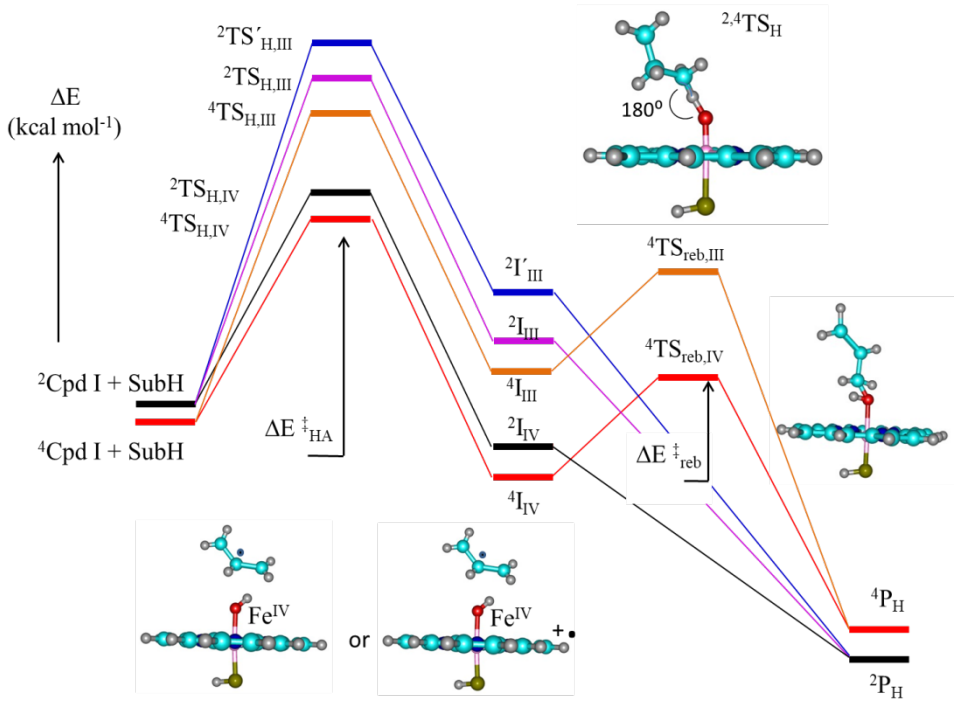

Figure 12: Typical two-state-reactivity potential energy profile for substrate hydroxylation by P450 Cpd I on competing doublet and quartet spin states and passing possible radical intermediate electromers.

Figure 12 displays a typical multistate-reactivity profile for aliphatic hydroxylation of a model substrate (propene) on competing doublet and quartet spin states.[176] The overall reaction mechanism starts from the degenerate doublet and quartet spin states of Cpd I and via an initial hydrogen atom abstraction followed by hydroxyl rebound to the radical restgroup gives 1-propenol products. Essentially, computation identified five low-lying reaction profiles via any of the $\mathbf{I}_{IV}$ or $\mathbf{I}_{III}$ intermediates. Obviously, these five radical intermediates connect to reactants via five different hydrogen atom abstraction barriers $\mathbf{TS}_H$. Radical rebound encounters significant barriers on the quartet spin state surface ($\mathbf{TS}_{reb}$), but is virtually barrierless on the low-spin surface. Nevertheless, the low-spin radical intermediates are local minima with real

frequencies only, but due to the small rebound barriers these states will have short lifetimes and collapse to the product complexes (^{2}**P**) spontaneously. By contrast, the quartet spin mechanisms have large barriers that will determine their lifetime during which the radical restgroup can undergo rearrangement leading to either by-products or stereochemical scrambling. These rearrangement patterns are not possible on the doublet spin state surface, hence the two spin state surfaces occasionally give differences in product distributions. The rebound barrier tend to be higher in energy for ^{4}**TS**$_{reb,III}$ than for ^{4}**TS**$_{reb,IV}$, since a double electron transfer takes place on the iron(III) surface. Thus, the quartet spin product (^{4}**P**) has orbital occupation $\pi^*_{xz}{}^{\uparrow}$ $\pi^*_{yz}{}^{\uparrow}$ $\sigma^*_z2^{\uparrow}$ $a_{2u}{}^2$, so that the process from ^{4}**I**$_{IV}$ will lead to electron transfer from substrate into the σ^*_z2 orbital, whereas the one starting from ^{4}**I**$_{III}$ gives an α-spin electron transfer from substrate to σ^*_z2 and a β-spin electron transfer from π^*_{xz} to a_{2u}. Because of this difference, the rebound barrier from ^{4}**I**$_{III}$ is larger than that for ^{4}**I**$_{IV}$, and consequently more rearrangement is expected on the quartet spin iron(III) surface.

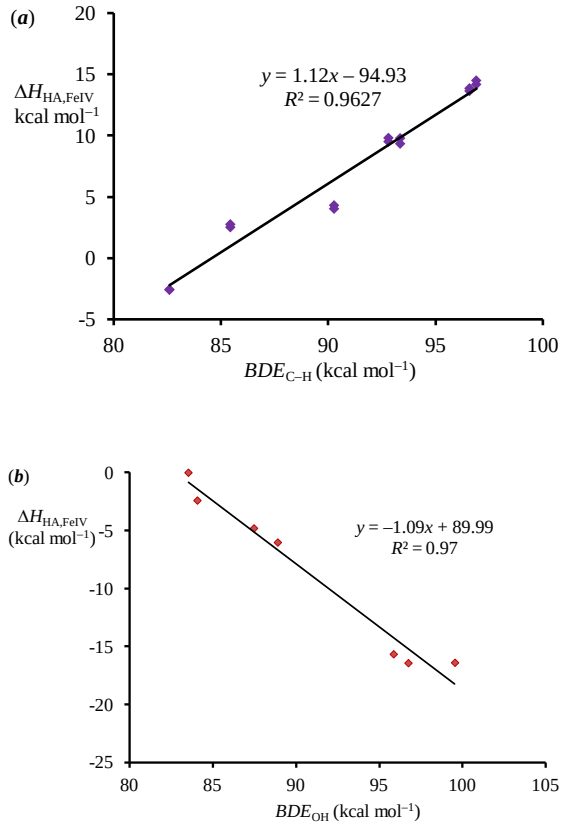

Figure 13: Hydrogen atom abstraction energy by Cpd I(P450) to form IIV intermediates as a function of (a) BDEC–H and (b) BDEO–H.

Let us in the following attempt to generalize and explain the energetics of the processes in Figure 12 and the corresponding reaction barriers. As shown in Eq 12 – 16 the reaction enthalpy for hydrogen atom abstraction is dependent on the strength of the C–H bond of the substrate that is broken or bond dissociation energy of the C–H bond ($BDE_{C–H}$) as well as on the strength of the O–H bond in the iron(IV)-hydroxo complex that is formed ($BDE_{O–H}$). The reaction enthalpy for the iron(IV)-process, therefore, can be written as the difference between $BDE_{C–H}$ and $BDE_{O–H}$.[177–179] This implies that the reaction energy from reactants to form $^4\mathbf{I}_{IV}$ should correlate with both $BDE_{C–H}$ and $BDE_{O–H}$. For the hydrogen atom abstraction from a range of substrates by a $^4[Fe^{IV}=O(Por^{+\bullet})SH]$ model of P450 Cpd I with Por = bare porphyrin ring without side chains, we plot the reaction enthalpy to form $^4\mathbf{I}_{IV}$ as a function of the calculated $BDE_{C–H}$ value of each substrate in Figure 13(*a*). As follows from Figure 13(*a*) the reaction enthalpy correlates linearly with $BDE_{C–H}$ and the correlation coefficient R^2 is close to unity. This implies that the standard deviation of the calculations is very small (within a few kcal mol^{-1}) and that indeed $\Delta H_{HA,FeIV}$ correlates with $BDE_{C–H}$ as predicted by Eq 16. The slope of the trend, however, deviates slightly from unity, probably because entropic effects were not taken into consideration in the calculations.

$$SubH \rightarrow Sub^{\bullet} + H^{\bullet} + BDE_{C–H} \quad (14)$$

$$[Fe^{IV}(OH)(heme)] \rightarrow [Fe^{IV}=O(heme^{+\bullet})] + H^{\bullet} + BDE_{O–H} \quad (15)$$

$$\Delta H_{HA,FeIV} = BDE_{C–H} - BDE_{O–H} \quad (16)$$

Subsequently, we calculated the hydrogen atom abstraction from propene by a range of iron(IV)-oxo species with either heme or nonheme ligand systems including a series of $[Fe^{IV}=O(Por^{+\bullet})X]$ intermediates with X = variable axial ligand.[180] A plot of the obtained $\Delta H_{HA,FeIV}$ enthalpies versus $BDE_{O–H}$ of these iron(IV)-oxo oxidants is given in Figure 14(*b*). As follows also the trend of $\Delta H_{HA,FeIV}$ against $BDE_{O–H}$ is linear with a correlation coefficient of $R^2 = 0.97$ and confirms the prediction made by Eq 14.

The Polanyi principle,[181] states that barrier heights of a chemical reaction are often proportional to the driving force of a reaction. Consequently for a

hydrogen atom abstraction from a substrate by Cpd I, the barrier height ($\mathbf{TS}_{H}$) should be proportional to ΔH_{HA} and also to either $BDE_{C–H}$ or $BDE_{O–H}$. In order to test this, two sets of calculations were performed. Firstly, for a model of P450 Cpd I the hydrogen atom abstraction of a range of substrates was calculated. Secondly, the aliphatic hydroxylation of propene was calculated for a set of iron(IV)-oxo species. These two sets of calculations aimed to correlate the barrier height of hydrogen atom abstraction against either $BDE_{C–H}$ or $BDE_{O–H}$.

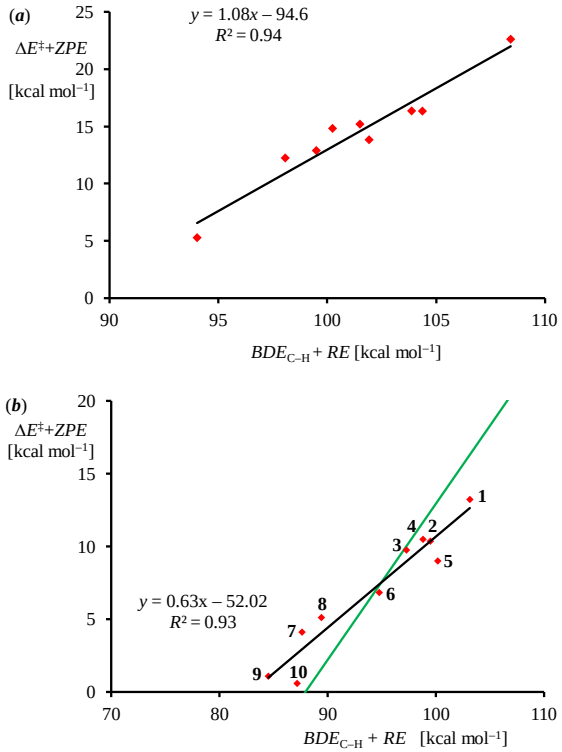

Figure 14: Trends of calculated hydrogen atom abstraction barrier height of an aliphatic group by an iron(IV)-oxo species versus the BDEC–H value of the substrate: (a) Using [Fe^{IV}=O(Por+•)SH] as an oxidant. (b) Using [Fe^{IV}=O(Cor+•)] as an oxidant. The green line in panel (b) gives the trend of panel (a).

In a first set of experiments we took one oxidant, [Fe^{IV}=O($Por^{+\bullet}$)SH] and calculated the hydrogen atom abstraction reaction of a set of substrates: methane, ethane, propane, propene, toluene, ethylbenzene, *trans*-methylphenylcyclopropane, *trans*-*i*-propylphenylcyclopropane, *N*,*N*-dimethylaniline and camphor. The hydrogen atom abstraction barrier was subsequently correlated to $BDE_{C–H}$ in Figure 14.[155,182] More recently, we also

calculated similar trends for [Fe^{IV}=O(corrole$^{+\bullet}$)],[183] displayed in Figure 15(*b*), and a model of the iron(IV)-oxo species of taurine/α-ketoglutarate dioxygenase (see section 4.4) and found similar trends. A corrole group resembles a porphyrin group but misses one of the *meso*-CH bridges and hence has overall charge –3 rather than –2. Because of this corroles are highly suitable ligand systems to stabilize transition metals in high oxidation states, such as Mn^{V} or Fe^{IV}. These figures give the $BDE_{C–H}$ energy corrected for the resonance energy of the substrate (*RE*), which reflects the distortions of the original substrate geometry in the transition state.[182] As can be seen from Figure 14 the hydrogen atom abstraction barrier correlates linearly with the strength of the C–H bond that is broken as predicted and found for experimentally observed trends by Bordwell, Mayer and their co-workers.[178,180]

As mentioned above substrate hydroxylation is a two step process with an initial hydrogen atom abstraction that is followed by OH rebound to Sub$^{\bullet}$ to form alcohol products. However, in some situations the latter step is replaced by a second hydrogen atom abstraction to give water and dehydrogenated substrate, such as an olefin or a ring-closure process. Technically, the dehydrogenation reaction competes with the hydroxylation reaction and the regioselectivity of these processes will be determined by the relative energies of the rebound *versus* dehydrogenation barriers.[184] Scheme 1 explains the competitive reaction mechanisms leading to alcohol and olefin products from aliphatic groups. Thus, both reactions start with a hydrogen atom abstraction from the substrate to form a radical intermediate. For simplicity we only show the iron(IV)-hydroxo intermediate in Scheme 1. Rebound of the OH group gives alcohol products with exothermicity $\Delta H_{reb,IV}$, but a second hydrogen atom abstraction from the substrate by the iron(IV)-hydroxo intermediate gives olefin and water products with reaction enthalpy $\Delta H_{dehydro}$.

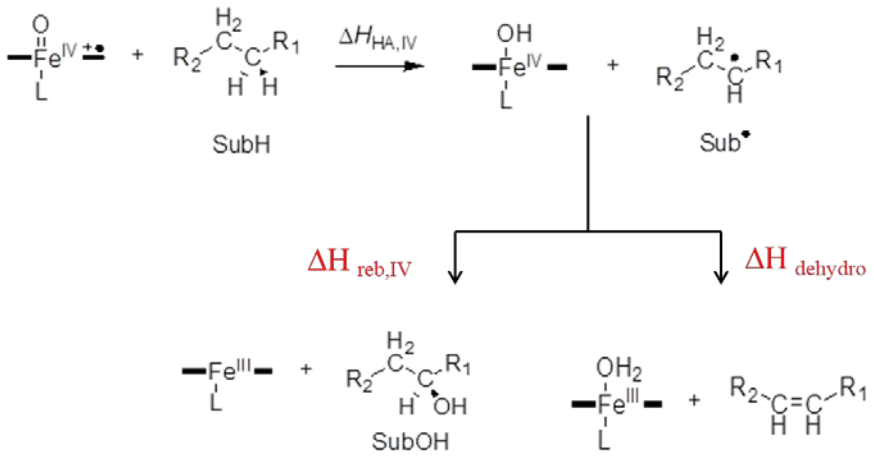

Scheme 1: Reaction mechanisms of Cpd I with alkanes leading to alcohol and olefin products.

Thermodynamically, the rebound barrier involves the breaking of the Fe^{IV}–OH bond in the radical intermediate and the formation of the Sub–OH bond. We calculated a value of 30.2 kcal mol^{-1} to break the Fe^{IV}–OH bond in the iron(IV)-hydroxo intermediate.[184] The bond dissociation energy of the C–O bond in the alcohol is defined as BDE_{COH} and we calculated this for a selection of substrates (Table 2). The bond is strong for aliphatic molecules such as ethane, *trans*-butane and cyclohexane, but is much weaker for olefins such as cyclohexene and cyclohexadiene. The dehydrogenation energy depends on the energy to break a C–H bond in $Sub^{\bullet}$ ($BDE_{C2–H}$) and the formation of an O–H bond to form water for which we calculated a value of 70.8 kcal mol^{-1} in $Fe^{III}(H_2O)$(heme). The values of $BDE_{C2–H}$ were calculated for a selection of substrates and are also given in Table 2.

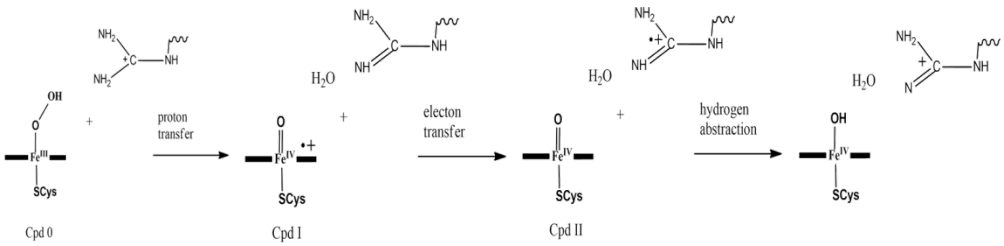

Scheme 2: Reaction mechanism of arginine hydroxylation by NOS enzymes as established by DFT.

Table 2: Calculated BDEs and reaction enthalpies for the reactions from Scheme 2.[a]

Substrate	$BDE_{C–H}$	$\Delta H_{HA,IV}$	$BDE_{C2–H}$	$\Delta H_{dehydro}$	BDE_{COH}	$\Delta H_{reb,IV}$
ethane	96.2	9.5	36.7	–34.0	85.8	–55.5
trans-butane	92.6	5.9	33.5	–37.3	85.4	–55.2
cyclohexane	93.0	6.4	33.6	–37.2	85.8	–55.6
cyclohexene	77.7	–9.0	47.5	–23.3	69.1	–38.9
cyclohexadiene	69.0	–17.6	21.8	–49.0	59.7	–29.5

[a] All values are in kcal mol^{-1} and taken from Ref 184.

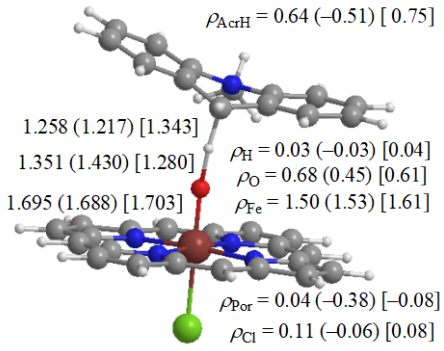

$\Delta E+ZPE$ = 5.6 (6.1) [11.9] kcal mol^{-1}

^{4}**TS**$_{H,HT}$ (^{2}**TS1**$_{H,HT}$) [^{4}**TS**$_{H,HA}$]

Figure 16: Optimized geometries of hydride transfer and hydrogen atom abstraction barriers from $AcrH_2$ by [Fe^{IV}=O(Por+•)Cl] with bond lengths in angstroms and group spin densities in atomic units.

Using these BDE values we then calculated reaction enthalpies for radical rebound and dehydrogenation from the iron(IV)-hydroxo complex and Sub•

and report these values in Table 2. As follows, for aliphatic substrates the rebound exothermicity is large mainly due to the formation of a strong C–O bond. With cyclohexene and cyclohexadiene the C–O bond formation is much lower. However, with cyclohexadiene the second hydrogen atom abstraction costs little energy, and, in addition, the formed product is benzene, which has considerable aromatic stabilization. By contrast, olefins formed from aliphatic groups do not have this resonance stabilization and hence have much lesser reaction exothermicities for dehydrogenation. As a consequence, cyclohexadiene will react with Cpd I by formation of benzene products through a dehydrogenation reaction, whereas linear alkanes give alcohol products instead. In principle, the reaction of Cpd I with an aliphatic group can lead to either hydrogen atom abstraction, proton transfer or hydride transfer. For the substrates discussed above only a hydrogen atom abstraction was observed, which was seen to be a separate electron and proton transfer to a different site, although the two events were found to be taking place during the same rate determining transition state. In the final paragraphs of this section we will give two examples of different reactivities. Firstly, we will give an example of a hydride transfer by Cpd I from a substrate with weak C–H bond strength, i.e., 10-methyl-9,10-dihydroacridine ($AcrH_2$). Secondly, we encountered a system, namely of the active site of nitric oxide synthase (NOS), where the reaction starts off with an initial electron transfer followed by a hydrogen atom abstraction.

The reaction of $[Fe^{IV}=O(Por^{+\bullet})Cl]$ with $AcrH_2$ was calculated with DFT methods and established a stepwise mechanism.[185] However, three barriers were located for the initial reaction step (Figure 16): $^{2,4}\mathbf{TS}_{H,HT}$ leading to a hydride transfer intermediate with orbital occupation $\delta_x 2_{-y} 2^2\ \pi^*_{xz}{}^2\ \pi^*_{yz}{}^1\ a_{2u}{}^2$ in the doublet spin state and $\delta_x 2_{-y} 2^2\ \pi^*_{xz}{}^1\ \pi^*_{yz}{}^1\ \sigma^*_z 2^1$ in the quartet spin state and configuration $[Fe^{III}(OH^-)(Por)Cl\text{---}AcrH^+]$. The third transition state ($^4\mathbf{TS}_{H,HA}$) is a hydrogen atom abstraction transition state similar to those discussed above that gives an iron(IV)-hydroxo radical intermediate. Thus, the hydride transfer transition states are substantially lower in energy than the hydrogen atom abstraction barrier. Furthermore, the cationic intermediates are also much lower in energy than the radical intermediates in this system.

However, although the overall reaction from reactants to intermediates implicates a hydride transfer step, actually, the charge and group spin densities in the $^{2,4}\mathbf{TS}_{H,HT}$ structures associate them as hydrogen atom abstraction barriers instead. In particular, the AcrH restgroup has considerable amount of unpaired spin density in all three transition states. Consequently, the hydride reaction step in the mechanism actually is a hydrogen atom transfer followed by a separate electron transfer. The hydrogen atom transfer then takes place in the transition states ($^{2,4}\mathbf{TS}_{H,HT}$), which are followed by an electron transfer en route from the transition state to the cationic intermediate. Replacement of the iron(IV) atom in Cpd I by manganese(V) gave similar reaction mechanisms of hydride versus hydrogen atom transfer reactions.[186]

Closely related to the P450 enzymes are the nitric oxide synthases (NOSs), which are involved in the biosynthesis of NO in the body. NO has diverse functions in the body, but due to its high reactivity it needs to be created close to the source where it is needed to avoid accidental damage. In the body NO functions as a neuronal messenger, and participates in blood pressure control and heart rate. NOS enzymes take one molecule of arginine and convert it to L-citrulline and NO through the use of two molecules of molecular oxygen on a heme centre. For a long time, it has been believed that the catalytic mechanism of the first step, i.e. the conversion of L-arginine into N^{ω}-L-hydroxy-arginine happens via a P450-type mechanism with an initial hydrogen atom abstraction followed by radical rebound. In order to understand its mechanism we did a series of DFT calculations on an active site model.[187,188] The calculations show that in the gas-phase protonated arginine substrate initially functions as a proton donor in the catalytic cycle, which can shuttle protons from the solvent to the iron(III)-superoxo and iron(III)-hydroperoxo (Cpd 0) intermediates. This eventually generates Cpd I and a neutral arginine residue. Test calculations for hydrogen atom abstraction or proton abstraction from protonated arginine by Cpd I revealed high energy barriers, and, therefore was ruled out as a possible mechanism. Neutral arginine transfers an electron to Cpd I rapidly in the gas phase to form Cpd II and ionized arginine. A hydrogen atom abstraction by Cpd II followed by OH rebound then gives N^{ω}-L-hydroxy arginine products.

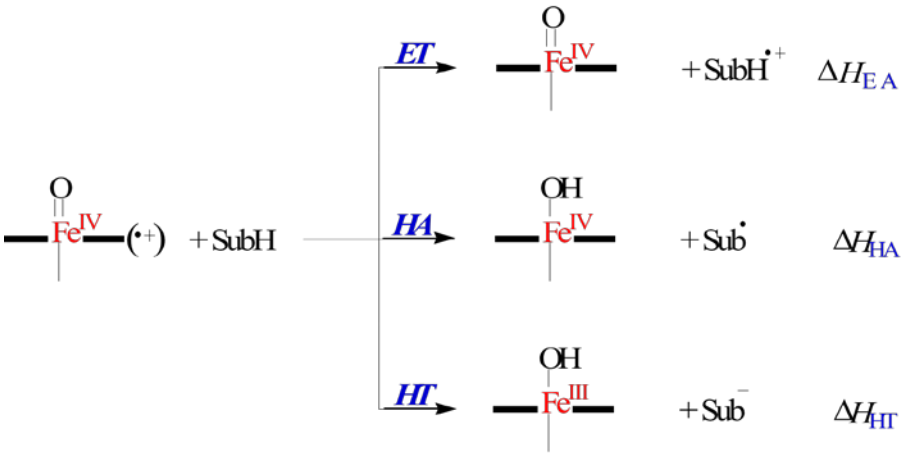

Figure 17: Possible reaction mechanisms between Cpd I and a substrate leading to electron transfer (ET), hydrogen atom abstraction (HA) and hydride transfer (HT).

In order to understand the reactivities of Cpd I with substrates and the possible mechanisms, i.e. electron transfer, hydrogen atom abstraction or hydride transfer, consider in Figure 17 the energetics for the individual processes. Thus, in a reaction where hydride transfer is preferential over hydrogen atom abstraction the reaction enthalpy ΔH_{HT} should be larger than ΔH_{HA}. Based on the strength of the C–H bond in the substrate and the electron affinity of Cpd I one can derive that the difference in enthalpy between hydrogen atom abstraction and hydride transfer is exactly equal to the electron affinity of a hydrogen atom minus the ionization potential of the hydrogen abstracted substrate (Sub):[185]

$$\Delta H_{HT} - \Delta H_{HA} > EA_H - IE_{Sub} \quad (18)$$

4.1.4 Olefin epoxidation by P450 Cpd I.

Olefin epoxidation is a common process catalyzed by P450 enzymes and, for instance, in the body takes place on unsaturated fatty acids in the liver,[189] whereas in cockroaches the epoxidation of methyl farnesoate by a P450 isozyme leads to the biosynthesis of a vital hormone.[190] A stepwise mechanism for substrate epoxidation by P450 Cpd I was established (Figure 18) with an initial C–O bond formation step to form a radical intermediate followed by a ring-closure barrier leading to epoxide products.[156] During the life-time of the radical intermediate stereochemical scrambling can occur leading, e.g., to *cis*-

epoxides from *trans*-olefins.[157] Furthermore, rearrangement patterns have been calculated leading to aldehyde and suicidal products via spin-state crossings from radical to cationic intermediates.[157,191,192] The features of the mechanism resemble that of aliphatic hydroxylation closely and were described as a stepwise process via a radical intermediate. As an example of a typical substrate epoxidation potential energy profile we present in Figure 19 the 1-butene epoxidation by ^{4,2}Cpd I of P450 as calculated with DFT.[145] In this study the geometries were optimized with a relatively large basis set, but despite this the energies were only a fraction different from those observed with UB3LYP/B1//UB3LYP/B2, hence the large basis set is not necessary for the geometry optimization itself. The potential energy profile resembles that of Figure 13 above and also can take place via either an iron(IV)(heme) or iron(III)(heme$^{+\bullet}$) radical intermediates, although we only give the low-lying iron(IV) structures here. Calculations on propene epoxidation by P450 Cpd I showed the mechanisms leading to iron(III) intermediates to be higher in energy by several kcal mol^{-1}, at least in the gas phase.[176] Ring closure of the epoxide ring leads to the product complexes and again the low-spin mechanism is virtually barrierless, whereas on the high-spin surface a small barrier (**TS**$_{rc}$) separates the radical intermediates from products. During the lifetime of the high-spin radical intermediate rearrangement patterns are possible leading to stereochemical scrambling. In addition, an internal electron transfer can take place to form two possible cationic intermediates; one that connects to suicidal intermediates and the other to aldehyde products.[157,191,192] The suicidal complexes originate from attack of the cationic site in Fe^{III}–OCH_2–CH^+–R onto a nitrogen atom of the porphyrin ring, which leads to a Fe–O–C–C–N five-membered ring. In enzymology these complexes have been detected and are called suicidal complexes as the formation of this highly stable complex destructs the activity of the heme.[193] We identified the cationic intermediate leading to these suicidal complexes as ^{4}**I**$_{III,cat,xy}$ with orbital occupation $\delta^2\ \pi^*_{xz}{}^1\ \pi^*_{yz}{}^1\ \sigma^*_{xy}{}^1\ a_{2u}{}^2\ \phi_R{}^0$.[157] An alternative cationic intermediate ^{4}**I**$_{III,cat,z2}$ with orbital occupation $\delta^2\ \pi^*_{xz}{}^1\ \pi^*_{yz}{}^1\ \sigma^*_z 2^1\ a_{2u}{}^2\ \phi_R{}^0$ was found to lead to a 1,2-hydrogen atom shift and the formation of aldehyde products.[191]

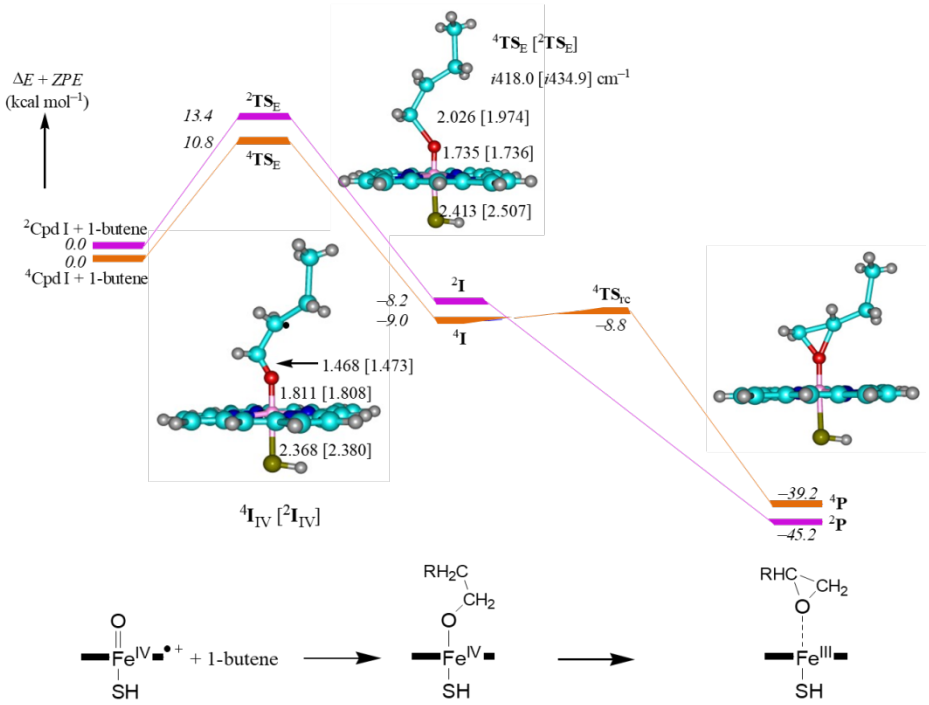

Figure 18: DFT calculated potential energy profile of 1-butene epoxidation by a Cpd I model. Bond lengths are in Ångstroms and relative energies in kcal mol–1. Data taken from Ref 145.

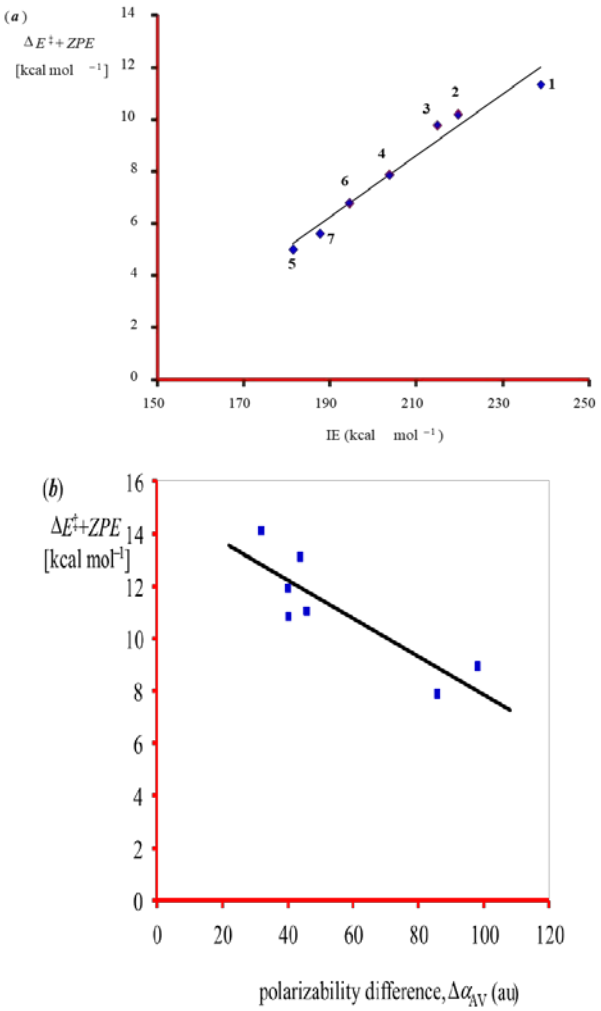

Figure 19: DFT calculated epoxidation barrier heights by Cpd I with a selection of substrates as a function of (a) the ionization potential of the substrate and (b) the polarizability change for the reaction. Data from Ref 145.

Subsequently, we investigated the intrinsic chemical properties of the oxidant and substrate that determine the barrier height or rate constant of olefin epoxidation. We first investigated olefin epoxidation by ^{4,2}Cpd I of P450 using a selection of substrates: ethene, propene, 1-butene, *trans*-2-butene, 1,3-cyclohexadiene, 1,4-cyclohexadiene and styrene. In a second set of calculations we took one substrate (propene) and varied the oxidant; this study included [Fe^{IV}=O($Por^{+\bullet}$)X] models with varying axial ligand X, as well as some nonheme iron(IV)-oxo complexes.[145] As the olefin epoxidation starts with the formation of a C–O bond and the transfer of an electron from the substrate into the a_{2u} molecular orbital, we attempted to correlate the barrier height ^{4,2}**TS**$_E$ with the ionization energy (IE) of the olefin. Figure 19 displays

the obtained correlation between epoxidation barrier height of olefins by ^{4}Cpd I(P450) as a function of IE. As follows a linear trend is observed that confirms that the rate constant is proportional to the ionization potential of the substrate. Recently, we showed that polarizability volume is a thermodynamic variable and is included in the van der Waals constants *a* and *b*.[194–196] To test if the barrier height of the reaction is proportional to the polarizability change from reactants to transition states, we extracted values of polarizability volume from the calculations and calculated the average value from the trace over α_{xx}, α_{yy} and α_{zz}. As follows from Figure 19(*b*) the polarizability volume correlates linearly with the barrier height, whereby the chemical system that undergoes the largest change in polarizability volume gives the lowest reaction barrier.

In a second set of calculations we investigated the properties of the oxidant in the epoxidation reaction process. We took one substrate (propene) and calculated its epoxidation by a set of iron(IV)-oxo complexes. Since, the epoxidation reaction is accomplished by the breaking of a π-bond in the substrate and the simultaneous formation of a C–O bond, we reasoned that the barrier height should correlate with the strength of the π-bond of the substrate that is broken and the strength of the C–O bond that is formed. The breaking of the π-bond, i.e. conversion of the double bond into a single bond, is essentially achieved upon ionizing the substrate as the π-orbital of the olefinic bond in most olefins is the HOMO. Indeed, the results in Figure 19 confirm a correlation between barrier height of substrate epoxidation with the ionization energy of the substrate. Subsequently, we mimicked the formation of the C–O bond between oxidant and substrate by the formation of an H–O bond. Thus, if the formation of a C–O bond is proportional to the formation of a H–O bond and the substrate encounters little stereochemical interactions with the oxidant then the $BDE_{O–H}$ value of the oxidant should correlate with the epoxidation barrier height for a range of oxidants. Our calculations indeed confirmed this for a range of iron(IV)-oxo complexes.[145]

4.1.5 Sulphoxidation reaction by P450 Cpd I.

Heteroatom oxidation, such as sulphoxidation and phosphorylation, are processes performed by P450 enzymes, for example in the biodegradation of neuroleptic drugs in the liver.[197] We studied the mechanism and detail and established a concerted, one-step, mechanism of heteroatom attack on the oxo group of Cpd I.[65,66,198–200] Experimental enzymology studies established a correlation between the rate constant of substrate sulphoxidation by P450 enzymes as a function of the substrate IE,[201] which was supported by a series of test calculations of sulphoxidation reactions catalyzed by Cpd I on a range of sulphides.[199] Since, both substrate epoxidation and sulphoxidation correlate with the IE of the substrate, these studies implicate that the regioselectivity of olefin epoxidation versus sulphide oxidation will be dependent on the nature of the substrate and can only be changed by external perturbations, such as in the substrate binding pocket that position the substrate for activation by Cpd I.

4.1.6 Rearrangement patterns in aliphatic hydroxylation reactions by P450 Cpd I.

Only recently P450 Cpd I was isolated and characterized as the active species in substrate hydroxylation reactions. Until that time studies were focused on establishing indirect evidence of its activity. A common method of this used, so-called, radical clock substrates.[58,61] From the kinetics of the reaction mechanism, it is believed that the lifetime of radical intermediates can be calculated. Thus, these P450 Cpd I reacts with the radical clock substrates via an initial hydrogen atom abstraction leading to a radical intermediate (Scheme 3) similarly to what was discussed in the previous section. During the lifetime of this intermediate, however, a rearranged may occur in the radical rest group Sub$^{\bullet}$. For instance, P450 Cpd I reacts with the radical clock substrate *trans*-methylphenylcyclopropane via aliphatic hydrogen atom abstraction from the methyl group. Rebound of the hydroxo group then gives the substrate with hydroxylated methyl group as unrearranged product (*U*) with rate constant $k_{reb,U}$. However, during the lifetime of the radical intermediate a ring-opening can take place with a rearrangement rate constant k_r, so that the subsequent

rebound with rate constant $k_{reb,R}$ leads to 4-hydroxo-4-phenyl-but-1-ene or rearranged products (*R*) instead. The product ratio [*U*/*R*] was used to experimentally determine the lifetime of the radical intermediate.[58] However, the obtained values were too short and a second-oxidant hypothesis was proposed to explain the observed trends, whereby Cpd 0 and Cpd I were considered as competing oxidants in the reaction mechanism.

To gain insight into the intricate details of the reaction mechanism, we performed a detailed DFT set of calculations on *trans*-methylphenylcyclo-propane hydroxylation by P450 Cpd I.[165,208,209] Figure 24 shows the calculated potential energy profile of the reaction leading to unrearranged and rearranged products. The initial mechanism is similar to that shown above in Figure 13 and starts with competing hydrogen atom abstraction barriers ($\mathbf{TS}_H$) on the doublet and quartet spin state surfaces leading to an iron(IV)-hydroxo intermediate with unrearranged radical rest group ($^{4,2}\mathbf{I}_U$). Radical rebound to form unrearranged products ($\mathbf{P}_U$) encounters a small barrier on the quartet spin state ($^{4}\mathbf{TS}_{reb,U}$) of 2.2 kcal mol^{-1} but is barrierless on the low-spin surface. The radical rest group in $^{4,2}\mathbf{I}_U$ can undergo a ring-opening to form the rearranged radical intermediate $^{4,2}\mathbf{I}_R$ via a barrier ($\mathbf{TS}_{rearr}$) of about 0.2 kcal mol^{-1} on the doublet as well as quartet spin state. The rearranged radical intermediate is considerably lower in energy than its unrearranged isomer and via subsequent radical rebound barriers ($\mathbf{TS}_{reb,R}$) it collapses to the rearranged product complexes ($^{4,2}\mathbf{P}_R$). As can be seen from Figure 24 the low-spin pathway has a lower radical rebound process then rearrangement barrier, so that the dominant pathway will lead to unrearranged products. By contrast, the high-spin unrearranged intermediate has lower rearrangement barrier than rebound barrier, hence the quartet spin profile will lead to dominant rearranged products instead. Therefore, the radical clock reaction mechanism gives an example of spin-state selective reactivity with different products on the doublet and quartet spin surfaces.

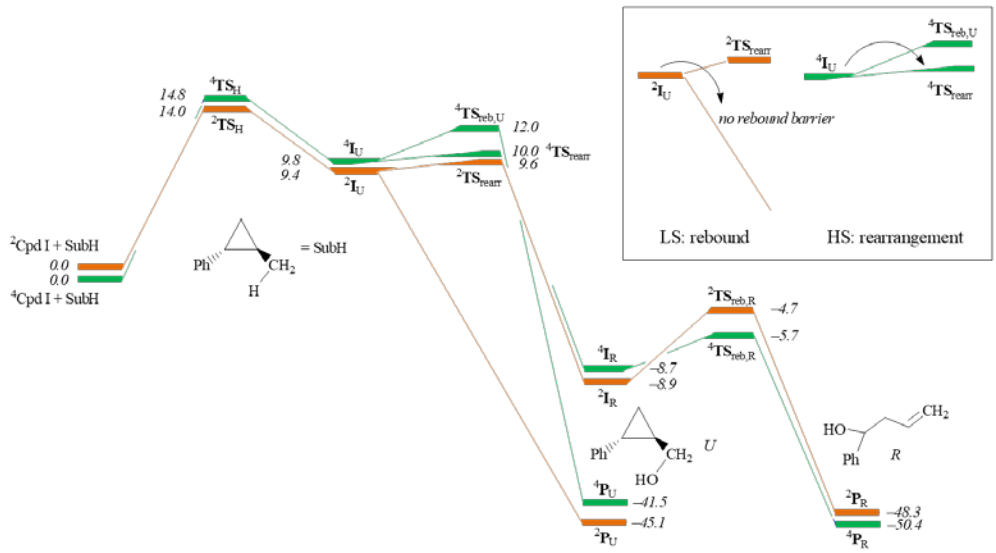

Figure 20: Potential energy profile for trans-methylphenylcyclopropane hydroxylation by P450 Cpd I leading to unrearranged (U) and rearranged (R) products. Energies are in kcal mol–1 and taken from Ref 208.

Experimental studies determined kinetic isotope effects (KIE) by replacement of the methyl hydrogen atoms by deuterium atoms and using the *U*/*R* product ratio a product isotope effect (PIE) was calculated.[58] In response to this we decided to calculate the KIEs for unrearranged and rearranged pathways and find the origin of the PIE values. Based on the mechanism in Figure 20 it can be envisaged that the KIE value for the unrearranged pathway originated from the low-spin surface and the KIE value for the rearranged mechanism from the high-spin surface, Eq 19.

$$\mathrm{PIE}(U/R) = \mathrm{KIE}(U)/\mathrm{KIE}(R) = \mathrm{KIE(LS)/KIE(HS)} \qquad (19)$$

DFT calculations established KIE values using the semiclassical Eyring equation (Eq 20) using 298 K free energies of activation ($\Delta G^{\ddagger}$) of the reaction using hydrogen and deuterium-substituted substrates. In Eq 20 the temperature is given by T and R is the gas constant.

$$\mathrm{KIE}_{\mathrm{Eyring}} = \exp[(\Delta G^{\ddagger}_{\mathrm{D}} - \Delta G^{\ddagger}_{\mathrm{H}})/RT] \qquad (20)$$

Further tunnelling-corrected KIEs due to Wigner (KIE_{Wigner}) and Bell (KIE_{Bell}) use models as described in Eq 21 – 23. In these equations, k_B is the Boltzmann constant, h is Planck's constant and ν is the imaginary frequency in the transition state.

$$KIE_{tunneling} = KIE_{Eyring} \times Q_{t,H}/Q_{t,D} \quad (21)$$

$$Q_{t,Wigner} = 1 + u_t^2/24 \text{ with } u_t = h\nu/k_B T \quad (22)$$

$$Q_{t,Bell} = \frac{u_t}{2\sin\left(\frac{1}{2}u_t\right)} - \sum_{n=1}^{\infty}(-1)^n \frac{\exp\left(\left(u_t - 2n\pi\right)\frac{\Delta E}{u_t}\right)}{\left(u_t - 2n\pi\right)/u_t} \quad (23)$$

DFT calculations for hydrogen atom abstraction by P450 Cpd I of *trans*-methylphenylcyclopropane versus *trans*-d_1-methylphenylcyclopropane gave values of PIE_{Eyring} = 1.03, PIE_{Wigner} = 1.07 and PIE_{Bell} = 1.20 in very good agreement with the experimentally reported PIE value of 1.14.[165,208] These calculations, therefore, ruled out a second oxidant in the reaction mechanism and explained the reactivity via Cpd I using multistate reactivity. To further ascertain that Cpd 0 cannot compete with Cpd I, the reaction mechanism of olefin epoxidation and dimethylsulphide oxidation by Cpd 0 and Cpd I was calculated.[63,65,66] Substantially higher barriers were obtained for the reactions starting with Cpd 0 than Cpd I, which implies that Cpd 0 is a sluggish oxidant that cannot compete with Cpd I.

4.2 Cysteine dioxygenase (CDO).

Cysteine dioxygenase, in contrast to TauD, has an active site with iron bound to a facial 3-His ligand system rather than the more common 2-His/1-Asp features of most nonheme iron dioxygenases. Computational studies were initially focussed on small model complexes,[118,119] but more recent work used QM/MM on the complete enzyme.[120] Due to the tight substrate binding pocket of CDO and the large number of stabilizing hydrogen bonds, a QM region was chosen that includes all characteristic features of the active site, namely most groups in the first and second coordination sphere of the metal: FeO_2, substrate

cysteine and the amino acid side chains of His_{86}, His_{88}, His_{140}, Arg_{60}, His_{155}, Tyr_{157} and Cys_{93}. The calculations revealed a mechanism as given in Figure 21(*a*) that starts from an iron(III)-superoxo complex (**A**), which has close lying singlet, triplet, quintet and septet spin states. The reaction proceeds with attack on the sulphur of cysteinate to for a bicyclic ring structure (**B**) on close-lying singlet, triplet and quintet spin state surfaces. Attempts to calculate this mechanism on the septet spin state surface failed and did not lead to products,[118] therefore, the experimentally trapped septet spin state iron(III)-superoxo intermediate may not be the catalytically relevant species, although the calculations showed it to be close in energy to the quintet spin state. During this process the O–O bond is significantly weakened from 1.338 to 1.513 Å, and in a subsequent step breaks to form an iron(IV)-oxo species with a bound cysteine sulfoxide (**C**). Figure 21(*b*) gives the results of the QM/MM calculations starting from the iron(IV)-oxo intermediate with extracts of the optimized geometries. Thus, in structure **C** the transfer of the second oxygen atom to the substrate is blocked by the sulfoxide group, so that an initial isomerisation step occurs, whereby the SO group rotates, the Fe–S bond breaks and the sulfoxide binds the metal instead to form isomer **C′**. In analogy to biomimetic nonheme iron(IV)-oxo species,[228,229] the ground state of both complexes **C** and **C′** is a triplet spin state. However, the triplet-quintet energy gap is strongly dependent on the ligands bound to the metal and whether cysteine-sulfoxide binds to metal with the sulphur or oxygen atom. The isomerisation step has barriers of 11.3 and 13.2 kcal mol^{-1} on the quintet and triplet spin state surfaces, therefore, a certain degree of spin equilibration is expected at this stage of the reaction with two-state reactivity patterns. After the isomerisation the second oxygen atom transfer takes place on a dominant quintet spin state surface to give cysteine sulphinic acid products (**D**).

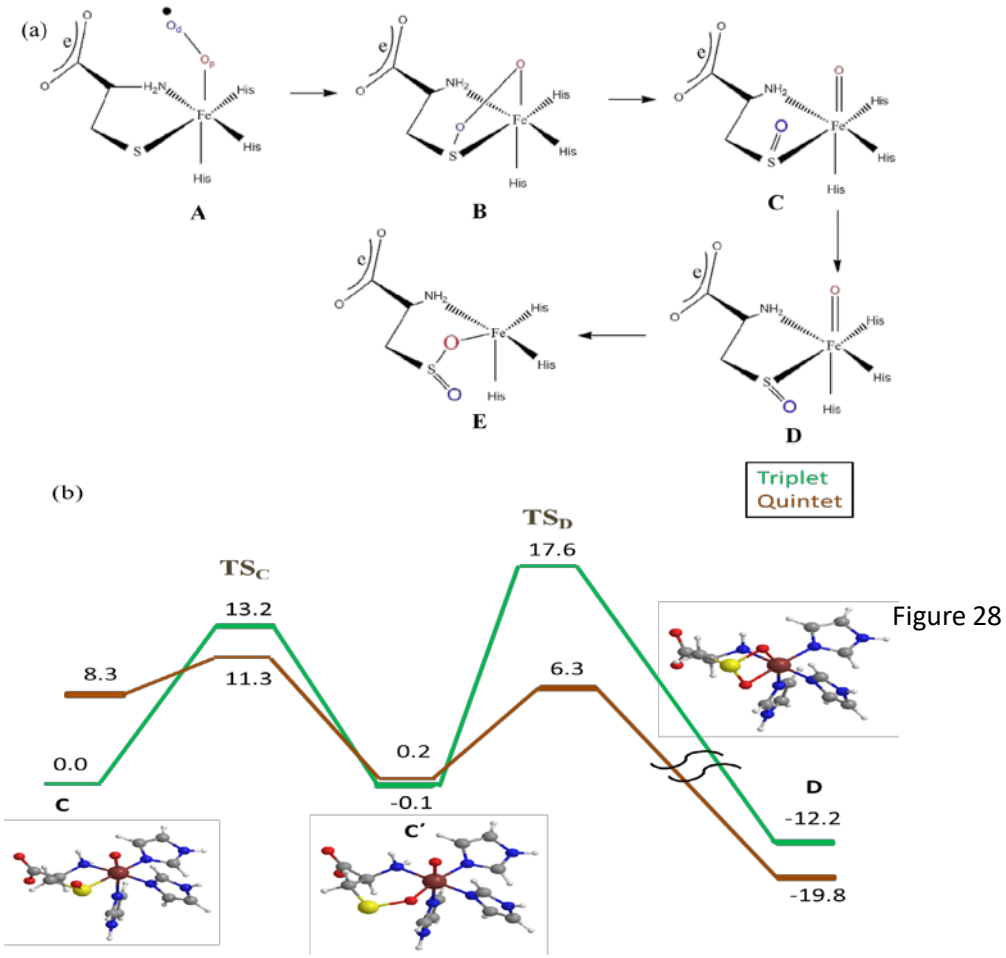

Figure 28

Figure 21: (a) Catalytic mechanism of CDO enzymes. (b) QM/MM calculated oxygenation of cysteine sulfinic acid by a nonheme iron(IV)-oxo intermediates. Energies are in kcal mol–1 and contain ZPE corrections.

Due to the structural differences between TauD and CDO, also calculations on active site mutants were performed where one of the three histidine ligands of the iron in CDO was replaced by a carboxylic acid group to create a 2-His/1-Asp bound motif, i.e. H86D, H88D and H140D mutants.[119] Thus, the mutants have higher dioxygenation barriers, which implies that the 3-His ligand motif in CDO is essential for optimal dioxygenation of the substrate. In particular, a weakening of the Fe–S bond is found for the situation where a carboxylic acid group located *trans* to this bond. On the other hand, a carboxylic acid group *trans* to the superoxo group increases the oxygen atom transfer barriers as a result of a pull-effect of electrons.

4.3 Synthetic nonheme iron complexes.

As discussed in the introduction, mononuclear nonheme iron(IV)-oxo complexes are potent catalysts of oxygenation reactions but the catalytic properties seem to be dependent on the ligands bound to the metal centre. Specifically, two types of interactions have been identified, namely from the axial ligand (i.e. the ligand *trans* to the oxo group) and the equatorial ligands (those perpendicular to the oxo group; the *cis*-ligands). To explain the differences in electronic properties of those types of systems and the factors that determine their reactivity patterns, a series of DFT studies have been performed to elucidate the electronic properties of the oxidants and their reactivity towards substrates. We will start this section with an in-depth overview of the factors that distinguish the individual iron(IV)-oxo catalysts as elucidated from quantum chemical modelling.

4.3.1 Electronic properties of iron(IV)-oxo complexes.

As described above, all experimentally characterized enzymatic mononuclear iron(IV)-oxo species have a quintet spin (S = 2) ground state, whereas most biomimetic complexes tend to have a triplet spin (S = 1) ground state. To understand these differences, we plot in Figure 29 the high-lying occupied and low-lying virtual orbitals of two mononuclear nonheme iron(IV)-oxo complexes, namely the active species of TauD and $[Fe^{IV}(O)(N4Py)]^{2+}$, N4Py = *N*,*N*-bis(2-pyridylmethyl)-*N*-bis(2-pyridyl)-methylamine.[205,215] Other non-heme mononuclear iron(IV)-oxo complexes give a similar set of occupied and virtual orbitals although small variations, e.g. due to differences in the axial ligand may occur. In particular, the axial ligand is known to entice a push-effect and thereby influence the orbitals along the molecular *z*-axis, i.e. along the Fe–O bond.[168,169] All orbitals originate from the metal type 3*d* atomic orbitals that split into a series of three t_{2g} and two e_g set of π^* and σ^* orbitals, where we allocate the *z*-axis along the Fe–O bond. A pair of orthogonal $3d_{xz}$ and $3d_{yz}$ atomic orbitals mix with $2p_x$ and $2p_y$ atomic orbitals on the oxo group to give a set of bonding and anti-bonding combinations, designated π_{xz},

π_{yz}, π^*_{xz}, and π^*_{yz}. The π^*_{xy} orbital is located in the equatorial ligand plane and its corresponding orbital in heme enzymes ($\delta_x 2_{-y} 2$) is nonbonding.[163] The same situation appears for $[Fe^{IV}(O)(N4Py)]^{2+}$ where the four equatorial ligands are identical. As a consequence, this orbital in $[Fe^{IV}(O)(N4Py)]^{2+}$ is significantly lowered in energy with respect to the other π^* orbitals, i.e. π^*_{xz} and π^*_{yz}, and hence the triplet spin state is the ground state.[226–228] High in energy and virtual are two σ-type anti-bonding combinations of the metal with the nitrogen atoms (in $\sigma^*_x 2_{-y} 2$) and along the O–Fe axis (in $\sigma^*_z 2$). The latter orbital also interacts with orbitals on the axial ligand and in particular this effect is strong with a sulfur atom in that position.[163] Indeed, in iron(IV)-oxo complexes the ligand environment has been shown to influence the energy level of, in particular, the $\sigma^*_z 2$ orbital.[145]

The set of orbitals displayed in Figure 22 is occupied with ten electrons but in the enzymatic system this gives a quintet spin ground state, whereas it is a triplet spin ground state in $[Fe^{IV}(O)(N4Py)]^{2+}$. These two states are close in energy for both systems, whereby the triplet/quintet spin state ordering is found to be dependent on the nature of the other ligand(s) bound to iron. In particular, with an increase of the electron-withdrawing power of the axial ligand the $\pi^*_{xy} - \sigma^*_x 2_{-y} 2$ energy gap decreases considerably and so does the quintet-triplet energy gap.[145] A consequence of close lying spin states is the phenomenon designated two-state reactivity (TSR) that originally was described to explain the reactivity patterns of iron(IV)-oxo heme systems, but has been extended to nonheme systems as well.[226–228] The next section explains this phenomenon in detail and how it affects reactivity patterns, product distributions and kinetic isotope effects.

Geometries of several mononuclear nonheme iron(IV)-oxo complexes were optimized with DFT methods in the triplet and quintet spin states.[205–207,226] Generally, the Fe–O bond in nonheme iron(IV)-oxo complexes is short (in the range of 1.65 Å) typical for a double bond. The four equatorial Fe–N distances are of similar size and the average value of these bonds ($r_{FeN,av}$) is shorter for the triplet spin state structures than for the quintet spin state systems, as a result of differences in orbital occupation. The axial Fe–N bond ($r_{FeN,ax}$) is

quite different in length to the equatorial Fe–N bonds again as a result of the orbital occupation in the structure.

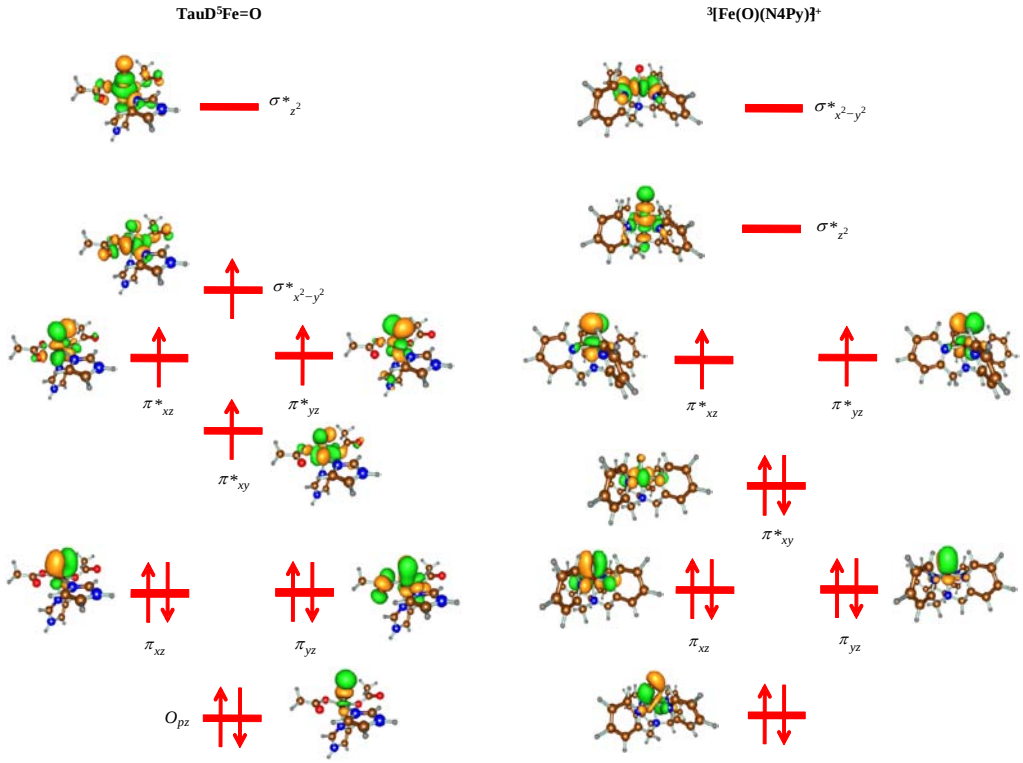

Figure 22: High-lying occupied and virtual orbitals and orbital occupation of the ground states of the iron(IV)-oxo species of TauD (left-hand-side) and [FeIV(O)(N4Py)]2+ (right-hand-side).

4.3.2 Two-state reactivity patterns of mononuclear nonheme iron-oxo complexes.

Enzymatic iron(IV)-oxo complexes have a quintet spin ground state, whereas biomimetic complexes have a lower lying triplet spin state. The oxygen transfer reaction with substrates, therefore, can take place on competing spin-state surfaces with different rate constants, KIEs and barrier heights on each of these spin state surfaces. This phenomenon has been termed two-state reactivity (TSR) and was originally designed to explain the reactivity patterns of the iron(IV)-oxo active species of the heme enzyme cytochrome P450

(P450).[8,16,164] In analogy to this, in nonheme iron(IV)-oxo complexes there are also close lying spin state surfaces, usually triplet and quintet spin. However, the two spin states in nonheme iron chemistry are not degenerate and the spin state energy is dependent on the interactions of the metal with its ligands. Figure 23 displays a schematic drawing of a TSR potential energy profile for a nonheme iron(IV)-oxo complex in a reaction with substrate AlkH. The reaction starts from the two close-lying reactant (**R**) spin states with triplet and quintet spin respectively that are identified with a superscript. These two spin states are generally close in energy in nonheme iron(IV)-oxo complexes, whereby in biomimetic model complexes the triplet spin is usually the ground state, although there are a few examples, where the quintet spin state is the ground state. The hydroxylation mechanism proceeds with an initial hydrogen atom abstraction via barriers $^{3,5}\mathbf{TS}_{HA}$ to form an iron(III)-hydroxo complex and a nearby Alk radical: the intermediate complex **I**. In a subsequent radical rebound step via barrier $^{3,5}\mathbf{TS}_{reb}$ the hydroxylated product (**P**) is formed. All hydroxylation studies of mononuclear nonheme iron(IV)-oxo complexes reported so far follow essentially this reaction mechanism.[205,207,226–228]

Although the triplet spin state is the ground state in all biomimetic iron(IV)-oxo complexes, in fact the hydrogen abstraction barriers on this spin state surface tend to be relatively high and in most cases much higher in energy than the corresponding quintet spin state hydrogen abstraction barriers. As a consequence, it is expected that along the reaction mechanism a spin state crossing from the triplet to quintet spin state takes place. The higher reactivity of the high-spin state has been explained with differences in substrate approach to the iron(IV)-oxo group.[226] In the triplet spin state mechanism the hydrogen abstraction step is accomplished by a simultaneous electron transfer from the substrate into the π^*_{xz} orbital and as a consequence the substrate attacks the Fe–O group sideways to get maximum orbital overlap with this orbital. By contrast, in the quintet spin state the electron transfer is into the $\sigma^*_{z}2$ orbital, which is along the Fe–O bond and the substrate, is aligned with this bond. In this particular orientation there is little electrostatic repulsion of the approaching substrate with the iron ligands, whereas in the triplet spin there is considerable repulsion that destabilizes this transition state. As a consequence

of these differences in electron transfer processes in the hydrogen abstraction step of the mechanism, the approach of the substrate onto the iron(IV)-oxo group also is different in the triplet and quintet spin states. The in-sets of Figure 30 show the geometries of the hydrogen abstraction transition states in the triplet and quintet spin states (^{3,5}**TS**$_{HA}$). In both transition states the O–H–C angle is around 180°, but due to differences in electron transfer the Fe–O–C angle is 180° in the quintet spin state while it is around 120° (dependent on the nature of the ligands bound to iron) in the triplet spin state.[226] Because of repulsive interactions of the approaching substrate with the ligands bound to iron, the triplet spin state barriers generally are higher in energy than those in the quintet spin state. Consequently, similarly to the heme models also biomimetic nonheme iron-oxo complexes give rise to two-state reactivity patterns on close lying triplet and quintet spin state surfaces. The difference, however, is that the orbital occupation of the triplet and quintet spin state is quite different, so that the nature of the other ligands determines the triplet-quintet energy splitting. In the next few sections we will give some examples of results of theoretical studies of oxygen atom transfer reaction by nonheme models and how TSR patterns affect the product distributions and KIEs. After the initial hydrogen abstraction step an iron(III)-hydroxo complex is formed with a radical rest group, and hydroxylated products (**P**) are formed via a radical rebound transition state (**TS**$_{reb}$). In most examples studied so far, the rebound barrier is significantly lower in energy than the hydrogen abstraction barrier that is the rate-determining step in the reaction mechanism.

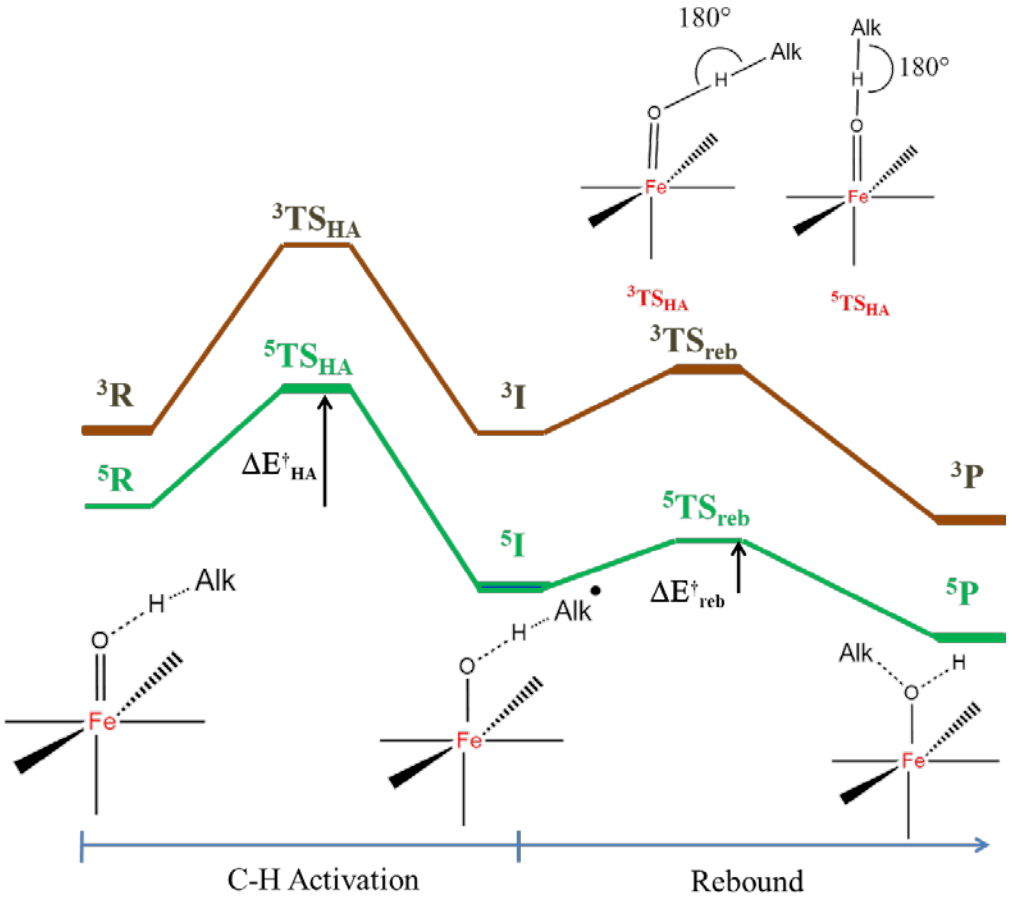

Figure 23: Reactivity differences of biomimetic iron(IV)-oxo species with triplet spin ground state as compared to enzymatic iron(IV)-oxo species with a quintet spin ground state.

A comparative DFT study on substrate hydroxylation by a TauD model vis-à-vis a heme model mimicking the active site of cytochrome P450 revealed that mononuclear nonheme iron(IV)-oxo oxidants are more efficient and powerful oxidants as compared to heme-type iron(IV)-oxo oxidants.[215,223] This was ascribed to the formation of a much stronger O–H bond in nonheme systems, which as a consequence also lowers the reaction barriers. More recent studies on the reactions of mononuclear iron(IV)-oxo oxidants with a 2-His/1-Asp ligand motif with a range of different substrates, with C–H bond strengths from 82.4 kcal mol^{-1} for ethylbenzene to 101.6 kcal mol^{-1} for methane, showed that the barrier of substrate hydroxylation is linearly related to the strength of the C–H bond that is broken in the process.[224]

4.3.3 The cis*-effect on the properties of the iron(IV)-oxo species.*

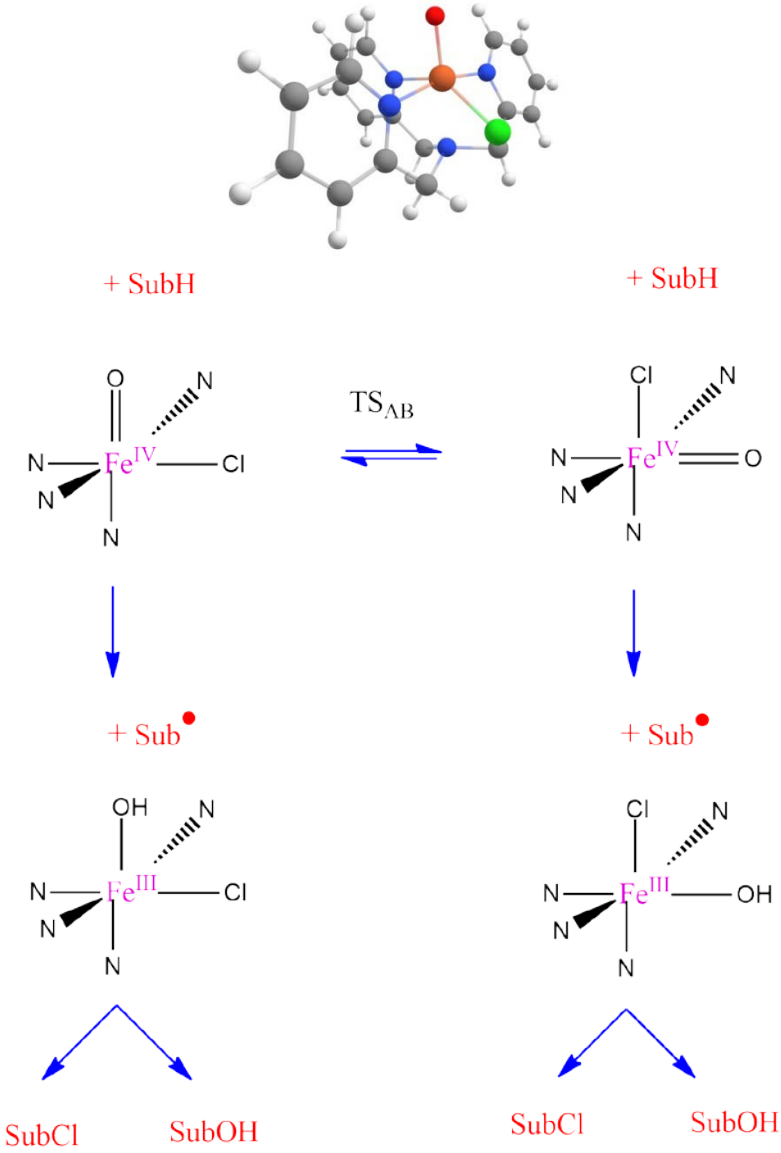

Scheme 2: Calculated reaction mechanisms of halogenation versus hydroxylation of a substrate with an iron(IV)-oxo(halide) system.

As shown in the previous section ligands *trans* to the oxo group (axial ligands) determine key properties of the iron(IV)-oxo centre and influence reactivity patterns. To establish whether or not ligands perpendicular to the iron(IV)-oxo bond influence the spectroscopic and catalytic properties of the system, a series of density functional theory studies on the nature of the *cis*-effect and *cis*-influence of ligands on iron(IV)-oxo nonheme complexes have been performed

using $[Fe^{IV}(O)(TPA)L]^+$ with L = F^-, Cl^-, and Br^-.[231] This particular ligand system with a hydroxyl group in the *cis*-position (L = OH^-) has been shown to react with olefins to give *cis*-dihydroxylation and epoxide products.[232–234] DFT calculations showed that the barrier leading to *cis*-dihydroxylation is 1 kcal mol^{-1} lower in energy than the one leading to epoxide products, hence both products are expected for the reactions as indeed observed by experiment.[235] Combined experimental and DFT studies using a mononuclear iron(IV)-oxo in a pentadentate bispidine ligand showed that it reacts with olefins to form competitive *cis*-dihydroxylation and epoxide products.[236,237]

The calculations of a series of $[Fe^{IV}(O)(TPA)X]^+$ complexes with X = F^-, Cl^- or Br^- showed that the interaction between the metal and a first-row element leads to an electronic *cis*-effect due to favourable orbital overlap, which is missing between the metal and second/third row elements.[231] As a consequence, the HOMO/LUMO energy gap is widened for the metal-second row element interaction with respect to the system with L = F^-. Despite the larger HOMO/LUMO gap no large differences in electron affinities of the complexes is observed. Similarly to other mononuclear nonheme iron-oxo complexes also $[Fe^{IV}(O)(TPA)X]^+$ with X = F^-, Cl^-, and Br^- have close lying triplet and quintet spin states, but only the quintet spin state is reactive with substrates. Therefore, the efficiency of the oxidant will be determined with the triplet-quintet spin state crossing of the reaction.

An interesting feature of iron(IV)-oxo complexes with a labile *cis*-ligand is the fact that under certain conditions this ligand is transferred to substrates. Thus, the α-ketoglutarate dependent halogenases have a catalytic cycle that closely resembles that of TauD reported in Figure 5 and all steps until the iron(IV)-oxo species are the same. However, in the halogenases, the *cis*-bound halide atom (usually Cl^-) is transferred to the radical to form halogenated products rather than rebound of the hydroxyl group to form alcohols. In biomimetic complexes substrate halogenation has been reported for $[Fe^{IV}(O)(Cl)(TPA)]^+$. Technically this system has two stable isomers, Scheme 4, with either the oxo or halide *trans* to the amide nitrogen atom of TPA. We calculated the isomerisation between the two forms as well as the hydrogen atom abstraction leading to radical intermediates and the halide and hydroxyl rebound to form halogenated

and hydroxylated products.[239] We show that the two isomers give different regioselectivities, where one isomer gives halogenated products, whereas the other gives dominant hydroxylation. As such we predict that it is essential for efficient substrate halogenation that an initial isomerisation takes place whereby the halide group is moved to a position *trans* to the amide nitrogen of TPA as it weakens its bond and makes the halide transfer to substrate more likely.

The all above discussion with elebortaded explainations and VB model explanations can be found in Ref. 261. There are nice discussions and detail experimental and theoretical presentation can be found in Ref. 262-271.

5. Conclusions and Summary

As highlighted in this dissertation, computational chemistry methods are highly accurate and these days are applicable to 'real life' systems including enzymatic intermediates and synthetic catalysts. As these oxidants tend to react very fast with substrates, computational methods can assist experimental studies in the field and gain valuable understanding on the chemical properties of the oxidant that drive the reaction mechanism and the nature of the active oxidant. Thus our studies established mechanisms for oxygen atom transfer reactions, including aliphatic and aromatic hydroxylation, olefin epoxidation, dehydrogenation of olefins and heteroatom oxidation (sulphoxidation/phosphorylation), of transition metal containing complexes. The research characterized the active oxidant in the reaction processes and the rate determining step in the mechanism. Moreover, in several cases we have devised models that rationalize reaction processes and barrier heights and that can be used to predict rate constants of processes. The work established the difference in reactivity of heme and nonheme iron(IV)-oxo intermediates and assigned the nonheme ones as the more reactive. The calculations rationalized the rate constants and reaction mechanisms and identified the origin of the rate constants, the electron/proton transfer processes involved and the regioselectivity preferences. These studies have set the scene for collaborative computational modelling in close relationship with experimental biomimetic and enzymatic work.

References:

1 M. Sono, M. P. Roach, E. D. Coulter and J. H. Dawson, *Chem. Rev*., 1996, **96**, 2841.

2 J. T. Groves, *Proc. Natl. Acad. Sci. USA*, 2003, **100**, 3569.

3 P. R. Ortiz de Montellano, Ed. *Cytochrome P450: Structure, Mechanism and Biochemistry*. 3rd ed.; Kluwer Academic/Plenum Publishers, New York, 2004.

4 B. Meunier, S. P. de Visser and S. Shaik, *Chem. Rev*., 2004, **104**, 3947.

5 A. W. Munro, H. M. Girvan and K. J. McLean, *Nat. Prod. Rep*., 2007, **24**, 585.

6 K. M. Kadish, K. M. Smith and R, Guilard, Eds. *Handbook of Porphyrin Science*. World Scientific Publishing Co., New Jersey, 2010.

7 P. R. Ortiz de Montellano, *Chem. Rev*., 2010, **104**, 932.

8 S. P. de Visser and D. Kumar, Eds. *Iron-containing enzymes: Versatile catalysts of hydroxylation reaction in nature*. RSC Publishing, Cambridge (UK), 2011.

9 I. G. Denisov, T. M. Makris, S. G. Sligar and I. Schlichting, *Chem. Rev*., 2005, **105**, 2253.

10 Y. Watanabe, H. Nakajima and T. Ueno, *Acc. Chem. Res*., 2007, **40**, 554.

11 J. T. Groves, *Models and Mechanisms of Cytochrome P450 Action*. In *Cytochrome P450: Structure, Mechanism and Biochemistry*. P. R. Ortiz de Montellano, Ed., 3rd Ed., Kluwer Academic/Plenum Publishers: New York, 2005, Chapter 1, pp 1–44.

12 W. Nam, *Acc. Chem. Res*., 2007, **40**, 522.

13 S. P. de Visser and W. Nam, *High-valent iron-oxo porphyrins in oxygenation reactions*. In *Handbook of Porphyrin Science*, K. M. Kadish, K. M. Smith and R. Guilard, Eds., World Scientific Publishing Co., New Jersey, 2010, Chapter 44, pp. 85–140.

14 J. T. Groves and G. A. McClusky, *J. Am. Chem. Soc*., 1976, **98**, 859.

15 J. Rittle and M. T. Green, *Science*, 2010, **330**, 933.

16 S. Shaik, D. Kumar, S. P. de Visser, A. Altun and W. Thiel, *Chem. Rev*., 2005, **105**, 2279.

17 P. E. M. Siegbahn, R. H. Crabtree and P. Nordlund, *J. Biol. Inorg. Chem*., 1998, **3**, 314.

18 P. R. Ortiz de Montellano, *Annu. Rev. Pharmacol. Toxicol.*, 1992, **32**, 89.

19 G. I. Berglund, G. H. Carlsson, A. T. Smith, H. Szöke, A. Henriksen and J. Hajdu, *Nature*, 2002, **417**, 463.

20 E. L. Raven, *Nat. Prod. Rep*., 2003, **20**, 367.

21 M. Sivaraja, D. B. Goodin, M. Smith and B. M. Hoffman, *Science*, 1989, **245**, 738.

22 M. Klingenberg, *Arch. Biochem. Biophys*., 1958, **75**, 376.

23 T. Omura and R. Sato, *J. Biol. Chem*., 1962, **237**, 1375.

24 T. Omura and R. Sato, *J. Biol. Chem*., 1964, **239**, 2370.

25 F. P. Guengerich, *Chem. Res. Toxicol.*, 2001, **14**, 611.

26 P. R. Ortiz de Montellano and J. J. De Voss, *Nat. Prod. Rep*., 2002, **19**, 477.

27 O. Pylypenko and I. Schlichting, *Annu. Rev. Biochem*., 2004, **73**, 991.

28 M. Costas, M. P. Mehn, M. P. Jensen and L. Que Jr, *Chem. Rev*., 2004, **104**, 939.

29 S. V. Kryatov, E. V. Rybak-Akimova and S. Schindler, *Chem. Rev*., 2005, **105**, 2175.

30 P. C. A. Bruijnincx, G. van Koten, R. J. M. Klein Gebbink, *Chem. Soc. Rev*., 2008, **37**, 2716

31 G. H. Loew and D. L. Harris, *Chem. Rev*., 2000, **100**, 407.

32 S. Shaik, S. Cohen, Y. Wang, H. Chen, D. Kumar and W. Thiel, *Chem. Rev*., 2010, **110**, 949.

33 S. P. de Visser, *Adv. Inorg. Chem.*, 2012, **64**, 1.

34 T. L. Poulos, B. C. Finzel, I. C. Gunsalus, G. C. Wagner and J. Kraut, *J. Biol. Chem*., 1985, **260**, 16122.

35 H. M. Berman, J. Westbrook, Z. Feng, G. Gilliland, T. N. Bhat, H. Weissig, I. N. Shindyalov and P. E. Bourne, *Nucleic Acids Res*., 2000, **28**, 235.

36 I. Schlichting, J. Berendzen, K. Chu, A. M. Stock, S. A. Maves, D. E. Benson, R. M. Sweet, D. Ringe, G. A. Petsko and S. G. Sligar, *Science*, 2000, **287**, 1615.

37 T. L. Poulos, B. C. Finzel and A. J. Howard, *Biochemistry*, 1986, **25**, 5314.

38 T. L. Poulos, B. C. Finzel and A. J. Howard, *J. Mol. Biol*., 1987, **195**, 687.

39 R. Raag and T. L. Poulos, *Biochemistry*, 1989, **28**, 7586.

40 J. H. Dawson, *Science*, 1988, **240**, 433.

41 M. T. Green, J. H. Dawson and H. B. Gray, *Science*, 2004, **304**, 1653.

42 M. T. Green, *Curr. Opin. Chem. Biol*., 2009, **13**, 84.

43 F. Ogliaro, S. P. de Visser and S. Shaik, *J. Inorg. Biochem*., 2002, **91**, 554.

44 K. L. Stone, R. K. Behan and M. T. Green, *Proc. Natl. Acad. Sci. USA*, 2005, **102**, 16563.

45 A. Dey, Y. Jiang, P. R. Ortiz de Montellano, P. O. Hodgson, B. Hedman and E. I. Solomon, *J. Am. Chem. Soc*., 2009, **131**, 7869.

46 S. G. Sligar, *Biochemistry*, 1976, **15**, 5399.

47 P. Rydberg, E. Sigfridsson and U. Ryde, *J. Biol. Inorg. Chem*., 2004, **9**, 203.

48 M. Swart, A. R. Groenhof, A. W. Ehlers and K. Lammertsma, *Chem. Phys. Lett*., 2005, **403**, 35.

49 A. Altun and W. Thiel, *J. Phys. Chem. B*, 2005, **109**, 1268.

50 A. R. Groenhof, M. Swart, A. W. Ehlers and K. Lammertsma, *J. Phys. Chem. A*, 2005, **109**, 3411.

51 P. R. Balding, C. S. Porro, K. J. McLean, M. J. Sutcliffe, J.-D. Maréchal, A. W. Munro and S. P. de Visser, *J. Phys. Chem. A*, 2008, **112**, 12911.

52 C. B. Brewer and J. A. Peterson, *J. Biol. Chem*., 1988, **263**, 791.

53 R. Davydov, T. M. Makris, V. Kofman, D. E. Werst, S. G. Sligar and B. M. Hoffman, *J. Am. Chem. Soc*., 2001, **123**, 1403.

54 I. G. Denisov, T. M. Makris and S. G. Sligar, *J. Biol. Chem*., 2001, **276**, 11648.

55 I. G. Denisov, S.-C. Hung, K. E. Weiss, M. A. McLean, Y. Shiro, S.-Y. Park, P. M. Champion and S. G. Sligar, *J. Inorg. Biochem*., 2001, **87**, 215.

56 J. E. Roberts, B. M. Hoffman, R. Rutter and L. P. Hager, *J. Am. Chem. Soc*., 1981, **103**, 7654.

57 A. D. N. Vaz, D. F. McGinnity and M. J. Coon, *Proc. Natl. Acad. Sci. USA*, 1998, **95**, 3555.

58 M. Newcomb, R. Shen, S.-Y. Choi, P. H. Toy, P. F. Hollenberg, A. D. N. Vaz and M. J. Coon, *J. Am. Chem. Soc*., 2000, **122**, 2677.

59 M. J. Cryle and J. J. De Voss, *Angew. Chem. Int. Ed*., 2006, **45**, 8221.

60 A. D. N. Vaz, S. J. Pernecky, G. M. Raner and M. J. Coon, *Proc. Natl. Acad. Sci. USA*, 1996, **93**, 4644.

61 P. R. Ortiz de Montellano and R. A. Stearns, *J. Am. Chem. Soc*., 1987, **109**, 3415.

62 M. Newcomb and P. H. Toy, *Acc. Chem. Res*., 2000, **33**, 449.

63 F. Ogliaro, S. P. de Visser, S. Cohen, P. K. Sharma and S. Shaik, *J. Am. Chem. Soc*., 2002, **124**, 2806.

64 T. Kamachi, Y. Shiota, T. Ohta and K. Yoshizawa, *Bull. Chem. Soc. Jpn*., 2003, **76**, 721.

65 P. K. Sharma, S. P. de Visser and S. Shaik, *J. Am. Chem. Soc*., 2003, **125**, 8698.

66 C. S. Porro, M. J. Sutcliffe and S. P. de Visser, *J. Phys. Chem. A*, 2009, **113**, 11635.

67 M. J. Park, J. Lee, Y. Suh, J. Kim and W. Nam, *J. Am. Chem. Soc*., 2006, **128**, 2630.

68 J. Kaizer, M. Costas and L. Que Jr., *Angew. Chem. Int. Ed*., 2003, **42**, 3671.

69 M. S. Seo, T. Kamachi, T. Kouno, K. Murata, M. J. Park, K. Yoshizawa and W. Nam, *Angew. Chem. Int. Ed*., 2007, **46**, 2291.

70 N. Hessenauer-Ilicheva, A. Franke, D. Meyer, W.-D. Woggon and R. van Eldik, *J. Am. Chem. Soc*., 2007, **129**, 12473.

71 A.-R. Han, Y. J. Jeong, Y. Kang, J. Y. Lee, M. S. Seo and W. Nam, *Chem. Commun*., 2008, 1076.

72 S. J. Lange and L. Que Jr, *Curr. Opin. Chem. Biol*., 1998, **2**, 159.

73 E. I. Solomon, T. C. Brunold, M. I. Davis, J. N. Kemsley, S.-K. Lee, N. Lehnert, F. Neese, A. J. Skulan, Y.-S. Yang and J. Zhou, *Chem. Rev*., 2000, **100**, 235.

74 T. D. H. Bugg, *Curr. Opin. Chem. Biol*., 2001, **5**, 550.

75 M. J. Ryle and R. P. Hausinger, *Curr. Opin. Chem. Biol*., 2002, **6**, 193.

76 M. M. Abu-Omar, A. Loaiza and N. Hontzeas, *Chem. Rev*., 2005, **105**, 2227.

77 J. M. Bollinger Jr and C. Krebs, *Curr. Opin. Chem. Biol*., 2007, **11**, 151.

78 C. Krebs, D. G. Fujimori, C. T. Walsh and J. M. Bollinger Jr, *Acc. Chem. Res*., 2007, **40**, 484.

79 C. J. Schofield and Z. Zhang, *Curr. Opin. Chem. Biol*., 1999, **9**, 722.

80 T. D. H. Bugg, *Tetrahedron*, 2003, **59**, 7075.

81 J. M. Simmons, T. A. Müller and R. P. Hausinger, *Dalton Trans*., 2008, 5132.

82 Y. Mishina, E. M. Duguid and C. He, *Chem. Rev*., 2006, **106**, 215.

83 P. J. O'Brien, *Chem. Rev*., 2006, **106**, 720.

84 C. Loenarz and C. J. Schofield, *Nat. Chem. Biol*., 2008, **4**, 152.

85 R. Chowdhury, A. Hardy and C. J. Schofield, *Chem. Soc. Rev*., 2008, **37**, 1308.

86 O. W. Choroba, D. H. Williams and J. B. Spencer, *J. Am. Chem. Soc*., 2000, **122**, 5389.

87 L. J. Higgins, F. Yan, P. Liu, H.-W. Liu and C. L. Drennan, *Nature*, 2005, **437**, 838.

88 M. C. Bodner, R. M. Phelan, M. F. Freeman, R. Li and C. A. Townsend, *J. Am. Chem. Soc*., 2010, **132**, 12.

89 E. L. Hegg and L. Que Jr., *Eur. J. Biochem*., 1997, **250**, 625.

90 E. G. Kovaleva and J. D. Lipscomb, *Nat. Chem. Biol*., 2008, **4**, 186.

91 Z. Zhang, J. Ren, D. K. Stammers, J. E. Baldwin, K. Harlos and C. J. Schofield, *Nat. Struct. Biol*., 2000, **7**, 127.

92 S. C. Trewick, T. F. Henshaw, R. P. Hausinger, T. Lindahl and B. Sedgwick, *Nature*, 2002, **419**, 174.

93 J. M. Simmons, T. A. Müller and R. P. Hausinger, *Dalton Trans*., 2008, 5132.

94 H. M. Hanauske-Abel and V. Günzler, *J. Theor. Biol*., 1982, **94**, 421.

95 K. I. Kivirikko, R. Myllyla and T. Pihlajaniemi, *FASEB J*., 1989, **3**, 1609.

96 A. D. Winter and A. P. Page, *Mol. Cell Biol*., 2000, 4084.

97 J. R. O'Brien, D. J. Schuller, V. S. Yang, B. D. Dillard and W. N. Lanzilotta, *Biochemistry*, 2003, **42**, 5547.

98 A. Bassan, T. Borowski and P. E. M. Siegbahn, *Dalton Trans*., 2004, 3153.

99 J. M. Bollinger Jr, J. C. Price, L. M. Hoffart, E. W. Barr, C. Krebs, *Eur. J. Inorg. Chem*., 2005, 4245.

100 S. P. de Visser, *Coord. Chem. Rev*., 2009, **253**, 754.

101 T. Borowski, A. Bassan and P. E. M. Siegbahn, *Chem. Eur. J*., 2004, **10**, 1031.

102 M. J. Ryle, R. Padmakumar and R. P. Hausinger, *Biochemistry*, 1999, **38**, 15278.

103 J. C. Price, E. W. Barr, B. Tirupati, J. M. Bollinger Jr and C. Krebs, *Biochemistry*, 2003, **42**, 7497.

104 D. A. Proshlyakov, T. F. Henshaw, G. R. Monterosso, M. J. Ryle and R. P. Hausinger, *J. Am. Chem. Soc*., 2004, **126**, 1022.

105 P. J. Riggs-Gelasco, J. C. Price, R. B. Guyer, J. H. Brehm, E. W. Barr, J. M. Bollinger Jr and C. Krebs, *J. Am. Chem. Soc*., 2004, **126**, 8108.

106 J. C. Price, E. W. Barr, T. E. Glass, C. Krebs, J. M. Bollinger Jr., *J. Am. Chem. Soc*., 2003, **125**, 13008.

107 M. H. Stipanuk, *Annu. Rev. Nutr*., 2004, **24**, 539.

108 C. A. Joseph and M. J. Maroney, *Chem. Commun*., 2007, 3338.

109 C. L. Weinstein, R. H. Haschemeyer and O. W. Griffin, *J. Biol. Chem*., 1988, **263**, 16568.

110 M. T. Heafield, S. Fearn, G. B. Steventon, R. H. Waring, A. C. Williams and S. G. Sturman, *Neurosci. Lett*., 1990, **110**, 216.

111 S. Ye, X. Wu, L. Wei, D. Tang, P. Sun, M. Bartlam and Z. Rao, *J. Biol. Chem*., 2007, **282**, 3391.

112 S. C. Chai, J. R. Bruyere and M. J. Maroney, *J. Biol. Chem*., 2006, **281**, 15774.

113 B. S. Pierce, J. D. Gardner, L. J. Bailey, T. C. Brunold and B. G. Fox, *Biochemistry*, 2007, **46**, 8569.

114 J. B. Lombardini, T. P. Singer and P. D. Boyer, *J. Biol. Chem*., 1969, **244**, 1172.

115 J. E. Dominy Jr, J. Hwang, S. Guo, L. L. Hirschberger, S. Zhang and M. H. Stipanuk, *J. Biol. Chem*., 2008, **283**, 12188.

116 T. Kleffmann, S. A. K. Jongkees, G. Fairweather, S. M. Wilbanks and G. N. L. Jameson, *J. Biol. Inorg. Chem*., 2009, **14**, 913.

117 E. P. Tchesnokov, S. M. Wilbanks and G. N. L. Jameson, *Biochemistry*, 2012, **51**, 257.

118 S. Aluri and S. P. de Visser, *J. Am. Chem. Soc*., 2007, **129**, 14846.

119 S. P. de Visser and G. D. Straganz, *J. Phys. Chem. A*, 2009, **113**, 1835.

120 D. Kumar, W. Thiel and S. P. de Visser, *J. Am. Chem. Soc*., 2011, **133**, 3869.

121 C. R. Simmons, K. Krishnamoorthy, S. L. Granett, D. J. Schuller, J. E. Dominy Jr, T. P. Begley, M. H. Stipanuk and P. A. Karplus, *Biochemistry*, 2008, **47**, 11390.

122 J. A. Crawford, W. Li and B. S. Pierce, *Biochemistry*, 2011, **51**, 10241.

123 M. J. Frisch *et al*. *Gaussian*-09, Revision A.02, Wallingford, CT, 2009.

124 *Jaguar* 7.6, Schrödinger LLC, New York NY, 2007.

125 R. Ahlrichs, M. Bär, M. Häser, H. Horn and C. Kölmel, *Chem. Phys. Lett*., 1989, **162**, 165.

126 F. Neese, *ORCA – an ab initio, DFT and semiempirical SCF-MO package*, Bonn, Germany, Version 2.7-00, 2009.

127 E. Schrödinger, *Phys. Rev.*, 1926, **28**, 1049.

128 P. W. Atkins and R. S. Friedman, *Molecular Quantum Mechanics*, 3rd Ed., Oxford University Press, 1997.

129 F. Jensen, *Introduction to Computational Chemistry*, 2nd Ed., John Wiley & Sons, Ltd., Chichester, 2007.

130 S. P. de Visser. *Introduction to quantum behaviour – a primer*. In *Quantum Tunnelling in Enzyme-Catalysed Reactions*, R. K. Alleman and N. S. Scrutton, Eds.; RSC Publishing, Cambridge, 2009, Chapter 2, p 18.

131 C. Møller and M. S. Plesset, *Phys. Rev*., 1934, **46**, 0618.

132 S. P. de Visser, *J. Biocatal. Biotransf*., 2012, **1**, 1.

133 P. Hohenberg and W. Kohn, *Phys. Rev. B*, 1964, **136**, 864.

134 W. Kohn and L. J. Sham, *Phys. Rev. A*, 1965, **140**, 1133.

135 J. C. Slater, *The self-consistent field for molecular and solids*. In *Quantum Theory of Molecular and Solids*, McGraw-Hill, New York, 1974, Vol. 4.

136 S. H. Vosko, L. Wilk and M. Nusair, *Can. J. Phys*., 1980, **58**, 1200.

137 C. Lee, W. Yang and R. G. Parr, *Phys. Rev. B*, 1988, **37**, 785.

138 J. P. Perdew and Y. Wang, *Phys. Rev. B*, 1992, **45**, 13244.

139 A. D. Becke, *J. Chem. Phys*., 1993, **98**, 5648.

140 M. Reiher, O. Salomon and B. A. Hess, *Theor. Chem. Acc*., 2001, **107**, 48.

141 T. Schwabe and S. Grimme, *Phys. Chem. Chem. Phys*., 2007, **9**, 3397.

142 E. Hückel, *Z. Physik*, 1931, **70**, 204.

143 H. Hellmann, *J. Chem. Phys*., 1935, **3**, 61.

144 P. J. Hay and W. R. Wadt, *J. Chem. Phys.*, 1985, **82**, 270.

145 D. Kumar, B. Karamzadeh, G. N. Sastry and S. P. de Visser, *J. Am. Chem. Soc*., 2010, **132**, 7656.

146 J. H. Jensen, *Molecular Modeling Basics*. CRC Press, Boca Raton, 2010.

147 J. Tomasi, B. Mennucci and R. Cammi, *Chem. Rev*., 2005, **105**, 2999.

148 H. M. Senn and W. Thiel, *Top. Curr. Chem*., 2007, **268**, 173.

149 D. Bakowies and W. Thiel, *J. Phys. Chem*., 1996, **100**, 10580.

150 A. K. Rappé, C. J. Casewit, K. S. Colwell, W. A. Goddard III and W. M. Skiff, *J. Am. Chem. Soc*., 1992, **114**, 10024.

151 W. D. Cornell, P. Cieplak, C. I. Bayly, I. R. Gould, K. M. Merz Jr., D. M. Ferguson, D. C. Spellmeyer, T. Fox, J. W. Caldwell and P. A. Kollman, *J. Am. Chem. Soc*., 1995, **117**, 5179.

152 A. D. MacKerell Jr, *et al*, *J. Phys. Chem. B*, 1998, **102**, 3586.

153 F. Ogliaro, N. Harris, S. Cohen, M. Filatov, S. P. de Visser and S. Shaik, *J. Am. Chem. Soc*., 2000, **122**, 8977.

154 S. P. de Visser, F. Ogliaro, P. K. Sharma and S. Shaik, *Angew. Chem. Int. Ed*., 2002, **41**, 1947.

155 S. P. de Visser, D. Kumar, S. Cohen, R. Shacham and S. Shaik, *J. Am. Chem. Soc*., 2004, **126**, 8362.

156 S. P. de Visser, F. Ogliaro, N. Harris and S. Shaik, *J. Am. Chem. Soc*., 2001, **123**, 3037.

157 S. P. de Visser, F. Ogliaro and S. Shaik, *Angew. Chem. Int. Ed*., 2001, **40**, 2871.

158 S. P. de Visser and S. Shaik, *J. Am. Chem. Soc*., 2003, **125**, 7413.

159 M. T. Green, *J. Am. Chem. Soc*., 1999, **121**, 7939.

160 F. Ogliaro, S. P. de Visser, S. Cohen, J. Kaneti and S. Shaik, *ChemBioChem*., 2001, **2**, 848.

161 F. Ogliaro, S. Cohen, S. P. de Visser and S. Shaik, *J. Am. Chem. Soc*., 2000, **122**, 12892.

162 J. C. Schöneboom, H. Lin, N. Reuter, W. Thiel, S. Cohen, F. Ogliaro and S. Shaik, *J. Am. Chem. Soc*., 2002, **124**, 8142.

163 S. P. de Visser, S. Shaik, P. K. Sharma, D. Kumar and W. Thiel, *J. Am. Chem. Soc*., 2003, **125**, 15779.

164 S. Shaik, S. P. de Visser, F. Ogliaro, H. Schwarz and D. Schröder, *Curr. Opin. Chem. Biol*., 2002, **6**, 556.

165 D. Kumar, S. P. de Visser and S. Shaik, *J. Am. Chem. Soc*., 2003, **125**, 13024.

166 P. Nicholls, I. Fita and P. C. Loewen, *Adv. Inorg. Chem*., 2000, **51**, 51.

167 N. G. Veitch and A. T. Smith, *Adv. Inorg. Chem.*, 2000, **51**, 107.

168 J. H. Dawson, R. H. Holm, J. R. Trudell, G. Barth, R. E. Linder, E. Bunnenberg, C. Djerassi and S. C. Tang, *J. Am. Chem. Soc*., 1976, **98**, 3707.

169 T. L. Poulos, *J. Biol. Inorg. Chem*., 1996, **1**, 356.

170 S. P. de Visser, *J. Phys. Chem. A*, 2005, **109**, 11050.

171 S. P. de Visser, *Inorg. Chem*., 2006, **45**, 9551.

172 R. Wang and S. P. de Visser, *J. Inorg. Biochem*., 2007, **101**, 1464.

173 C. A. Bonagura, B. Bhaskar, H. Shimizu, H. Li, M. Sundaramoorthy, D. E. McRee, D. B. Goodin and T. L. Poulos, *Biochemistry*, 2003, **42**, 5600.

174 E. O'Reilly, V. Köhler, S. L. Flitch and N. J. Turner, *Chem. Commun*., 2010, **47**, 2490.

175 H. M. Girvan, C. W. Levy, P. Williams, K. Fisher, M. R. Cheesman, S. E. Rigby, D. Leys and A. W. Munro, *Biochem. J*., 2010, **427**, 455.

176 S. P. de Visser, F. Ogliaro, P. K. Sharma and S. Shaik, *J. Am. Chem. Soc*., 2002, **124**, 11809.

177 L. E. Friedrich, *J. Org. Chem*., 1983, **48**, 3851.

178 F. G. Bordwell and J.-P. Cheng, *J. Am. Chem. Soc*., 1991, **113**, 1736.

179 J. M. Mayer, *Acc. Chem. Res*., 1998, **31**, 441.

180 S. P. de Visser, *J. Am. Chem. Soc*., 2010, **132**, 1087.

181 M. G. Evans and M. Polanyi, *J. Chem. Soc., Faraday Trans*., 1936, **32**, 1340.

182 S. Shaik, D. Kumar and S. P. de Visser, *J. Am. Chem. Soc*., 2008, **130**, 10128.

183 R. Latifi, J. S. Valentine, W. Nam and S. P. de Visser, *Chem. Commun*., 2012, **48**, 3491.

184 D. Kumar, L. Tahsini, S. P. de Visser, H. Y. Kang, S. J. Kim and W. Nam, *J. Phys. Chem. A*, 2009, **113**, 11713.

185 L. Tahsini, M. Bagherzadeh, W. Nam and S. P. de Visser, *Inorg. Chem*., 2009, **48**, 6661.

186 R. Latifi, L. Tahsini, B. Karamzadeh, N. Safari, W. Nam and S. P. de Visser, *Arch. Biochem. Biophys*., 2011, **507**, 4.

187 S. P. de Visser and L. S. Tan, *J. Am. Chem. Soc*., 2008, **130**, 12961.

188 S. P. de Visser, *Biochem. Soc. Trans*., 2009, **37**, 373.

189 B. E. Daikh, J. M. Lasker, J. L. Raucy and D. R. Koop, *J. Pharmacol. Exp. Therap*., 1994, **271**, 1427.

190 C. Helvig, J. F. Koener, G. C. Unnithan and R. Feyereisen, *Proc. Natl. Acad. Sci. USA*, 2004, **101**, 4024.

191 S. P. de Visser, D. Kumar and S. Shaik, *J. Inorg. Biochem*., 2004, **98**, 1183.

192 D. Kumar, S. P. de Visser and S. Shaik, *Chem. Eur. J*., 2005, **11**, 2825.

193 K. L. Kunze, B. L. K. Mangold, C. Wheeler, H. S. Beilan and P. R. Ortiz de Montellano, *J. Biol. Chem*., 1983, **258**, 4202.

194 S. P. de Visser, *Phys. Chem. Chem. Phys*., 1999, **1**, 749.

195 S. P. de Visser, *J. Phys. Chem. B*, 2011, **115**, 4709.

196 S. P. de Visser, *Chem. Phys. Lett*., 2011, **515**, 170.

197 J. Wójcikowski, P. Maurel and W. A. Daniel, *Drug Metabol. Disp*., 2006, **34**, 471.

198 D. Kumar, S. P. de Visser, P. K. Sharma, H. Hirao and S. Shaik. *Biochemistry*, 2005, **44**, 8148.

199 D. Kumar, G. N. Sastry and S. P. de Visser, *Chem. Eur. J*., 2011, **17**, 6196.

200 K. A. Prokop, H. M. Neu, S. P. de Visser and D. P. Goldberg, *J. Am. Chem. Soc*., 2011, **133**, 15874.

201 Y. Watanabe, T. Iyanagi and S. Oae, *Tetrahedron Lett*., 1982, **23**, 533.

202 S. P. de Visser, *Chem. Eur. J*., 2006, **12**, 8168.

203 C. Hazan, D. Kumar, S. P. de Visser and S. Shaik, *Eur. J. Inorg. Chem*., 2007, 2966.

204 D. Kumar, G. N. Sastry and S. P. de Visser, *J. Phys. Chem. B*, 2012, **116**, 718.

205 S. P. de Visser, K. Oh, A.-R. Han and W. Nam, *Inorg. Chem*., 2007, **46**, 4632.

206 S. P. de Visser, L. Tahsini and W. Nam, *Chem. Eur. J*., 2009, **15**, 5577.

207 S. P. de Visser, R. Latifi, L. Tahsini and W. Nam, *Chem. Asian J*., 2011, **6**, 493.

208 D. Kumar, S. P. de Visser, P. K. Sharma, S. Cohen and S. Shaik, *J. Am. Chem. Soc*., 2004, **126**, 1907.

209 D. Kumar, S. P. de Visser and S. Shaik, *J. Am. Chem. Soc*., 2004, **126**, 5072.

210 S. P. de Visser, *Chem. Commun*., 2007, 171.

211 I. A. Topol, A. V. Nemukhin, K. Salnikow, R. E. Cachau, Y. G. Abashkin, K. S. Kasprzak and S. K. Burt, *J. Phys. Chem. A*, 2006, **110**, 4223.

212 A. R. Diebold, C. D. Brown-Marshall, M. L. Neidig, J. M. Brownlee, G. R. Moran and E. I. Solomon, *J. Am. Chem. Soc*., 2011, **133**, 18148.

213 L. M. Mirica, K. P. McCusker, J. W. Munos, H.-w. Liu and J. P. Klinman, *J. Am. Chem. Soc*., 2008, **130**, 8122.

214 E. Godfrey, C. S. Porro and S. P. de Visser, *J. Phys. Chem. A*, 2008, **112**, 2464.

215 S. P. de Visser, *J. Am. Chem. Soc*., 2006, **128**, 9813.

216 S. Sinnecker, N. Svensen, E. W. Barr, S. Ye, J. M. Bollinger Jr, F. Neese and C. Krebs, *J. Am. Chem. Soc*., 2007, **129**, 6168.

217 A. V. Nemukhin, I. A. Topol, R. E. Cachau and S. K. Burt, *Theor. Chem. Acc*., 2006, **115**, 348.

218 S. Ye and F. Neese, *Proc. Natl. Acad. Sci. USA*, 2011, **108**, 1228.

219 B. Karamzadeh, D. Kumar, G. N. Sastry and S. P. de Visser, *J. Phys. Chem. A*, 2010, **114**, 13234.

220 P. K. Grzyska, E. H. Appelman, R. P. Hausinger and D. A. Proshlyakov, *Proc. Natl. Acad. Sci. USA*, 2010, **107**, 3982.

221 Z. Gross, *J. Biol. Inorg. Chem*., 1996, **1**, 368.

222 M. T. Green, *J. Am. Chem. Soc*., 2006, **128**, 1902.

223 S. P. de Visser, *Angew. Chem. Int. Ed*., 2006, **45**, 1790.

224 R. Latifi, M. Bagherzadeh and S. P. de Visser, *Chem. Eur. J*., 2009, **15**, 6651.

225 C. Geng, S. Ye and F. Neese, *Angew. Chem. Int. Ed*., 2010, **49**, 5717.

226 S. P. de Visser, *J. Am. Chem. Soc*., 2006, **128**, 15809.

227 D. Kumar, H. Hirao, L. Que Jr. and S. Shaik, *J. Am. Chem. Soc*., 2005, **127**, 8026.

228 H. Hirao, D. Kumar, L. Que Jr. and S. Shaik, *J. Am. Chem. Soc*., 2006, **128**, 8590.

229 K. A. Prokop, S. P. de Visser and D. P. Goldberg, *Angew. Chem. Int. Ed*., 2010, **49**, 5091.

230 P. Leeladee, R. A. Baglia, K. A. Prokop, R. Latifi, S. P. de Visser and D. P. Goldberg, *J. Am. Chem. Soc*., 2012, **134**, 10397.

231 S. P. de Visser and W. Nam, *J. Phys. Chem. A*, 2008, **112**, 12887.

232 K. Chen and L. Que Jr, *J. Am. Chem. Soc*., 2001, **123**, 6327.

233 A. Company, Y. Feng, M. Güell, X. Ribas, J. M. Luis, L. Que Jr. and M. Costas, *Chem. Eur. J*., 2009, **15**,3359.

234 I. Prat, J. S. Mathieson, M. Güell, X. Ribas, J. M. Luis, L. Cronin and M. Costas, *Nature Chem*., 2011, **3**, 788.

235 A. Bassan, M. R. A. Blomberg, P. E. M. Siegbahn and L. Que Jr, *Angew. Chem. Int. Ed*., 2005, **44**, 2939.

236 J. Bautz, P. Comba, C. Lopez de Laorden, M. Menzel and G. Rajaraman, *Angew. Chem. Int. Ed*., 2007, **46**, 8067.

237 P. Comba and G. Rajaraman, *Inorg. Chem*., 2008, **47**, 78.

238 S. P. de Visser and R. Latifi, *J. Phys. Chem. B*, 2009, **113**, 12.

239 M. G. Quesne and S. P. de Visser, *J. Biol. Inorg. Chem*., 2012, **17**, 841.

240 S. J. Lange, H. Miyake and L. Que Jr, *J. Am. Chem. Soc*., 1999, **121**, 6330.

241 M. P. Jensen, S. J. Lange, M. P. Mehn, E. L. Que and L. Que Jr, *J. Am. Chem. Soc*., 2003, **125**, 2113.

242 N. Y. Oh, M. S. Seo, M. H. Lim, M. B. Consugar, M. J. Park, J.-U. Rohde, J. Han, K. M. Kim, J. Kim, L. Que Jr and W. Nam, *Chem. Commun*., 2005, 5644.

243 M. R. Bukowski, K. D. Koehntop, A. Stubna, E. L. Bominaar, J. A. Halfen, E. Münck, W. Nam and L. Que Jr, *Science*, 2005, **310**, 1000.

244 Y. M. Badlei, M. Siegler and D. P. Goldberg, *J. Am.Chem. Soc*., 2011, **133**, 1274.

245 M. Sallmann, I. Siewert, L. Fohlmeister, C. Limberg and C. Knispel, *Angew. Chem., Int. Ed*., 2012, **51**, 2234.

246 D. Kumar, G. N. Sastry, D. P. Goldberg and S. P. de Visser, *J. Phys. Chem. A*, 2012, **116**, 582.

247 L. E. Gonzalez-Ovalle, M. G. Quesne, D. Kumar, D. P. Goldberg and S. P. de Visser, *Org. Biomol. Chem*., 2012, **10**, 5401.

248 S. P. de Visser, J. S. Valentine and W. Nam, *Angew. Chem. Int. Ed*., 2010, **49**, 2099.

249 A. K. Vardhaman, C. V. Sastri, D. Kumar and S. P. de Visser, *Chem. Commun*., 2011, **47**, 11044.

250 J. Annaraj, J. Cho, Y.-M. Lee, S. Y. Kim, R. Latifi, S. P. de Visser and W. Nam, *Angew. Chem. Int. Ed*., 2009, **48**, 4150.

251 R. Latifi, L. Tahsini, D. Kumar, G. N. Sastry, W. Nam and S. P. de Visser, *Chem. Commun*., 2011, **47**, 10674.

252 R. Latifi, L. Tahsini, W. Nam and S. P. de Visser, *Phys. Chem. Chem. Phys*., 2012, **14**, 2518.

253 R. Latifi, M. Bagherzadeh, B. F. Milne, M. Jaspars and S. P. de Visser, *J. Inorg. Biochem*., 2008, **102**, 2171.

254 S. J. Kim, R. Latifi, H. Y. Kang, W. Nam and S. P. de Visser, *Chem. Commun*., 2009, 1562.

255 S. P. de Visser, *J. Phys. Chem. B*, 2006, **110**, 20759.

256 S. P. de Visser, *J. Phys. Chem. B*, 2007, **111**, 12299.

257 S. P. de Visser, *The axial ligand effect on substrate monoxygenation by the oxo-iron active species of heme enzymes. How does cytochrome c peroxidase compare to cytochrome P450?* In *Inorganic Biochemistry: Research Progress*, J. G. Hughes and A. J. Robinson, Eds.; Nova Science Publishers, Inc., New York, 2008, Chapter 7, pp. 197–224.

258 S. P. de Visser, *J. Biol. Inorg. Chem*., 2006, **11**, 168.

259 S. P. de Visser, Y.-M. Lee and W. Nam, *Eur. J. Inorg. Chem*., 2008, 1027.

260 S. P. de Visser, *Chem. Eur. J*., 2008, **14**, 4533.

261 S. P. De Visser, **D.Sc. Thesis**, University of Mancestor, 2012

262 S. Kumar, A. S. Faponle, P. Barman, A. K. Vardhaman, C. V. Sastri, Devesh Kumar, and S. P. de Visser, *J. Am. Chem. Soc.*, 2014, **136**, 17102.

263 B. Karamzadeh, D. Singh, W. Nam, Devesh Kumar and S. P. de Visser, *Phys. Chem. Chem. Phys*., 2014, **16**, 22611.

264 M. A. Sainna, S. Kumar, Devesh Kumar, S. Fornarini, M. E. Crestoni, and S. P. de Visser, *Chem.Sci.*, 2015, **6**, 1516.

265 M. A. Sainna, Devendra Singh, Devesh Kumar, and S. P. de Visser, *Organometallics* 2015, **34**, 1651.

266 Li Ji, A. S. Faponle, M. G. Quesne, M. A. Sainna, J. Zhang, A. Franke, Devesh Kumar, R. van Eldik, W. Liu, and S. P. de Visser, *Chem. Eur. J*. 2015, **21**, 9083.

267 Madleen Sallmann, Suresh Kumar, Petko Chernev, Joscha Nehrkorn, Alexander Schnegg, Devesh Kumar, Holger Dau, Christian Limberg, and Sam P. de Visser, *Chem. Eur. J*. 2015, **21**, 7470.

268 P. Barman, P. Upadhyay, A. S. Faponle, J. Kumar, S. S. Nag, Devesh Kumar, C. V. Sastri, and S. P. de Visser, *Angew. Chem. Int. Ed*., 2016, **55**, 11091.

269 F. G. C. Reinhard, P. Barman, G. Mukherjee, J. Kumar, D. Kumar, Devesh Kumar, Chivukula V. Sastri, and Sam P. de Visser, *J. Am. Chem. Soc.*, 2017, **139**, 18328.

270 G Mukherjee, A Alili, P Barman, Devesh Kumar, C V Sastri, and S P de Visser, *Chem.–A Euro. J.*, 2019, **25**, 5086.

271 P Barman, F C Reinhard, U K Bagha, Devesh Kumar, C V Sastri, and S P de Visser *Angew. Chem. Int. Ed.* 2019, **58**, 10639.

Appendix

Paper #1:

P Barman, F C Reinhard, U K Bagha, **Devesh Kumar**, C V Sastri, S P de Visser

Hydrogen by Deuterium Substitution in an Aldehyde Tunes the Regioselectivity by a Nonheme Manganese (III)-Peroxo Complex.

***Angew. Chem. Int. Ed.* 2019**, *58*, 10639 –10643

Paper #2:

G Mukherjee, A Alili, P Barman, **Devesh Kumar**, C V Sastri, S P de Visser

Interplay Between Steric and Electronic Effects: A Joint Spectroscopy and Computational Study of Nonheme Iron (IV)-Oxo Complexes.

***Chem.–A Euro. J.* 2019**, *25*, 5086-5098.

Paper #3:

F S T Khan, S Banerjee, **Devesh Kumar**, S P Rath

Diheme Cytochrome c: Structure–Function Correlation and Effect of Heme−Heme Interactions.

Inorg. Chem. **2018**, *57*, 11498-11510.

Paper #4:

G. Mukherjee, C WZ Lee, S. Sekhar Nag, A. Alili, F. G Cantú Reinhard, **Devesh Kumar**, C V Sastri, S P de Visser

Dramatic rate-enhancement of oxygen atom transfer by an iron (iv)-oxo species by equatorial ligand field perturbations.

Dalton Trans. **2018**, *42*, 14945-14957.

Paper #5:

F. G. C. Reinhard, P. Barman, G. Mukherjee, J. Kumar, D. Kumar, **Devesh Kumar**, Chivukula V. Sastri, and Sam P. de Visser

Keto−Enol Tautomerization Triggers an Electrophilic Aldehyde Deformylation Reaction by a Nonheme Manganese(III)-Peroxo Complex.

***J. Am. Chem. Soc.* 2017**, *139*, 18328−18338.

Paper #6:

F. G. C. Reinhard, M. A. Sainna, P. Upadhyay, G. A. Balan, **Devesh Kumar**, S. Fornarini, M. E. Crestoni, Sam P. de Visser

A Systematic Account on Aromatic Hydroxylation by a Cytochrome P450 Model Compound I: A Low-Pressure Mass Spectrometry and Computational Study.

Chem. Eur. J. **2016**, *22*, 18608 – 18619.

Paper #7:

P. Barman, P. Upadhyay, A. S. Faponle, J. Kumar, S. S. Nag, **Devesh Kumar**, C. V. Sastri, S. P. de Visser

Deformylation Reaction by a Nonheme Manganese(III)–PeroxoComplex via Initial Hydrogen-Atom Abstraction.

Angew. Chem. Int. Ed. **2016**, *55*, 11091 –11095.

Paper #8:

M. G. Quesne, D. Senthilnathan, D. Singh, **Devesh Kumar**, P. Maldivi, A. B. Sorokin, Sam P. de Visser

Origin of the Enhanced Reactivity of μ-Nitrido-Bridged Diiron(IV)-Oxo Porphyrinoid Complexes over Cytochrome P450 Compound I.

ACS Catal. **2016**, *6*, 2230−2243.

Paper #9:

Madleen Sallmann, Suresh Kumar, Petko Chernev, Joscha Nehrkorn, Alexander Schnegg, **Devesh Kumar**, Holger Dau, Christian Limberg, Sam P. de Visser

Structure and Mechanism Leading to Formation of the Cysteine Sulfinate Product Complex of a Biomimetic Cysteine Dioxygenase Model.

Chem. Eur. J. **2015**, *21*, 7470 – 7479.

Paper #10:

Li Ji, A. S. Faponle, M. G. Quesne, M. A. Sainna, J. Zhang, A. Franke, **Devesh Kumar**, R. van Eldik, W. Liu, S. P. de Visser

Drug Metabolism by Cytochrome P450 Enzymes: What Distinguishes the Pathways Leading to Substrate Hydroxylation Over Desaturation?

Chem. Eur. J. **2015**, *21*, 9083 – 9092.

Paper #11:

M. A. Sainna, Devendra Singh, **Devesh Kumar**, S. P. de Visser

A Trimetal Carbene with Reactivity Reminiscent of Fischer−Tropsch Catalysis.

Organometallics **2015**, *34*, 1651-1660.

Paper #12:

M. A. Sainna, S. Kumar, **Devesh Kumar**, S. Fornarini, M. E. Crestoni, S. P. de Visser

A comprehensive test set of epoxidation rate constants for iron(IV)--oxo porphyrin complexes.

Chem.Sci. **2015**, *6*, 1516–1529.

Paper #13:

S. Kumar, A. S. Faponle, P. Barman, A. K. Vardhaman, C. V. Sastri, Devesh Kumar, S. P. de Visser

Long-Range Electron Transfer Triggers Mechanistic Differences between Iron(IV)-Oxo and Iron(IV)-Imido Oxidants.

J. Am. Chem. Soc. **2014**, *136*, 17102-17115.

Paper #14:

B. Karamzadeh, D. Singh, W. Nam, **Devesh Kumar,** S. P. de Visser

Properties and reactivities of nonheme iron(IV)–oxo versus iron(V)–oxo: long-range electron transfer versus hydrogen atom abstraction.

Phys. Chem. Chem. Phys. **2014**, *16*, 22611-22622.

Paper #15:

. D. Saha, Ravi Verma, **Devesh Kumar**, S. Pathak, S. Bhunya, A. Sarkar

A “Hemilabile” Palladium−Carbon Bond: Characterization and Its Implication in Catalysis.

Organometallics **2014**, *33*, 3243−3246.

Paper #16:

L. R. Widger, Y. Jiang, A. C. McQuilken, T. Yang, M. A. Siegler, H. Matsumura, P. Moënne-Loccoz, **Devesh Kumar**, S. P. de Visser, D. P. Goldberg

Thioether-ligated iron (II) and iron (III)-hydroperoxo/alkylperoxo complexes with an H-bond donor in the second coordination sphere.

Dalton Transactions **2014**, *43*, 7522-7532.

Paper #17:

M. G. Quesne, R. Latifi, L. E. Gonzalez-Ovalle, **Devesh Kumar**, and S. P. de Visser

Quantum Mechanics/Molecular Mechanics Study on the Oxygen Binding and Substrate Hydroxylation Step in AlkB Repair Enzymes.

Chem. Eur. J. **2014**, *20*, 435 – 446.

Paper #18:

Anil Kumar Vardhaman, Prasenjit Barman, Suresh Kumar, C. V. Sastri, **Devesh Kumar**, Sam P. de Visser

Mechanistic insight into halide oxidation by non-heme iron complexes. Haloperoxidase versus halogenase activity.

***Chem.Commun.* 2013**, 49, 10926-10928.

Paper #19:

A. K. Vardhaman, P. Barman, S. Kumar, C. V. Sastri, **Devesh Kumar**, Sam P. de Visser

. Comparison of the Reactivity of Nonheme Iron(IV)–Oxo versus Iron(IV)–Imido Complexes: Which is the Better Oxidant?

Angew. Chem. Int. Ed.* 2013, 52,*12288-12292.

Paper #20:

L. R. Widger, Y. Jiang, M. Siegler, **Devesh Kumar**, R. Latifi, S. P. de Visser, G. N. L. Jameson, D. P. Goldberg

Synthesis and Ligand Non-Innocence of Thiolate-Ligated (N4S) Iron(II) and Nickel(II) Bis(imino)pyridine Complexes.

InorgChem* 2013, 52,* 10467–10480.

Paper #21:

S. M. Pratter, C. Konstantinovics, C. L. M. DiGiuro, E. Leitner, **Devesh Kumar**, S. P. de Visser, G. Grogan, and G. D. Straganz

. Inversion of Enantioselectivity of a Mononuclear Non-Heme Iron(II)-dependent Hydroxylase by Tuning the Interplay of Metal-Center Geometry and Protein Structure.

Angew. Chem. Int. Ed. 2013*, 52,*9677-9681,

Paper #22:

Devesh Kumar, R. Latifi, S. Kumar, E. V. Rybak-Akimova, M. A. Sainna, Sam P. de Visser

Rationalization of the Barrier Height for p-Z-styrene Epoxidation by Iron(IV)-Oxo Porphyrin Cation Radicals with Variable Axial Ligands.

***Inorg. Chem.* 2013**, *52*, 7968–7979.

Paper #23:

P. Leeladee, G. Jameson, M. Siegler, **Devesh Kumar**, Sam de Visser, David P. Goldberg

Generation of a High-Valent Iron Imido Corrolazine Complex and NR Group Transfer Reactivity.

Inorg. Chem. **2013**, *52*, 4668-4682.

Paper #24:

L. E. Gonzalez-Ovalle, M. G. Quesne, **Devesh Kumar**, D. P. Goldberg, Sam P. de Visser

Axial and equatorial ligand effects on biomimetic cysteine dioxygenase model complexes.

Org. Biomolec. Chem. **2012**, *10*, 5401-5409.

Paper #25:

Devesh Kumar, G. Narahari Sastry, Sam P. de Visser

Axial Ligand Effect On The Rate Constant of Aromatic Hydroxylation By Iron(IV)- Oxo Complexes Mimicking Cytochrome P450 Enzymes.

J. Phys. Chem. B **2012**, *116*, 718-730.

Paper #26:

Devesh Kumar, G. Narahari Sastry, David P. Goldberg, Sam P. de Visser

Mechanism of S-Oxygenation by a Cysteine Dioxygenase Model Complex.

J. Phys. Chem. A **2012**, *116*, 582-591.

Paper #27:

A. K. Vardhaman, C. V. Sastri, **Devesh Kumar**, Sam P. de Visser

Nonheme Ferric Hydroperoxo Intermediates Are Efficient Oxidants of Bromide Oxidation.

ChemComm 2011, *47*, 11044 - 11046.

Paper #28:

R. Latifi, L. Tahsini, **Devesh Kumar**, G. Narahari Sastry, W. Nam, Sam P. de Visser

Oxidative properties of a nonheme Ni(II)(O_2) complex: Reactivity patterns for C–H activation, aromatic hydroxylation and heteroatom oxidation.

ChemComm 2011, *47*, 10674-10676.

Paper #29:

Devesh Kumar

Drug metabolism by Cytochrome P450: A tale of multistate reactivity.

In:

"*Iron-Containing Enzymes: Versatile Catalysts of Hydroxylation Reactions in Nature", Eds. S. P. Visser, D. Kumar, The Royal Society of Chemistry, U.K., (2011) Ch. 9 pp 281-329.*

Paper #30:

Sam P. de Visser and Devesh Kumar (Eds.)

Iron-containing enzymes: Versatile catalysts of hydroxylation reactions in nature;

Royal Society of Chemistry Publishing, Cambridge (UK),

2011.

Paper #31:

Devesh Kumar, Walter Thiel, S. P. de Visser

Theoretical study on the mechanism of the oxygen activation process in cysteine dioxygenase enzymes.

***J. Am. Chem. Soc.* 2011**, *133*, 3869-3882.

Paper #32:

Devesh Kumar, G. N. Sastry, S. P. de Visser

Effect of the Axial Ligand on Substrate Sulfoxidation Mediated by Iron (IV)–Oxo Porphyrin Cation Radical Oxidants.

Chem. Eur. J. **2011**, *17*, 6196-6205.

Paper #33:

Devesh Kumar, A. Altun, S. Shaik, W. Thiel

Water as biocatalyst in cytochrome P450.

Faraday Discussions* 2011, 148*, 373-383.

Paper #34:

B. Karamzadeh, **Devesh Kumar**, G. N. Sastry, S. P. de Visser

Steric Factors Override Thermodynamic Driving Force in Regioselectivity of Proline Hydroxylation by Prolyl-4-hydroxylase Enzymes.

J. Phys. Chem. A **2010**, *114*; 13234-13243.

Paper #35:

Devesh Kumar, B. Karamzadeh, G. Narahari Sastry, S. P. de Visser

What Factors Influence the Rate Constant of Substrate Epoxidation by Compound I of Cytochrome P450 and Analogous Iron(IV)-Oxo Oxidants.

***J. Am. Chem. Soc.* 2010**,*132*, 7656–7667.

Paper #36:

M. Altarsha, T. Benighaus, **Devesh Kumar**, W. Thiel

Coupling and uncoupling mechanisms in the methoxythreonine mutant of cytochrome P450cam: a quantum mechanical/ molecular mechanical study.

Biol. Inorg. Chem. **2010**, *15*, 361-372.

Paper #37:

S. Shaik, S. Cohen, Y. Wang, H. Chen, **D. Kumar** & W. Thiel

. P450 Enzymes: Their Structure, Reactivity and Selectivity, Modeled by QM/MM Calculations.

***Chem. Rev*. 2010**, *110*, 949-1017.

Paper #38:

Devesh Kumar, L. Tahsini, S. P. de Visser, H. Y. Kang, S. J. Kim, W. Nam

Effect of Porphyrin Ligands on the Regioselective Dehydrogenation versus Epoxidation of Olefins by Oxoiron(IV) Mimics of Cytochrome P450.

***J. Phys. Chem. A* 2009**, *113*, 11713-11722.

Paper #39:

C. S. Porro, **Devesh Kumar**, S. P. de Visser

Electronic properties of pentacoordinated heme complexes in cytochrome P450 enzymes: Search for an Fe(I) Oxidation State

Phys. Chem. Chem. Phys. **2009**, *11*, 10219-10226.

Paper #40:

M. Altarsha, W. Dongqi, T. Benighaus, **Devesh Kumar**, W. Thiel

QM/MM Study of the Second Proton Transfer in the Catalytic Cycle of the D251N Mutant of Cytochrome P450cam.

J. Phys. Chem. B **2009**, *113*, 9577-9588.

Paper #41:

M. Altarsha, T. Benighaus, **Devesh Kumar**, W. Thiel

How is the Reactivity of Cytochrome P450cam Affected by Thr252X Mutation? A QM/MM Study for X = Serine, Valine, Alanine, Glycine.

J. Am. Chem. Soc. **2009**, *131*, 4755-4763.

Paper #42:

A. Altun, **Devesh Kumar**, F. Neese, W. Thiel

Multi-reference Ab Initio QM/MM Study on Intermediates in the Catalytic Cycle of Cytochrome P450cam.

J. Phys. Chem. A **2008**, *112*, 12904-12910.

Paper #43:

S. Shaik, **Devesh Kumar**, S. P. de Visser

A Valence Bond Modeling of Trends in Hydrogen Abstraction Barriers and Transition States of Hydrogen Reactions Catalyzed by Cytochrome P450 Enzymes.

***J. Am. Chem. Soc.* 2008**, *130*, 10128-10140.

Paper #44:

Y. Wang, **Devesh Kumar**, C. Yang, K. Han, S. Shaik

Theoretical Study of N-Demethylation of Substituted N,N-Dimethylanilines by Cytochrome P450: The Mechanistic Significance of Kinetic Isotope Effect Profiles.

J. Phys. Chem. B **2007**, *111*, 7700-7710.

Paper #45:

C. Hazan, **Devesh Kumar**, S. P. de Visser, S. Shaik

A Density Functional Study of the Factors that Influence the regioselectivity of Toluene Hydroxylation by Cytochrome P450 enzyme?

Eur. J. Inorg. Chem. **2007**, 2966-2974.

Paper #46:

S. Shaik, H. Hirao, **Devesh Kumar**

Reactivity patterns of cytochrome P450 enzymes: Multifunctionality of the active species and the two states – two oxidants conundrum.

Natural Product Reports **2007**, *24*, 533-552..

Paper #47:

S. Shaik, H. Hirao, **Devesh Kumar**

Reactivity of High-Valent Iron Oxo Species in Enzymes and Synthetic Reagents: A Tale of Many States.

***Acc. Chem. Res.* 2007**, *40*, 532-542.

Paper #48:

C. A. Grapperhaus, P. M. Kozlowski, **Devesh Kumar**, H. N. Frye, K. B. Venna, S. Poturovic

Singlet Diradical Character of an Oxidized Ruthenium Trithiolate: Electronic Structure and Reactivity.

Angew. Chem. Int. Ed. **2007**, *46*, 4085-4088..

Paper #49:

K.-B. Cho, Y. Moreau, **DeveshKumar**, D. Rock, J. P. Jones, S. Shaik

Formation of the Active Species of Cytochrome P450 Using Iodosylbenzene: A Case for Spin Selective Reactivity.

Chem. Eur. J. **2007,** *13*, 4103 - 4115.

Paper #50:

H. Hirao, **Devesh Kumar**, S. Shaik

On the Identity and Reactivity Patterns of the "Second Oxidant" of the T252A Mutant of Cytochrome P450cam in the Oxidation of 5-Methylenenylcamphor.

***J. Ing. Biochem.* 2006**, *100*, 2054-2068.

Paper #51:

Devesh Kumar, H. Hirao, S. Shaik, P. M. Kozlowski

Proton-shuffle mechanism of O-O activation for formation of a high-valent oxo-iron species of Bleomycin.

***J. Am. Chem. Soc.* 2006,** *128*, 16148-16158.

Paper #52:

H. Hirao, **Devesh Kumar**, Lawrence Que Jr. & S. Shaik

Two-State Reactivity in Alkane Hydroxylation by Non-Heme Iron-Oxo Complexes.

***J. Am. Chem. Soc.* 2006**, *128*, 8590-8606.

Paper #53:

S. Cohen, **Devesh Kumar**, S. Shaik

In silico design of a mutant of cytochrome P450 containing selenocysteine.

***J. Am. Chem. Soc.* 2006,** *128*, 2649-2653.

Paper #54:

E. Derat, **Devesh Kumar**, H. Hirao, S. Shaik

Gauging the Relative Oxidative Powers of Compound I, Ferric-Hydroperoxide and the Ferric-Hydrogen Peroxide Species of Cytochrome P450 Towards C-H Hydroxylation of a Radical Probe Substrate.

***J. Am. Chem. Soc.* 2006**, *128*, 473-484.

Paper #55:

C. Li, W. Wu, **Devesh Kumar**, S. Shaik

Kinetic Isotope Effect is A Sensitive Probe of Spin State Reactivity in C-H Hydroxylation of N,N-Dimethyl Aniline by Cytochrome P450.

***J. Am. Chem. Soc.* 2006**, *128*, 394-395.

Paper #56:

Devesh Kumar, H. Hirao, S. P. de Visser, J. Zheng , D. Wang, W. Thiel, S. Shaik

New Feature in the Catalytic Cycle of Cytochrome P450 during the formation of Compound I from Compound 0.

J. Phys. Chem. B **2005,** *109*, 19946-19951.

Paper #57:

H.Hirao, **Devesh Kumar**, W. Thiel, S. Shaik

Two States and Two More in the Mechanisms of Hydroxylation and Epoxidation by Cytochrome P450.

***J. Am. Chem. Soc.* 2005,** *127*, 13007-13018.

Paper #58:

S. Shaik, **Devesh Kumar**, S. P. de Visser, A. Ahmet, W. Thiel

A Theoretical Perspective on Structure and Mechanisms of Cytochrome P450 Enzymes.

***Chem. Rev*. 2005**, *105*, 2279-2328.

Paper #59:

Devesh Kumar, S. P. de Visser, P. K. Sharma, H. Hirao, S. Shaik

Sulfoxidation Mechanisms Catalyzed by Cytochrome P450 and Horseradish Peroxidase Models: Spin-Selection Induced by the Ligand.

Biochemistry **2005,** *44*, 8148-8158.

Paper #60:

Devesh Kumar, S. P. de Visser, S. Shaik

Theory Favors A Stepwise Mechanism of Porphyrin Degradation By a Ferric Hydroperoxide Model of Active Speices of Heme Oxygenase.

***J. Am. Chem. Soc.* 2005**, *127*, 8204-8213.

Paper #61:

Devesh Kumar, H. Hirao, Lawrence Que Jr., S. Shaik

Theoretical Investigation of C-H Hydroxylation by $(N_4Py)Fe^{IV}=O^{2+}$: An Oxidant More Powerful than P450?

J. Am. Chem. Soc. **2005,** *127*, 8026 -8027.

Paper #63:

Devesh Kumar, S. P. de Visser, S. Shaik

Multi-state Reactivity in Styrene Epoxidation by Compound I of Cytochrome P450: Mechanisms of Products and Side Product Formations.

***Chem. Eur. J.* 2005,** *11*, 2825–2835.

Paper #64:

S. Shaik, S. P. de Visser, **Devesh Kumar**

One oxidant, many pathways: A theoretical perspective of monoxygenation mechanisms by cytochrome P450 enzymes.

J. Biol. Inorg. Chem. **2004,** *9*, 661-668.

Paper #65:

S. Shaik, S. P. de Visser, **Devesh Kumar**

External Electric Field Will Control the Selectivity of Enzymatic-Like Bond Activations.

***J. Am. Chem. Soc.* 2004,** *126*, 11746-11749.

Paper #66:

S. P. de Visser, **Devesh Kumar**, S. Cohen, R. Shacham, S. Shaik

A Predictive Pattern of Computed Barriers for C-H Hydroxylation by Compound I of Cytochrome P450.

***J. Am. Chem. Soc.* 2004,** *126*, 8362-8363.

Paper #67:

S. Shaik, S. Cohen, S. P.de Visser, P. K. Sharma, **Devesh Kumar**, S. Kozuch, F. Ogliaro, D. Danovich

The "Rebound Controversy": An Overview and Theoretical Modeling of the Rebound Step in C-H Hydroxylation by Cytochrome P450.

***Eur. J. Inorg. Chem*. 2004**, 207-226.

Paper #68:

S. P. de Visser, **Devesh Kumar**, S. Shaik

How Do Aldehyde Side Products Occur During Alkene Epoxidation by Cytochrome P450? Theory Reveals a State-Specific Multi-State Scenario Where the High-Spin Component Leads to All Side Products.

***J. Inorg. Biochem*. 2004,** *98*, 1183-1193.

Paper #69:

Devesh Kumar, S. P. de Visser, S. Shaik

Oxygen Economy of Cytochrome P450: What is the Origin of the Mixed Functionality as a Dehydrogenating-Oxidase Enzyme Compared with its Normal Function?

***J. Am. Chem. Soc.* 2004,** *126*, 5072-5073.

Paper #70:

P. K. Sharma, R. Kerkokiants, S. P. de Visser, **Devesh Kumar**, S. Shaik

Porphyrin Traps its Terminator! Concerted and Stepwise Porphyrin Degradation Mechanisms Induced by Heme-Oxygenase and Cytochrome P450.

***Angew. Chem. Int. Ed.* 2004**, *43*, 1129-1132.

Paper #71:

Devesh Kumar, S. P. de Visser, P. K. Sharma, S. Cohen, S. Shaik

Radical Clock Substrates, their C–H Hydroxylation Mechanism by Cytochrome P450 and Other Reactivity Patterns:; What Does Theory Reveal About the Clocks'- Behavior?

***J. Am. Chem. Soc.* 2004**, *126*, 1907-1920.

Paper #72:

S. P. de Visser, S. Shaik, P. K. Sharma, **Devesh Kumar**, W. Thiel

Active Species of Horseradish Peroxidase (HRP) and Cytochrome P450: Two Electronic Chameleons.

J. Am. Chem. Soc. **2003,** *125*, 15779-15788.

Paper #73:

Devesh Kumar, S. P. de Visser, S. Shaik

How Does Product Isotopes Effect Prove the Operation of a Two-State 'Rebound' Mechanism in C-H Hydroxylation by Cytochrome P450?

***J. Am. Chem. Soc.* 2003,** *125*, 13024 - 13025.